1-1-2012

# Virus-Size Nanoparticles Coated with a Synthetic "Self" Peptide inhibit Phagocytic Clearance and Enhance Delivery of an Anti-Cancer Drug

Pia Lorena Rodriguez Nunez
*University of Pennsylvania*, piarod@seas.upenn.edu

# Virus-Size Nanoparticles Coated with a Synthetic "Self" Peptide inhibit Phagocytic Clearance and Enhance Delivery of an Anti-Cancer Drug

**Abstract**
Professional phagocytes are white blood cells of the innate immune system that protect humans and other animals from attacks by foreign pathogens by ingesting potentially harmful circulating particles. However, phagocytes such as macrophages may also attack elements that have been intentionally introduced into the body, such as implants, artificial tissues, artificial organs and vesicles bearing therapeutic agents, reducing their lifetime in the body. Nanoparticles and liposomes are similar in size to viruses, and are frequently decorated with antibodies for targeted therapeutics or imaging purposes. Although such particles are sufficiently small to avoid passive entrapment within capillaries in vivo, macrophages in the spleen and liver are known to clear these particles within hours or days after injection into the circulation, limiting proper delivery to target disease sites. This dissertation describes the engineering of long-circulating nanoscale carriers bearing a universal marker that avoids macrophage clearance by mimicking the process of recognition of "self"cells *in vivo*. The membrane protein CD47 is a marker of "self" that impedes phagocytosis of "self" cells by signaling through a species-specific, highly polymorphic receptor named SIRPα. Among natural mouse variants, only NOD.SCID gamma chain (NSG) mice express a mouse polymorph of SIRPα that cross-reacts with human CD47, and thus provided an ideal platform for our in vivo assessment of human CD47 on synthetic particles. Based on the co-crystallized structure of the CD47-SIRPα complex, polypeptides were designed by simulation and then synthesized with the further reductionist goal of identifying and then exploiting the most minimal components necessary for CD47-SIRPα complex interactions. This thesis details a reductionist approach that avoids many potentially confounding biological factors, and constitutes a first example of a synthetic, human ligand that is easily attached to synthetic surfaces and can successfully mediate binding and signaling to phagocyte receptors to inhibit phagocytic uptake. By understanding how both the full-length as well as the minimal component of the hCD47-SIRPα interaction works *in vivo*, this dissertation was able to elucidate potential therapeutic roles for anti-hCD47 antibody targeting in biodistribution of drugs delivered to solid tumors, among other applications.

**Degree Type**
Dissertation

**Degree Name**
Doctor of Philosophy (PhD)

**Graduate Group**
Chemical and Biomolecular Engineering

**First Advisor**
Dennis E. Discher

**Keywords**
Biocompatability, Blood Cells, In vivo, Macrophages, Nanoparticles, Tumor

# VIRUS-SIZE NANOPARTICLES COATED WITH A SYNTHETIC “SELF” PEPTIDE INHIBIT PHAGOCYTIC CLEARANCE AND ENHANCE DELIVERY OF AN ANTI-CANCER DRUG

Pía Lorena Rodríguez Núñez

A DISSERTATION

in

Chemical and Biomolecular Engineering

Presented to the Faculties of the University of Pennsylvania

in

Partial Fulfillment of the Requirements for the

Degree of Doctor of Philosophy

2012

Supervisor of Dissertation

_____

Dennis E. Discher,

Robert D. Bent Chaired Professor

Graduate Group Chairperson

_____

Raymond J. Gorte, Professor and Graduate Group Chair

Dissertation Committee:

Dr. Dianne Cox, Professor of Anatomy and Structural Biology

Dr. Matthew J. Lazzara, Assistant Professor of Chemical and Biomolecular Engineering

Dr. Casim A. Sarkar, Assistant Professor of Bioengineering

VIRUS-SIZE NANOPARTICLES COATED WITH A SYNTHETIC “SELF” PEPTIDE INHIBIT PHAGOCYTIC CLEARANCE AND ENHANCE DELIVERY OF AN ANTI-CANCER DRUG

*A mi Família*

# ABSTRACT

VIRUS-SIZE NANOPARTICLES COATED WITH A SYNTHETIC “SELF” PEPTIDE INHIBIT PHAGOCYTIC CLEARANCE AND ENHANCE DELIVERY OF AN ANTI-CANCER DRUG

Pía Lorena Rodríguez Núñez

Dr. Dennis E. Discher

Professional phagocytes are white blood cells of the innate immune system that protect humans and other animals from attacks by foreign pathogens by ingesting potentially harmful circulating particles. However, phagocytes such as macrophages may also attack elements that have been intentionally introduced into the body, such as implants, artificial tissues, artificial organs and vesicles bearing therapeutic agents, reducing their lifetime in the body. Nanoparticles and liposomes are similar in size to viruses, and are frequently decorated with antibodies for targeted therapeutics or imaging purposes. Although such particles are sufficiently small to avoid passive entrapment within capillaries *in vivo*, macrophages in the spleen and liver are known to clear these particles within hours or days after injection into the circulation, limiting proper

delivery to target disease sites. This dissertation describes the engineering of long-circulating nanoscale carriers bearing a universal marker that avoids macrophage clearance by mimicking the process of recognition of “self” cells *in vivo.* The membrane protein CD47 is a marker of “self” that impedes phagocytosis of “self” cells by signaling through a species-specific, highly polymorphic receptor named SIRPα. Among natural mouse variants, only NOD.SCID gamma chain (NSG) mice express a mouse polymorph of SIRPα that cross-reacts with human CD47, and thus provided an ideal platform for our *in vivo* assessment of human CD47 on synthetic particles. Based on the co-crystallized structure of the CD47-SIRPα complex, polypeptides were designed by simulation and then synthesized with the further reductionist goal of identifying and then exploiting the most minimal components necessary for CD47-SIRPα complex interactions. This thesis details a reductionist approach that avoids many potentially confounding biological factors, and constitutes a first example of a synthetic, human ligand that is easily attached to synthetic surfaces and can successfully mediate binding and signaling to phagocyte receptors to inhibit phagocytic uptake. By understanding how both the full-length as well as the minimal component of the hCD47-SIRPα interaction works *in vivo*, this dissertation was able to elucidate potential therapeutic roles for anti-hCD47 antibody targeting in biodistribution of drugs delivered to solid tumors, among other applications.

## TABLE OF CONTENTS

# LIST OF TABLES

# LIST OF FIGURES

# CHAPTER 1: Introduction to CD47-SIRPα

## 1.1 – Background

The immune system has evolved to counteract assault on the body by non-“self” entities that may compromise an individual’s health. This tight regulation involves complex interactions between membrane proteins on Macrophages that play key roles in both the innate and adaptive immune responses. Viable cells are normally not phagocytosed since CD47 on their surface can interact with the phagocytosis inhibitor receptor signal regulatory protein alpha (SIRPα) on the macrophage (Oldenborg 2000). Both CD47 and SIRPα are critical aspects of this doctoral dissertation, and therefore we start by providing some important background information on both of them.

The ubiquitously expressed protein CD47 is an Ig superfamily member that interacts specifically with SIRPα found on macrophages (Jiang 1999; Seiffert 1999; Vernon-Wilson 2000) and innate immune cell as a regulator or toll receptor signaling (Kong 2007). CD47 interacts with signal regulatory protein-α (SIRPα), thrombospondin (TSP)-1 and -2 to mediate various cellular functions (Oldenborg 2001). In particular, CD47 signaling through SIRPα inhibits the phagocytosis of CD47-expressing target cells by SIRPα-expressing macrophages. Phosphorylation of the immune-receptor tyrosine-based inhibitory motif (ITIM) in the cytoplasmic domain of SIRPα upon ligation with CD47 leads to the recruitment of SHP-1 and deactivation of phagocytosis (Vernon-Wilson 2000;

Seiffert 2001). The loss of CD47 protein in red blood cells (RBCs), platelets, apoptotic cells and lymphocytes results in their rapid elimination by splenic macrophages (Oldenborg 2001; Krieser 2002; Oldenborg 2004, Gardai 2005; Majeti 2009). Anti-CD47 monoclonal antibodies inhibiting the interaction of CD47 and SIRPα promote the phagocytosis of tumor cells by macrophages, and also by monocytes and neutrophils (Gresham 1989, Jaiswal 2009). Anti-CD47 monoclonal antibodies have been shown to inhibit phagocytosis *in vitro* and significantly inhibit myeloma growth in human fetal bone-free and –bearing xenotransplantation models *in vivo* (Kim 2012).

The receptor SIRPα is composed of three immunoglobulin superfamily (IgSF) domains while CD47 contains only a single IgSF domain with a disulfide link across one of the loops between the transmembrane regions (Tsai 2008), which may be required for optimal binding of SIRPα. The crystal structure of the SIRPα-CD47 complex indicates a high degree of flexibility in the SIRPα loops, and that CD47 binds SIRPα at its N-terminal ligand-binding domain (Hatherley 2008).

Expression of both SIRPα and CD47 on the surface of macrophages raises the possibility that these proteins interact on the same macrophage surface (*in cis*). The occurrence of cis interactions would have implications for SIRPα's ability to bind to CD47 on target cells (*in trans*) (Doucey 2004).

CD47 binds to SIRPα with relatively low affinity, and the interaction does not result in strong cell-cell adhesion (Hatherley 2007; Subramanian 2007). The lower affinity interaction of CD47-SIRPα instead allows for transient cis or trans interactions during intracellular or intercellular binding. CD47 expression is not limited to red blood cells, being present in many other cell types including macrophages. SIRPα belongs to the “paired receptors” class of membrane proteins, and exhibits homology to other receptors on innate immune cells including natural killer (NK) cells, as well as to major histocompatibility complex (MHC) proteins (Lanier 2005).

Recently, research on the high degree of polymorphisms in the SIRPα N-terminal domain reported by Takenaka et al. (2007) implicated the SIRPα locus in the more efficient engraftment of human bone marrow stem cells into the non-obese diabetic severe combined immunodeficiency (NOD.SCID) mouse strain over other strains. In general, there is little cross reaction between CD47 from one species and SIRPα of another (Subramanian 2006, 2007). However, the allele of SIRPα in the NOD.SCID mouse is sufficiently different from other mouse strains to enable binding to human CD47 and mediate protection of human cells from host macrophages, allowing for xenogenenic engraftment. (Barclay 2009). Recent studies have showed that some transgenic BALB/c mice exhibited increased engraftment of human hematopoietic cells improved functionality of the human immune cells over NOD.SCID, and NOD.SCID gamma (NSG) mice

(Strowig 2011, Legrand 2011). However, further analysis of the SIRPα proteins in these strains need to be done to show the binding affinity constant of those SIRPα to hCD47. In this dissertation, we have adopted a conservative approach by electing to utilize the NSG strain as the host in which to study the CD47-SIRPα interaction.

### 1.2 – Motivation for reductionist approach with particles

A major challenge in injecting particles or implanting biomaterials into the body is the possibility that they will activate an immune response. The internalization of extracellular material into cells is commonly performed by a process called endocytosis, which is divided into two general categories: phagocytosis, which involves the uptake of particles, and pinocytosis, which involves the uptake of fluid and solutes. Phagocytosis is an essential arm of the immune response whose main function is to clear and destroy invading pathogens (Allen 1996). This chore is conducted primarily by highly specialized cells, such as macrophages, monocytes and neutrophils, with the goal of clearing pathogens and/or debris (Stuart 2008). Interestingly, macrophages have a surface receptor mechanism which prevents them from phagocytosing one's own "self" cells. During initial macrophage engulfment, macrophages recognize both foreign and "self" targets because both display antibodies or plasma complement proteins on their surface. However, before macrophage engulfment, "self" cells

are checked for the presence of the surface protein CD47. While it has been shown that macrophages are efficient at discriminating between foreign cells and particles in the micrometer size range (Tsai 2008), little is known about how this "self" signal, CD47, behaves in targets that are less than 500 nanometers in size. In fact, particles that are in the nanometer length scales may undergo a process other than traditional phagocytosis (Wright 1984, Koval 1998; Rejman 2004). Therefore, new research is needed in order to enhance our understanding of how macrophage targets use the CD47 "self" signal in the nanometer range, which is precisely the focus of this dissertation. In this thesis work, we employ a reductionist approach by designing short peptides that can easily attach to nanobeads. This allowed us to quantify binding to and signaling of these peptides as well as of soluble-CD47 to its receptor, SIRPα. Inhibition of phagocytosis mediated either by peptide-coated or by CD47-coated beads was also quantified, as well as the beads' *in vivo* clearance kinetics in NSG mice.

### 1.3 – Phagocytosis after opsonization

The extent of macrophage signaling induced by the interaction between CD47 ligand to its receptor SIRPα is affected by the expression levels of both proteins. Macrophages sense foreign and self through SIRPα recognition of self protein, CD47 on target cells stimulate tyrosine activation of the immune-receptor tyrosine-based inhibitory motif (ITIM) which leads to recruitment of SHP-1 and

subsequent deactivation of cytoskeletal proteins (Tsai 2008). The process of phagocytosis is often activated when opsonins such as antibodies attach and are recognized by $F_c$ receptors ($F_cR$). Foreign cells and viruses as well as autologous cells are typically Ig-opsonized by antibodies (McCullough 1988; Turrini 1993; Wilflingseder 2007). Also, since particles are rapidly cleared whenever an antibody is added to a nanoparticle, the tradeoff between the amount of Opsonin and CD47 protein added onto particle surfaces needs to be studied. For our purposes, as NSG mice lack IgG and since IgG is one of the three most commonly adsorbed serum proteins, we added the IgG opsonin to the nanobeads before injection in order to render the system more analogous to normal animals and humans.

Similarly, in order to study the effect of the ligand-receptor interaction in phagocytosis after opsonization, we designed an experimental system in which sheep and human red blood cells (RBC) were IgG-opsonized and fed to macrophages. We found that the opsonization levels linearly correlated with anti-serum dilution (**Fig 1.1**), while phagocytosis of sheep RBC by human-derived THP-1 macrophages was non-linear, exhibiting a response that could be saturated.

This is consistent with one of our previous findings (Tsai 2010) wherein opsinized particles were fed to human or mouse macrophages that lacked membrane proteins such as Rh proteins. The particles were avidin-coated and

IgG-opsonized with anti-streptavidin in order to allow for FcγR-mediated phagocytosis. Human macrophages phagocytosed the uncoated, “CD47-null” beads significantly more than beads displaying hCD47. The two ligands, CD47 and IgG-opsonin, do not compete and do not interfere with SIRPα binding (Tsai 2008). Thus, the dependence on the level of IgG-opsonization fit that of a saturating binding process, which was indicative of the specificity of Fcγ-R mediated phagocytosis, as seen with RBC.

The “decision” of a macrophage to phagocytose a target is in part made by assessing the extent of target opsonization. Ig concentrations are typically very high in bodily fluids, which seems to lead to absorption or at least weak binding in some level to all cells (Turrini 1993)-- especially aged blood cells (Fossati-Jimack 2002). Our binding, signaling, and phagocytosis results motivated additional characterization of CD47 expression levels on all cells involved, especially in light of changes in CD47 expression levels that are seen on hematopoietic stem cells (HSC) (Jaiswal 2009).

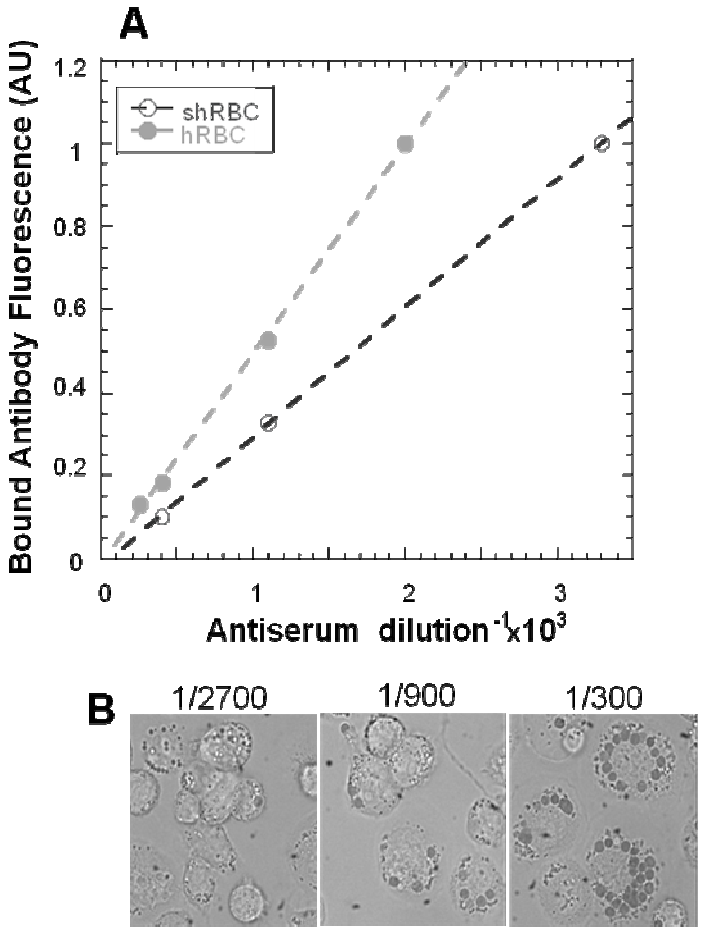


**Fig.1.1.- Phagocytosis of Ig-opsonized sheep RBC by human-THP-1 macrophages.**

**(A)** Fresh sheep and human RBC were incubated with anti-serum at different dilution ratios and detected by FITC-anti-RBC, exhibiting a linear opsonization based on flow cytometry. **(B)** Phagocytosis of shRBC by human-derived THP-1 macrophages at different opsonization level observed by DIC microscopy showed a saturable type of response.

The goal of this dissertation was to design polypeptides that could avoid species-specific clearance to enhance xenotrasplantation. We quantified CD47-SIRPα binding by investigating the inhibitory mechanisms of phagocytosis and

their implications in body clearance. Based on recent research and collaborative work with former graduate students, we followed a bottom-up approach to study this “self” recognition protein. CD47 was used to study the phagocytic mechanism in macrophages. We were able to show a species-specific recognition of “self” by using RBC from sheep and humans as non-“self” and “self” targets *in vitro*. We also developed a mathematical model to understand the trans and cis interactions of the “self”-receptor SIRPα in macrophages that expressed CD47, and how the cis interaction may impede the ability to effectively differentiate between “self” and non-“self” due to inherent inhibitory signals.

As part of the innate immune response neutrophils are also involved in phagocytosis of non-“self” targets. Neutrophils, as with all phagocytizing immune cells, are strongly driven to phagocytose by the presence of opsonins such as antibodies, highlighting the cooperative nature of the innate and adaptive immune responses. Therefore, we extended our studies of phagocytosis into migration effects of hCD47 and “self” peptide on neutrophils.

We also explored the species-specific interaction of SIRPα-CD47 with NSG macrophages and RBCs in order to determine the effects of affinity and phagocytosis in the clearance process of foreign nanoparticles by the immune system. Finally, we explored the potential for enhanced imaging of tumors with near-infrared nanobeads conjugated with hCD47 or “self” peptide. If tumor perfusion of the particles and the subsequent enhanced permeability and

retention (EPR) effect of immune system evasion were increased, there would be potential for biomedical applications. Specifically, we studied whether recombinant hCD47 protein or the small synthetic “self” peptide could enhance the effects of an anti-cancer drug and whether it could improve the delivery of nanoparticles to tumor sites when they contained bioactive antibodies against a therapeutic target.

### 1.4 – Reference


1. Allen, L. A. and A. Aderem (1996). "Molecular definition of distinct cytoskeletal structures involved in complement- and Fc receptor-mediated phagocytosis in macrophages." J Exp Med 184(2): 627-37.
2. Barclay, A. N. (2009). “Signal regulatory protein alpha (SIRPalpha)/CD47 interaction and function.” Curr Opin Immunol. 21(1):47-52.
3. Doucey, M. A., et al. (2004). "Cis association of Ly49A with MHC class I restricts natural killer cell inhibition." Nat Immunol 5(3): 328-36.
4. Fossati-Jimack, L., S. Azeredo da Silveira, T. Moll, T. Kina, F. A. Kuypers, P. A. Oldenborg, L. Reininger and S. Izui (2002). "Selective increase of autoimmune epitope expression on aged erythrocytes in mice: implications in anti-erythrocyte autoimmune responses." J Autoimmun 18(1): 17-25.
5. Gardai, S. J., et al. (2005). "Cell-Surface Calreticulin Initiates Clearance of Viable or Apoptotic Cells through trans-Activation of LRP on the Phagocyte." 123(2): 321.
6. Gresham H.D., Goodwin J.L., Allen P.M., Anderson D.C., Brown E.J. (1989). “A novel member of the integrin receptor family mediates Arg-Gly-Asp-stimulated neutrophil phagocytosis.” J Cell Biol. 108(5):1935-43.
7. Hatherley, D., et al. (2008). "Paired receptor specificity explained by structures of signal regulatory proteins alone and complexed with CD47." Mol Cell 31(2): 266-77.
8. Hatherley, D., et al. (2007). "The structure of the macrophage signal regulatory protein alpha (SIRPalpha) inhibitory receptor reveals a binding face reminiscent of that used by T cell receptors." J Biol Chem 282(19): 14567-75.
9. Jaiswal, S., et al. (2009)." CD47 Is Upregulated on Circulating Hematopoietic Stem Cells and Leukemia Cells to Avoid Phagocytosis ". Cell 138(2): 271-85
10. Jiang, P., et al. (1999). "Integrin-associated protein is a ligand for the P84 neural adhesion molecule." J Biol Chem 274(2): 559-62.

11. Kim D., Wang J, Willingham SB, Martin R, Wernig G, Weissman IL. (2012). “Anti-CD47 antibodies promote phagocytosis and inhibit the growth of human myeloma cells. Leukemia”. May 30. doi: 10.1038/leu.2012.141.
12. Krieser, R. J. and K. White (2002). "Engulfment mechanism of apoptotic cells." Curr Opin Cell Biol 14(6): 734-8.
13. Kong, X. N., et al (2007). "LPS-induced down-regulation of signal regulatory protein {alpha} contributes to innate immune activation in macrophages." J Exp Med 204(11): 2719-31.
14. Koval, M., K. Preiter, C. Adles, P. D. Stahl and T. H. Steinberg (1998). "Size of IgG-opsonized particles determines macrophage response during internalization." Exp Cell Res 242(1): 265-73.
15. Lanier, L. L. (2005). "NK cell recognition." Annu Rev Immunol 23: 225-74.
16. Legrand N, Huntington ND, Nagasawa M, Bakker AQ, Schotte R, Strick-Marchand H, J de Geus S, Pow, SM, Bohne Ma, Voordouw A, Wejer K, Di Santos JP, Spits H. (2011). “Functional CD47/signal regulatory protein alpha (SIRP(alpha)) interaction is required for optimal human T- and natural killer- (NK) cell homeostasis in vivo.” Proc Natl Acad Sci USA. 108(32):13224-9.
17. Majeti, R., Chao, M.P., Alizadeh, A.A., Pang, W.W., Jaiswal,S., Gibbs, K.D., Van Rooijen, N., Weissman, I.L. (2009). “CD47 is an adverse prognostic factor and therapeutic antibody target on human acute myeloid leukemia stem cells. Cell. 138(2):286-99.
18. McCullough, K. C., D. Parkinson and J. R. Crowther (1988). "Opsonization-enhanced phagocytosis of foot-and-mouth disease virus." Immunology 65(2): 187-91.
19. Oldenborg, P. A., et al. (2000). "Role of CD47 as a marker of self on red blood cells." Science. 288(5473): 2051-4.
20. Oldenborg, P. A., H. D. Gresham and F. P. Lindberg (2001). "CD47-signal regulatory protein alpha (SIRPalpha) regulates Fcgamma and complement receptor-mediated phagocytosis." J Exp Med 193(7): 855-62.
21. Oldenborg, P. A. (2004). “Role of CD47 in erythroid cells and in autoimmunity.” Leuk Lymphoma. 45(7):1319-27.
22. Olsson, M., A. Nilsson and P. A. Oldenborg (2007). "Dose-dependent inhibitory effect of CD47 in macrophage uptake of IgG-opsonized murine erythrocytes." Biochem Biophys Res Commun 352(1): 193-7.
23. Rejman, J., V. Oberle, I. S. Zuhorn and D. Hoekstra (2004). "Size-dependent internalization of particles via the pathways of clathrin- and caveolae-mediated endocytosis." Biochem J 377(Pt 1): 159-69.
24. Seiffert, M., et al. (2001). "Signal-regulatory protein alpha (SIRPalpha) but not SIRPbeta is involved in T-cell activation, binds to CD47 with high affinity, and is expressed on immature CD34(+)CD38(-) hematopoietic cells." Blood 97(9): 2741-9.
25. Seiffert, M., et al. (1999). "Human signal-regulatory protein is expressed on normal, but not on subsets of leukemic myeloid cells and mediates cellular adhesion involving its counterreceptor CD47." Blood 94(11): 3633-43.
26. Stuart, L.M., and Ezekowitz, R.A. (2008). “Phagocytosis and comparative innate immunity: learning on the fly.” Nat Rev Immunol 8(2):131-41.

27. Subramanian, S., et al. (2006). “Species- and cell type-specific interactions between CD47 and human SIRPalpha”. Blood. 107(6): 2548-2556.
28. Subramanian, S., et al. (2007). "Phylogenetic divergence of CD47 interactions with human signal regulatory protein alpha reveals locus of species specificity. Implications for the binding site." J Biol Chem 282(3): 1805-18.
29. Strowig, T., et al. (2011). Transgenic expression of human signal regulatory protein alpha in Rag2−/−γc −/− mice improves engraftment of human hematopoietic cells in humanized mice. *Proc Natl Acad Sci USA.* 108(32):13218-23.
30. Takenaka, K., et al. (2007). Polymorphism in SIRPα modulates engraftment of human hematopoietic stem cells. *Nature Immunology.* 8(12): 1313-23.
31. Tsai, R. K. and D. E. Discher (2008). "Inhibition of "self" engulfment through deactivation of myosin-II at the phagocytic synapse between human cells." J Cell Biol 180(5): 989-1003.
32. Tsai, R.K., P.L. Rodriguez, and D.E. Discher. 2010. Self inhibition of phagocytosis: The affinity of 'marker of self' CD47 for SIRPalpha dictates potency of inhibition but only at low expression levels Blood Cells. Mol.Dis. doi: 10.1016/j.bcmd.2010.02.016.
33. Turrini, F., et al. (1993). Low, Characterization of the autologous antibodies that opsonize erythrocytes with clustered integral membrane proteins. *Blood.* 81: 3146 – 3152.
34. Vernon-Wilson, et al. (2000). "CD47 is a ligand for rat macrophage membrane signal regulatory protein SIRP (OX41) and human SIRPalpha 1." Eur J Immunol. 30(8): 2130-7.
35. Wilflingseder, D., et al. (2007). IgG opsonization of HIV impedes provirus formation in and infection of dendritic cells and subsequent long-term transfer to T cells. J Immunol. 178(12):7840-8.
36. Wright, S. D. and S. C. Silverstein (1984). "Phagocytosing macrophages exclude proteins from the zones of contact with opsonized targets." Nature 309(5966): 359-61.

# CHAPTER 2 - ‘Active Stealth’ signaling with a synthetic “self” peptide - inhibiting phagocytic clearance of virus-size nanoparticles

Pia L. Rodriguez, Diego Pantano, Richard K. Tsai, Kevin Hsu, Pierre Bhoorasingh, David A. Christian, and Dennis E. Discher

Dr. Pantano provided the molecular dynamics simulations. P. Bhoorasingh helped with the Western blotting. Dr. Christian helped with general discussion of the subject. Dr. Tsai and K. Hsu provided construction, expression, and assays of ten hSIRPα variants and Dr. Tsai also provided the initial studies of effects of particle size and inhibitors in phagocytosis.

**Abstract**

Foreign particles and cells are rapidly cleared from the body by professional phagocytes that incessantly encounter and recognize “self” cells. The membrane protein CD47 appears to be a ‘Marker of Self’ that impedes phagocytosis of self cells, with signaling through a species-specific, highly polymorphic receptor, SIRPα. Here, minimal “self” peptides were computationally designed from human-CD47, synthesized with anchoring groups, and attached to virus-size nanoparticles for injection into NOD.SCID (NSG) mice that are known to exhibit unique compatibility with human cells. The hCD47-peptides delay splenic clearance of particles by macrophages with an exponential advantage in persistent circulation. The affinity of hCD47 for NSG-SIRPα proves weak but within the broad range (0.1~5 μM) measured for ten constructed variants of human-SIRPα; several versions of hCD47-peptide are likewise shown to bind and potently inhibit nanoparticle uptake by an unexpected cytoskeletal mechanism. The reductionist approach reveals the importance and utility as well as some limits of a human ‘Marker of Self’.

## 2.1 – Introduction

Macrophages engulf invading microbes and dying cells in a highly coordinated and active process that evolved over eons and occurs also now in foreign body responses to injected particles and implants. This clearance

function of phagocytes is delayed but not eliminated by dense ‘Stealth’ brushes such as with polyethylene glycol (PEG) on circulating nanoparticles and liposomes used in therapeutics and imaging (Klibanov 1991, Photos 2003, Bartlett 2007). Coating with PEG of (<500 nm) indeed helps to delay rapid clearance and to thereby provide more time for circulation through disease sites such as tumors, but neither PEG nor targeting groups can stop the clearance of a majority of particles from the circulation by macrophages in the spleen and liver (e.g. Klibanov 1991, Photos 2003, Turk 2004, Bartlett 2007, Rossin 2008). Delivery to disease sites can also be limited by phagocytic uptake by tumor-associated macrophages for example (Turk 2004), and the acquired immunity to foreign polymers has become an additional concern (Armstrong 2007). In contrast, “self” cells and tissues are in constant contact *with* and well-tolerated by macrophages, which has suggested critical mechanisms of self recognition. Here we describe a reductionist approach to a synthetic but humanized “Active Stealth” peptide that specifically binds and signals “self” to phagocytes in blocking clearance of particles as small as viruses.

CD47 glycoprotein is a putative ‘Marker of Self’ (Oldenborg 2000) normally expressed on all cell membranes in humans, mice and other higher organisms (Bentley 2010), and it often associates in *cis* with integrins (Brown 2001) and in other *species-specific*, immunogenic macrocomplexes on cells (Bruce 2003, Mouro-Chanteloup 2003, Subramanian 2006) Mouse knockouts of CD47

(mCD47) are surprisingly viable, but when red blood cells from these mice (mRBCs) are injected into the circulation of control mice, the deficient cells are cleared within hours by macrophages of the spleen compared to normal mRBC that circulate for weeks (Oldenborg 2000). CD47's extracellular domain interacts with SIRPα (Signal Regulatory Protein-α) on phagocytes (Brown 2001), and the binding is species-specific (Subramanian 2006) in part because SIRPα is highly polymorphic within a species (Takenaka 2007). Indeed, NOD.SCID strains of mice happen to express one variant of mouse-SIRPα that cross-reacts with human-CD47, which explains why *human* hematopoietic cells engraft and circulate in NOD.SCID better than any other mouse strain (Takenaka 2007, Strowig 2011). *In vitro*, the CD47-SIRPα interaction inhibits mouse macrophage uptake of antibody-coated mRBCs (Oldenborg 2000) as well as human macrophage uptake of both human-RBC and human-CD47 (hCD47)-coated microparticles (Tsai 2008). SIRPα signaling ultimately inhibits contractility-driven uptake of micron-size cells and particles (Tsai 2008), but while contractile forces exerted by the cytoskeleton are sensible for uptake of such large objects they are widely considered unimportant to internalization of *nano*particles and viruses.

We address whether human-CD47 and a synthetic "self" peptide on such small particles can minimize phagocytic uptake and thereby enhance delivery *in vivo* here using NOD.SCID/Il2rg$^{-/-}$ mice (NSG). Our reductionist approach eliminates confounding, biological factors on cell membranes (e.g. integrins), and

the results with a minimal “self” peptide constitute a first example of a synthetic, human ligand that binds and signals to phagocyte receptors to passivate macrophages.

## 2.2 – Results

### 2.2.1 – Human CD47 and a “self”-peptide prolong circulation of nanoparticles *in vivo*

To check that CD47 is effective in the NSG mouse strain and to also establish a method for comparing circulation times, we first sought to show that blocking of mCD47 accelerates clearance of mouse-RBCs in NSG mice. Competitive circulation studies were designed to maximize accuracy in quantitation for each mouse (**Fig. 2.1A**), with cells (or nanobeads) split into two samples with one sample labeled by red fluorophore and the other sample labeled by far-red fluorophore plus anti-mCD47. The samples were then mixed 1:1 for injection into the same mouse. Bleeds at subsequent time points (including $t$ = 0) are analyzed by flow cytometry for both colors (**Fig. 2.S1A**), providing a ratio result that minimizes variations mouse-to-mouse. Since NSG mice lack serum IgG (~100 μM in normal mice), cells were also heavily opsonized by anti-mRBC to controllably accelerate clearance *via* phagocytosis (Cox 2001). IgG is also found in abundance on normal RBC *in vivo* (Turrini 1993) as well as on nanoparticles (Lundqvist 2008) and on viruses (Wilflingseder

2010), and so clearance signals are ever-present. Consistent with a 'Marker of Self' function of mCD47, the persistence ratio for the mixed sample [mRBC / (mRBC with blocked mCD47)] increased exponentially ($R^2$ = 0.93) with a doubling time of $T$ = 33 min (**Fig. 2.1B**); single color results give T = 30 min (**Fig. 2.S1B**), such a doubling time advantage sustained over one full day would yield *~10-trillion more RBC with CD47* (= $2^{24h/33min}$) compared to every circulating *RBC without CD47*. This exceeds the daily production of RBCs in humans by about 100-fold and begins to suggest the potency of CD47 and/or co-factors on RBC.

RBC membranes are complicated with hundreds of different interacting proteins, and some involved in clearance are distinct between mouse and man (Mouro-Chanteloup 2003, Glodek 2010). Beads have much better defined surface properties and enable addition of 'Marker of Self' ligands, but it is well-appreciated that rigid beads must be far smaller than highly flexible RBC to avoid first-pass clearance from the microcirculation (Deplaine 2010). Nanoparticles are thus needed but can be a challenge to characterize *in vivo*. The extracellular, Ig-like domain of human-CD47 (hCD47) that binds SIRP$\alpha$ was recombinantly expressed, site-specifically biotinylated, and then bound to Streptavidin-coated, 160 nm polystyrene nanobeads for *in vivo* and *in vitro* studies. Beads were also labeled with red or near-infrared dyes (or left unlabeled) and opsonized equally with anti-Streptavidin before injection into the tail-vein of an NSG mouse. Whole blood analysis by flow cytometry clearly identified these nanobeads in the

circulation based on both distinctive scatter and fluorescence detection of anti-Streptavidin (**Fig. 2.1A, inset**; **Fig. 2.S1C**). The persistence ratio for (Nanobead+hCD47 / Nanobead) is again well-controlled at every time-point and increases exponentially with a relative doubling time $T$ = 30 min (**Fig. 2.1C**), which is about the same as mouse-RBC above ("doubling time" for beads does not refer to an actual ability to replicate, but is instead used as an analogy to demonstrate that beads behave similarly to RBC). Mice injected with just a single color of nanobead gave similar results (**Fig. 2.S1D**). In order to test whether any other opsonins would have similar effects in circulation, we tested a targeting antibody that yielded similar results (**Fig. 2.S1E**). As one of two controls, PEG-biotin modified beads gave a flat persistence curve with $T$ > 200 min (**Fig. 2.1C, Fig. 2.S2B)**. Additionally, longer circulation studies with PEGylated particles (**Fig. 2.S2A**) provided some evidence that adding CD47 to these particles increase the circulation time *in vivo* even when targeting or opsonizing antibodies are not pre-attached onto the beads, which correlates with the phagocytosis assays *in vitro* (**Fig. 2.S2D).** Human-CD47 on virus-size nanoparticles thus acts as an inhibitor of *in vivo* clearance, thereby prolonging circulation.

Minimizing the 117 amino acid, recombinant hCD47 domain to a binding site peptide could provide, we thought, the clearest evidence that binding and signaling of hCD47 to mSIRP$\alpha$ is the molecular mechanism of inhibition *in vivo*. Mouse and human CD47 differ by about 40% in the sequence of SIRP$\alpha$'s N-

terminal domain, and these differences include one or more amino acids in each of three distinct binding sequences in the co-crystal structure of hCD47-hSIRP$\alpha$ (Hatherley, 2008). Multiple mutations in each sequence decrease binding substantially (Hatherley, 2008), but the highest density of interactions with hSIRP$\alpha$ are in one loop in hCD47 between canonical $\beta$-strands 'F' and 'G', where a nine amino acid sequence constitutes 40% of hCD47's contacting residues. Our first guess design was a 21 amino acid "self"-peptide, which was simulated for stability and interactions (see below) and then synthesized with the aims of (*i*) minimizing species specificity (Strowig 2011), (*ii*) eliminating the glycosylation of CD47 that impedes binding (Subramanian 2007), and (*iii*) developing Scrambled, inactive peptides. Biotinylation on an amino-terminal PEG linker provided a means of attachment to Streptavidin-beads for *in vivo* studies. Surprisingly, the "self"-peptide increased persistence of beads in the circulation compared even to recombinant hCD47: the faster growing exponential has a 40% smaller doubling time of $T$ = 18 min compared to control nanobeads (**Fig. 2.1C**). In comparison, Scrambled-peptide has little impact on circulation, which suggests specificity to interactions as analyzed in detail below for these and additional synthetic designs. An apparent difference between hCD47 and 'Self' peptide is not significant ($p = 0.18$).

### 2.2.2 – hCD47 binds NSG-SIRPα weakly but within a broad range of affinities for human polymorphisms

Flow cytometry enables detailed analysis of the surface of nanobeads before injection (**Fig. 2.S2C)** and in blood drawn at various time points post-injection. While anti-streptavidin IgG remains stably bound to beads, a fraction of the biotinylated-hCD47 is often lost from the bead surface (30% in **Fig. 2.2A**, inset bargraph; **Fig. 2.S4A**), even though the biotin part of the protein was strongly attached to avidin present on the bead surface. This could be due to the presence of a biotinylase enzyme in circulation that has been shown to compromise avidin:biotin binding (Kuroishi 2008; Jeong Lee 2000). Thus, CD47 could be binding free biotin upon detaching from the beads. Covalent attachment of biotinylated-hCD47 might ameliorate this problem. Nonetheless, the %-Clearance of nanobeads at 35 min *versus* the measured density of hCD47 at 35 min fit well to a simple inhibition model that also fits our "self"-peptide results (**Fig. 2.2 A**) with:

$$K_{i,\text{in-vivo}} = 110 \text{ molecules } \textit{per } 160 \text{ nm Nanobead}$$

This appears independent of circulating bead number over at least a ~ten-fold range (**Fig. 2.S4 B**).This corresponds to a density of hCD47 that is about ten-fold higher than the lowest densities reported for human RBC (i.e. ~25 hCD47 molecules/$\mu m^2$ (Mouro-Chanteloup 2003)). Indeed, saturable binding of soluble hCD47 to fresh, NSG-SIRPα$^+$ phagocytes yields a weak, effective affinity

of just $K_d$ = 4 μM (**Fig. 2.2B**). Lymphocytes do not express SIRPα (Seiffert 1999) and show no binding to CD47.

To compare the affinity for NSG-mouse to human-SIRPα (hSIRPα), ten reported human polymorphic variants of hSIRPα (Takenaka 2007) were constructed here as C-terminal GFP fusions and expressed on CHO cell membranes as done previously with CD47-GFP (Subramanian2007). Many of the amino acid changes in SIRPα occur near but not in the hCD47 binding site (Hatherley 2008), making predictions difficult. Saturation binding of soluble hCD47 to each variant yields a surprisingly broad, 60-fold range of affinities with $K_d$ = 0.08 – 5 μM (**Fig. 2.2C**). Soluble protein showed the same trend (**Fig. 2.S5**). The co-crystal structure of hCD47-hSIRPα shows all of the amino acid differences in these variants occur outside of the binding interface (Hatherley 2008), and so the effects here seem likely to reflect allosteric and conformational mechanisms, including SIRPα homodimers (Lee 2010). When plotted *versus* human allele frequency of SIRPα, variants of intermediate affinity (e.g. v1, v2) are most common and are similar to results for soluble- SIRPα(v1) binding to CHO-displayed hCD47-GFP (Subramanian 2007). Importantly, the 4 μM affinity for NSG-SIRPα phagocytes proves weak but within the range of ten human variants, consistent with the cited success of human xenografts in NOD.SCID mice.

In addition, to show that the CD47-SIRPα interaction is indeed involved in the delay of clearance of the beads *in vivo*, we blocked mouse-SIRPα in NSG mice by pre-injecting anti(mSIRPα) antibodies that block binding of mSIRPα to CD47 *in vitro*. After nanoparticles were injected to these pre-injected mice, the circulating particle ratio at 35 min was measured as in **Fig. 2.2A.** CD47 particles provided no advantage in circulation (**Fig. 2.2B**, inset) when blocking SIRPα antibody is bounded to splenic macrophages.

### 2.2.3 – Minimal "self": conformational constraints limit activity

Given the important, allosteric effects of SIRPα variants on affinity for hCD47, the impact of "self"-peptide conformation on binding and signaling is conceivably just as important. The recent co-crystal structure of the hCD47 Ig-like domain in association with the hSIRPα Ig-like domain suggested important electrostatic interactions of the "self"-peptide's loop, but stability of this hairpin was unknown and seemed important to binding. Three versions of the peptide were therefore designed and simulated by all-atom Molecular Dynamics (**Fig. 2.2D**; **Fig. 2.S6**): (*i*) the 21-aa "self"-peptide that was shown functional above, and also (*ii*) a 12-aa "self"-SS-peptide with a T107C substitution opposite in the hairpin to C96 intended to disulfide-stabilize the β-hairpin, together with (*iii*) a 10-aa "self"-hairpin centered on the loop. Equilibration of the three peptide designs and also hCD47 respectively show that, relative to the "self"-SS-peptide, the "self"-peptide maintains a smaller β-hairpin (**Fig. 2.2D**, upper plot) that achieves

more salt bridges in docking simulations with hSIRPα (**Fig. 2.2D**, lower plots). The “self”-SS-peptide undergoes a large torsional distortion that alters the surface charge distribution, whereas the short “self”-hairpin completely loses its initial loop but is not over-constrained in a misfolded state.

Synthesis of the three designs and Scrambled-peptides (with or without biotin attached via a PEG linker or an aminohexanoic acid linker ‘C6’), enabled functional testing of binding to hSIRPα as well as inhibition of nanobead phagocytosis. When immobilized on beads, the “self”-peptide’s affinity for soluble hSIRPα ($K_d$ ≈ 0.1-0.2 μM; **Fig. 2.2E-*i,ii***) proves high on the affinity scale for polymorphisms (**Fig. 2.2C**) and consistent with functionality of peptide *in vivo* (**Fig. 2.1**) and *in vitro* (see below). In contrast, the disulfide-stapled “self”-SS-peptide showed no significant affinity for hSIRPα and no statistically significant inhibition of phagocytosis, thus revealing the importance of flexibility in maintaining the β-hairpin’s surface charge distribution. While the PEG linker between biotin and peptide improves solubility, the more hydrophobic C6 linker has little impact on hSIRPα binding, whereas scrambling the peptide eliminates binding as well as any statistically significant inhibition of phagocytosis (**Fig. 2.2E-*ii***).

The 10-aa “self”-hairpin was also synthesized without attachment of biotin for use as a soluble inhibitor of hSIRPα binding to hCD47-beads. While the scrambled peptide lacked function once again, this short “self”-hairpin inhibited

hCD47-hSIRPα interactions, and although the extent of inhibition was less than with the longer "self"-peptide, a similar $K_i \approx 0.1 - 0.2$ μM (**Fig. 2.2E-*iii***) proves consistent with the affinities measured above. The results all substantiate the general approach to specific binding and signaling (see below) from a minimal 'Marker of Self' peptide.

### 2.2.4 – *In vivo* persistence of "self" correlates with inhibition of phagocytosis *in vitro*.

Whether phagocytosis of nanoparticles – including viruses – involves mechanisms similar to larger particles remains a significant question in the field of phagocytosis (Swanson 2004), and CD47 on nanobeads here could help clarify the minimal limits to phagocytic uptake. The spleen generally clears nanoparticles (**Fig. 2.S3A-D**), and fluorescence imaging of tissue sections shows the strong tendency of nanobeads to colocalize with macrophages (**Fig. 2.3A, inset-*i***), consistent with the well-established role of the mononuclear phagocyte system. Human-derived THP1 macrophages express one of the common variants of hSIRPα (*v1*), which is why hCD47 has been reported to inhibit phagocytosis of microparticles by these cells *in vitro* (Tsai 2008). Nanoparticles are not sufficiently large or dense to settle to the bottom of a culture dish, which limits bead contact with such cells, but since binding is a surface-based process, opsonized nanobeads that are added at the same total surface area as micro-beads (**Fig. 2.S7A**) are seen to be taken up just as efficiently in culture by THP1

macrophages (**Fig. 2.3A, *iia***). Myosin-II accumulates at the phagocytic synapse formed with opsonized beads except when hCD47 is attached to beads (**Fig. 2.3A, *iia*-inset, *ii*b**). The result is similar to results with micro-particles and microbes (*i.e.* bacteria) (**Fig. 2.S7B**).

The mechanism for inhibiting phagocytosis appears independent of length-scale or curvature. Indeed, the amount of hCD47 required to impede uptake *in vitro* by THP1 cells further proves independent of particle size from at least 100 nm to 10 μm (**Fig. 2.3A, *ii*c**; **Fig. 2.S7C**). Similar inhibition of nanobead uptake was found with the biotinylated "self"-peptide, using two types of linkers, whereas both Scrambled and "self"-SS peptides showed no significant inhibition of phagocytosis (**Fig. 2.2E, *i,ii*-insets**). Inhibition with hCD47 is remarkably potent with

$K_{i,in\text{-}vitro} \approx 1.0 \pm 0.3$ molecule / $[4\pi(\textit{Equiv. Radius})^2]$ for *Equiv. Radius* = 60nm.

This very low density of hCD47 is about the same as the lowest densities reported for human RBC (Mouro-Chanteloup 2003), and despite the fact that maximum inhibition for any particle studied here is incomplete (<80%), the above $K_{i,in\text{-}vitro}$ indicates that a nanoparticle of 60 nm *Radius* requires *only 1* CD47 molecule to inhibit uptake. Nanobeads used throughout the studies here were significantly larger to ensure that the vast majority of particles start with at least a few molecules of hCD47, but the results highlight the potency of this 'Marker of Self'.

Our previous knockdown and overexpression of myosin-II in THP1 cells demonstrated that – unless hCD47 is on the target particles – IgG driven uptake is linearly proportional to myosin-II activity (Tsai 2008). This is consistent with a specialized and signal-responsive role for the cytoskeleton in phagocytosis (Cox 2001, Swanson 2004). With nanobeads here, hCD47 blocks uptake and so does acute inhibition of myosin-II with blebbistatin (**Fig. 2.3A, inset-*iic***). Myosin-II's enrichment near the nanobead extends deeply into the cytoplasm (~5 μm) relative to bead size, suggestive of a diffuse signal that directs cytoskeletal assembly. When CD47 binds SIRPα, Tyrosines in SIRPα's cytoplasmic tail are hyperphosphorylated and activate the hematopoietic-restricted phosphatase SHP1 (Matozaki 2009) which dephosphorylates multiple proteins, including myosin-II (Tsai 2008). Inhibition of SHP1 here produces the expected increase in phagocytosis of hCD47-nanobeads as well as hCD47-microbeads (**Fig. 2.3A, inset-*iic***; **Fig. 2.S7D**). Consistent with inhibition of this signal in THP1 macrophages, binding of hCD47 and "self"-peptide leads to a significant increase in phospho-SIRPα whereas Scrambled-peptide shows no significant effect relative to controls (**Fig. 2.3B**). Consistent with a common mechanism in vitro and in vivo, uptake of the various nanoparticles by THP1 cells correlates inversely with persistence in NSG mice (**Fig. 2.3C**).

*In vitro* uptake by the human-derived THP1 cells (at 45 min) correlates inversely with the *in vivo* persistence ratio in the NSG mice at a similar time point

($y$ = 1/$x$, **Fig. 2.3C**). hCD47 inhibits the number of opsonized particles taken up per cell *in vitro* by ~60% and "self"-peptide inhibits by ~75%, whereas PEG and scrambled peptide lead to only a slight reduction in phagocytosis (average of ~25%). The results thus establish a major inhibitory effect and suggest that potency might be engineered further with CD47-inspired peptides.

## 2.3 – Discussion

Phagocytes are found in all tissues of the body in addition to the spleen and liver, and they have key roles in recognizing and clearing foreign cells and particles as well as contributing to inflammatory responses with cytokine release and oxidative burst. Recently we showed that implantation of polyurethane slabs coated with hCD47 will inhibit oxidation of the polymer (Stachelek 2011), indicating a general capacity of this 'Marker of Self' to passivate *via* active signaling to Macrophages – a form of 'Active Stealth' (**Fig. 2.4**). A potency here as low as 1 molecule per 60 nm particle is far smaller than the PEG densities needed to inhibit phagocytes, and because CD47 is naturally expressed on all cells, it seems far less likely to be as antigenic as PEG (Armstrong 2007).

The nanobead results suggest CD47 on viruses might also be useful or important, especially since viruses are likewise cleared from circulation by spleen and liver (Pan 2002). Initial results for HIV-related Lentivirus that display CD47-GFP indeed show decreased infection of macrophages (*not shown*). Moreover,

a putative homolog of CD47 encoded by at least one type of poxvirus has been reported to maximize virulence (Cameron 2005). Structure analyses had questioned interactions of the viral protein with SIRPα (Hatherley 2008), but the minimal “self” peptides here lack amino acids that contribute in full length hCD47 to SIRPα binding, and yet binding is strong. Likewise, the ten human-SIRPα variants here involve mutations far from the hCD47 binding site, and yet affinities vary ~60-fold. Allosteric mechanisms are clearly in need of further study.

Whether CD47 or peptides are displayed on particles, viruses, or surfaces, “self” signaling across length scales offers further opportunities in application as well as understanding. In terms of molecular mechanisms and likely limits, the synthetic “self”-peptide here works similar to or better than recombinant hCD47, probably because the latter possesses five carbohydrate chains that inhibit binding (Subramanian2007). On the other hand, conformation requirements of the peptide will likely limit further reductionism (**Fig. 2.2D**). Based on the polymorphism studies, an intermediate affinity for SIRP$\alpha$ is best and is understandable (**Fig. 2.2C**) as a trade-off between adhesion that is not too strong (‘must let go’) and signaling that is not too weak (‘don’t eat me’). Polymorphisms in CD47 have been recently listed in databases as “damaging” [www.1000genomes.org], but validation of these as well as the variants reported for SIRPα are needed. Additionally, since CD47 is reportedly lacking in the genome of amphibia and other lower species (Bentley 2010), and since the

CD47-knockout mouse is viable if immune compromised (Oldenborg 2000), additional and more ancient ‘Marker of Self’ proteins seem likely to contribute to homeostasis in shifting the innate immune system further away from clearance by macrophages in the liver, spleen, (tumors), and other tissues. Further elaboration and application of “self” peptides might therefore help deliver imaging agents and therapeutics more effectively to disease sites rather than to phagocytes.

## 2.4 – Materials and Methods

### 2.4.1 – Chemicals

Streptavidin polystyrene beads were of different radius: 160nm, 1.1μm, 3.5μm, (Spherotech) and 100nm (Ademtech). Dulbecco’s phosphate-buffered saline (DPBS) without Ca2+ or Mg2+ (Invitrogen) was supplemented with 1% BSA and 0.05% Tween 20 (Sigma-Aldrich). TBS (Tris-buffered saline) and TTBS (TBS with Tween 20) were used in Western blotting. Hoechst 33342 (Invitrogen, Carlsbad, CA) was used for DNA stains. RBC lysis Buffer (Roche Diagnostics Corporation) was used in Neutrophil isolation from NSG mice. The near-infrared lipophilic dye, DiR, and the deep red dye, DiD, were purchased from Invitrogen, Inc. and PKH26 Red Fluorescent Cell Linker Kit for General Cell Membrane Labeling from Sigma Aldrich. Chloroform, methanol, and hydrochloric acid were purchased from Fisher Scientific. N-Biotinyl-NH-(PEG)4-COOH was purchased

from EMD Chemicals, PEG Biotin, MW 550 was purchased from Nanocs Inc., and mPEG-Biotin, MW 5,000 from Laysan Bio Inc. Blebbistatin (±) was purchased from EMD Biosciences, and NSC-87877 was from Sigma.

### 2.4.2 – Antibodies

The fluorescein-labeled antibody B6H12-FITC (BD Biosciences) and mIAP301-FITC (BD Biosciences) were used against human CD47 and mouse CD47 respectively. Quantification of SIRPα was performed using anti-SIRPα (SE7C2) (Santa Cruz Biotech). Human SIRPα$^{ex}$ (this laboratory) used for experiments comparing binding affinities between species. Antibodies against NMM IIA, actin was obtained from Sigma-Aldrich. Opsonizing antibodies against mouse RBCs included rabbit anti-mouse RBC (Sigma-Aldrich); Opsonizing antibodies streptavidin coated polystyrene beads (Spherotech) included rabbit anti-streptavidin (Sigma-Aldrich), rabbit anti-streptavidin conjugated with FITC (Rockland Immunochemicals) and Biotin anti-human CD47 Antibody (BioLegend) were used as IgG opsonin. Secondary antibodies used for detecting opsonin levels and uningested beads included goat anti-rabbit FITC or goat anti-rabbit F(ab')$_2$ R-PE (Sigma-Aldrich). Secondary antibodies used for detecting soluble SIRPαex or biotinylated CD47 binding included anti-GST Alexa 488 (Invitrogen) and Cy5 conjugated Affinity Purified Anti-Biotin goat (Rockland Immunochemicals) respectively. Primary antibody used to measure the level of

PEG molecules and Biotin anti-human CD47 bounded to streptavidin coated polystyrene beads was Biotin-4–fluorescein (Anaspec).

### 2.4.3 – Proteins and Peptides

We followed the protocol described by (Tsai 2008) for the production of recombinant human CD47 and soluble human SIRPα, proteins were storage at -20˚C in PBS. Human was the focus due to a lack of in vivo experiments on human-CD47 and known differences with mouse.

In considering synthesis of a 'Self'-peptide, mouse and human CD47 differ by about 40% in the sequence that binds SIRPα's N-terminal domain, and these differences include one or more amino acids in each of three distinct binding sequences in the co-crystal. 'Self'-Peptides were simulated for stability and interactions and then synthesized by standard solid phase methods in order to assess whether a synthetic, human-based ligand binds and signals to phagocyte receptors to passivate the innate immune cells responsible for clearing foreign objects of many forms. The peptides are:

(1a) 21 aa, >80% purity, Biotin-Acp (N-Terminal) – GNYTCEVTELTREGETIIELK

(1b) 21 aa, >90% purity, Biotin-dPEG4 (N-Terminal) – GNYTCEVTELTREGETIIELK

(2) 12 aa, >80% purity, Biotin-Acp – CEVTELTREGEC (disulfide bridged)

(3) 10 aa, 10 mg, >90% purity, Biotin-dPEG4 (N-Terminal) – EVTELTREGE

(4) 10 aa, 10 mg, >90% purity, Biotin-dPEG4 (N-Terminal) – EGERTLETVE (Scrambled)

### 2.4.4 – SIRPα reverse transcriptase PCR and sequence

The SIRPα variant expressed in THP-1 macrophages were confirmed by RNA extraction (Qiagen) and using a one step reverse transcriptase PCR (RT-PCR) amplification (Invitrogen). Samples of the PCR product were run on 1% agarose gel and gel purified for sequencing. Primers used for both RT-PCR sequencing include the following 5′-GGGTGAGGAGGAGCTGCAGGTGATT-3′ and 5′-GCGCTCGAGCCGTTCATTAGATCC -3′.

### 2.4.5 – Plasmid construction and polymorphism mutations

The plasmid vector containing a cytomegalovirus promoter in pEGFP-N1 (Clontech laboratories, Mountain View, CA) containing the DNA fragment encoding full length human SIRPα using primers 5′-GCAGAGCTGGTTTAGTGAACCG-3′ and 5′-CGTCGCCGTCCAGCTCGACCAG-3′. Full-length human SIRPα variants 1-10 as denoted (Takenaka 2007) were generated by making point mutants based on human SIRPα variant 2; using the QuikChange Site-Directed Mutagenesis kit (Stratagene). For convenience human SIRPα variants 1-10 are denoted as hSIRPα v1-10. hSIRPα variant 2 to 1 was constructed based on multiple mutagenesis by using the following primers:

5′-CTGGAGAGACGGCCACTCTGCGCTGCACTGCGACCTCCC-3′ and
5′- GGGAGGTCGCAGTGCAGCGCAGAGTGGCCGTCTCTCCAG-3′
for mutations S54T, I56T, H58R, V61A;
5′-GAGGAGCTGGACCAGGCCGGGAATTAATCTA-3′ and
5′-TAGATTAATTCCCGGCCTGGTCCAGCTCCTC-3′ for mutations A79G;

5′-CACTTCCCCCGGGTAACAACTGTTTCAGATTTAACAAAGAGAGAAAACA-3′ and

5′-TGTTTTCTCTCTTTGTTAAATCTGAAACAGTTGTTACCCGGGGGAAGTG-3′ for mutations E99D;

5′- ATTCAGCCTGACAAGTCCGTATTAGTTGCAGCTGG-3′ and

5′-CCAGCTGCAACTAATACGGACTTGTCAGGCTGAAT-3′ for mutations S48L;

5′- GTTTCAGATTTAACAAAGAGAAATAACATGGACTTTTCCATCAGG-3′ and

5′-CCTGATGGAAAAGTCCATGTTATTTCTCTTTGTTAAATCTGAAAC-3′

for mutations E104N;

5′-CATGGACTTTTCCATCAGGATCGGTAACATCACCCCAGCAG-3′ and

5′-CTGCTGGGGTGATGTTACCGATCCTGATGGAAAAGTCCATG-3′

for mutations S111R, S113G;

5′-GGAAAGGGAGCCCTGACGTGGAGTTTAAGTCTGGAG-3′ and

5′-CTCCAGACTTAAACTCCACGTCAGGGCTCCCTTTCC-3′ for mutations T135V;

5′-GAAAGGGAGCCCTGACGACGTGGAGTTTAAGTCTGG-3′ and

5′-CCAGACTTAAACTCCACGTCGTCAGGGCTCCCTTTC-3′ for inserting D at 135.

hSIRPα variant 2 to 3 was constructed with the primers

5′- GTCGGCCATTCTGCTCTGCACTGTGACCT-3′ and

5′- AGGTCACAGTGCAGAGCAGAATGGCCGAC-3′ for mutations H58L.

hSIRPα variant 2 to 4 was constructed using primers:

5′-GCGGGTGAGGAGGGGCTGCAGGTGATT-3′ and

5′- AATCACCTGCAGCCCCTCCTCACCCGC-3′ for mutations E37G;

5′-TCTGCACTGCACTGCGACCTCCCTGATCC-3′ and

5′- GGATCAGGGAGGTCGCAGTGCAGTGCAGA-3′ for mutations V61A.

hSIRPα variant 2 to 7 was constructed using the following primers:

5′- CTGTCTGTGCGTGGCAAACCCTCTGCC-3′ and

5′- GGCAGAGGGTTTGCCACGCACAGACAG-3′ for mutations A149G.

hSIRPα variant 2 to 10 was constructed using primers

5′- TGCGCCTGGTCAAGAGTGGCGGGTG-3′ and

5′-CACCCGCCACTCTTGACCAGGCGCA-3′ for mutations G31R.

hSIRPα variant 1 to 5 was constructed using primers

5′- GGTGATTCAGCCTGACAAGTTCGTATTAGTTGCAG-3′ and

5′- CTGCAACTAATACGAACTTGTCAGGCTGAATCACC-3′ for mutations S46F.

hSIRPα variant 1 to 6 was constructed using primers:

5′- AGATTTAACAAAGAGAAATAACATGGACTTTCCCATCAGGATCGGTAA-3′ and

5′- TTACCGATCCTGATGGGAAAGTCCATGTTATTTCTCTTTGTTAAATCT-3′ for mutations S109P.

hSIRPα variant 1 to 9 was constructed using primers

5′- ACTTTTCCATCAGGATCAGTAACATCACCCCAGCA-3′ and

5′-TGCTGGGGTGATGTTACTGATCCTGATGGAAAAGT-3′.

All constructs were confirmed by sequencing.

### 2.4.6 – Cells culture and transfection

COS-1, CHO-K1, A549, THP-1 cells (American Type Culture Collection) were respectively maintained in DMEM, MEMα, F-12, RPMI 1640, and DMEM low glucose media (Invitrogen) supplemented with 10% heat inactivated FBS (Sigma-Aldrich). Cells were detached using 0.25% Trypsin/0.5mM EDTA (Invitrogen) for passaging. Differentiation of THP-1 cells was achieved in 100 ng/mL phorbol myristate acetate (PMA) (Sigma-Aldrich) for 2 days and confirmed by attachment of these cells to tissue-culture plastic. Peripheral blood monocytes from human donors were obtained through the Human Immunology Core (University of Pennsylvania). Human blood was obtained from finger pricks of healthy donors. Blood from other species was obtained from Covance and washed 3x in PBS plus 0.4% BSA.

hSIRPα v1-10 was transfected into CHO-K1 cells with Lipofectamine 2000 (Invitrogen) according to manufacturer's instructions. Clones resistant to 400 μg/ml G418 (Invitrogen) were selected. Expression of hSIRPα was confirmed. Transfected cells were harvested using DPBS supplemented with 2 mM EDTA (Invitrogen) 1-2 days post-transfection for analysis. In addition to detection for GFP signals, anti-SIRPα (Santa Cruz Biotech) was used to confirm surface expression by fluorescent microscopy and flow cytometry.

### 2.4.7 – Preparation and characterizations of Nanobeads with CD47, 'Self' peptide, and Opsonin

Beads enable facile addition of 'Marker of Self' ligands, but rigid beads must be far smaller than highly flexible RBC to avoid first-pass clearance from the microcirculation (Deplaine 2010). Nanoparticles are thus needed but if they are too small, then they can be a challenge to controllably modify and fully characterize after injection.

Streptavidin-coated polystyrene beads of 160 nm radius (SVP-03-10; Spherotech, Lake Forest, IL) were washed and blocked 3x in PBS plus 0.4% BSA. Manufacturer specifications of about 3x104 Biotin–fluorescein sites per nanobead were confirmed by flow cytometry with fluorescence calibration beads and equate to about 1 biotin site per 10 sq.nm (Fig. S2A). This is the maximum density of modification (eg. PEGylation) achievable with these nanobeads, and compares well with useful densities in related contexts. Malmsten et al. reported 95% suppression of protein adsorption (at a specified time point) for PEG surfaces with 1 polymer per 10 sq.nm although protein adsorption was still measurable. In addition, with liposomes the area per lipid is 0.7 sq.nm, and PEGylated liposomes exhibit 'stealth' in circulation with 2-5% PEGylation (eg. Photos2003), which equates to one PEG chain per 14 - 35 sq.nm.

Recombinant biotinylated hCD47 or synthetic biotinylated 'Self'-peptide were attached to the beads and then rabbit anti-Streptavidin conjugated with

FITC was added as an opsonizing IgG-antibody (Rockland Immunochemicals). Beads were incubated at room temperature for 30 min, washed 3x, and re-suspended in PBS plus 0.4% BSA. The density of hCD47or 'Self' on the beads was determined by binding to soluble hSIRPα at 1 μM (see Binding Isotherms below) and, for hCD47, labeling with 15 μl of anti-hCD47-FITC (clone B6H12, BD Biosciences). Binding of hSIRPα was thus used to confirm similar levels of attachment of hCD47or 'Self' on the beads (see Fig. 3A). The opsonin density on the beads was determined with 1 μl goat anti-rabbit F(ab')2 R-PE incubated for 30 min at room temperature. Beads were washed and resuspended in PBS for flow cytometry and further analyses.

Zeta potential measurements (Malvern Zetasizer) on key samples of Fig. 1C showed no significant differences: for (anti-streptavidin nanobeads), (hCD47 + anti-streptavidin nanobeads), ('Self'-peptide + anti-streptavidin nanobeads), (Scrambled peptide + anti-streptavidin nanobeads) all had a measured Zeta potential = -3.5 ± 1 mV. Sizes from light scattering for these nanobeads as well as PEGylated nanobeads conformed to manufacturer's specifications within about 10%. Forward and Side scatter in flow cytometry from pre-injected nanobeads provided additional evidence of uniformity of size even after the modifications.

### 2.4.8 – Binding isotherm for soluble hSIRPα for hCD47 and Polypeptides

The binding isotherm of soluble hSIRPα was performed for Polypeptides and hCD47 attached to the streptavidin polystyrene beads as noted over a range of concentration using flow cytometry. Forward scatter, side scatter and fluorescence (FL1, FL2, FL3, FL4 channels in logarithmic mode) were acquired for at least $10^4$ events using a FACScan or FACSCalibur (BD Immunocytometry Systems). Data points from flow cytometry were plotted and fitted to obtain the $K_d$ values as shown.

### 2.4.9 – Phagocytosis Assay

For phagocytosis assays, macrophages were plated in $4cm^2$ Lab-Tek II Chambered Coverglass (Nalge Nunc International) at $1 \times 10^5/4cm^2$. Streptavidin polystyrene beads were added to macrophages at a number ratio of 20:1 and allowed to incubate at 37˚C for 45 min. Non-phagocytosed beads were washed with PBS. Cells were fixed with 5% formaldehyde (Fischer Scientific) for 5 min, followed by immediate replacement with PBS. For differentiation of non-internalized beads, beads were labeled with a primary antibody, rabbit anti-streptavidin (Sigma) at 1:1,000 in PBS for 20 min at 25℃. A second antibody, anti-rabbit R-PE (Sigma) was added at 1:1,000 in PBS to the cells and incubated for an additional 20 min at 25℃. Cells were then w ashed with PBS/ 0.4% BSA and then quantified by light and fluorescent microscopy. At least 200 cells were scored per well and experiments were repeated at least three times.

For stimulated phagocytosis assays, beads with or without Polypeptide, PEG or CD47 were incubated with rabbit anti-streptavidin as the opsonin. Beads were opsonized at the respective concentration for 30 min at RT. Opsonized beads were washed 2x and resuspended in 50 µl of PBS/0.4% BSA. Phagocytes were washed with PBS beads were labeled as described above.

For cytoskeletal involvement at the phagocytic synapse, streptavidin beads opsonized with rabbit anti-streptavidin FITC. Opsonized beads of different sizes were added to PMA treated THP-1 cells and immediately placed at 4℃ for 10 min to synchronize phagocytosis. The temperature of the cells was then immediately increased to 37℃ for 10 min and then fixed with 5% formaldehyde for immunofluorescence. For studies involving blebbistatin (EMD Biosciences), macrophages were treated for 10 min at 4ºC prior to temperature increase to 37ºC or for 45 min. Macrophages treated with DMSO were used to verify no solvent effects.

Images were acquired with an inverted microscope (Olympus; IX71) with a 60x and 150x (oil, 1.4 NA) objective using a Cascade CCD camera (Photometrics, Tuscon, AZ). Image acquisition was performed with Image Pro software (Media Cybernetics, Silver Spring, MD). All subsequent image analysis was done using ImageJ.

### 2.4.10 – SHP-1 inhibitor effect on phagocytosis

PMA activated THP-1 macrophage was treated with a SHP-1 inhibitor (NSC-87877) provided by Dr. Frank L. Conlon (University of North Carolina) from 0-100 nM in DI water for 5 min prior to the addition of IgG-opsonized particles. Phagocytosis assay of IgG-opsonized particles coated with or without CD47 at 100 nm and 1.1 μm radius were conducted as described above.

### 2.4.11 – Inhibition of nanoparticle uptake

THP-1 macrophages activated with PMA were incubated with 10 μg/ml chlorpromazine in distilled water or 30 μM cytochalasin B in DMSO (Sigma-Aldrich) for 30 min at 37℃. Control cells were inc ubated with the medium with solvent. Followed by incubation with the above inhibitors, THP-1 cells were used for uptake studies with or without IgG-opsonized 100 nm radius particles targets as described above.

### 2.4.12 – Immunofluorescence microscopy

Immunostaining was performed after cells were fixed and blocked for 1 h with 5% BSA in PBS. Staining with primary antibody anti-rabbit PE-conjugated (1:200) was used for detection of non-phagocytosed beads for 1 h at room temperature in PBS. After washing, samples were fixed with 5% formaldehyde and imaged. In order to ensure that the cells were not permeable to labeling an

antibody against myosin IIA was used to confirm not labeling occurred (Sigma-Aldrich).

Images were acquired on an inverted microscope (IX71; Olympus) with a 40x or a 60× (oil, 1.4 NA) objective using a Cascade CCD camera (Photometrics). Image acquisition was performed with Image Pro software (Media Cybernetics, Inc.). All subsequent image analysis was done using ImageJ.

### 2.4.13 – Immunoprecipitation and Western blotting

Human Phagocytes, THP-1 wild-type ($2x10^6$) were cultured and differentiated in 6-well plates for 48 hours after PMA differentiation. Human CD47, PEG and Polypeptides were attached to 2.1µm diameter beads at specific densities as described above and added at a bead to cell ratio of 20:1 for 10 minutes. Following the incubation time, the cells were washed with ice-cold PBS and then lysed on ice in 300 µl of lysis buffer (50 mM Tris-HCl (pH 7.4), 150 mM NaCl, 1mM EDTA, 1% NP-40, 1% protease inhibitor cocktail [Sigma-Aldrich] and 2mM activated sodium orthovanadate). For immunoprecipitation, whole lysate was mixed with 1:200 anti-SIRPα (SE7C2) antibody (Santa Cruz Biotechnology, Inc.) with Protein G agarose (Pierce) at 4˚C overnight. Precipitated proteins was placed in 4-12% SDS-PAGE in MOPS buffer (Invitrogen), transferred to PVDF membrane, blocked and labeled via phosphotryosine IgG HRP-conjugated (Cell

Signaling) and anti-SIRPα (C-20) (Santa Cruz Biotechnology, Inc.) as primary antibodies and anti-goat-HRP (Amersham). All Westerns were run in duplicate, along with an additional blot for actin to ensure constant protein load among samples.

### 2.4.14 – Biodistribution Study with dye-labeled Beads

All mice were treated in accordance with approved IACUC protocols at the University of Pennsylvania. Near Infrared Fluorophore (NIRF)-labeled and unlabeled streptavidin coated polystyrene beads were injected into the tail veins of healthy Adult Immune-deficient (NSG) Mice (4-8 weeks). The range of injected beads was ~$10^7$ per ml, with some variability due to accuracy of locating the tail vein. Every 10 min, 5 µl blood samples were collected by retro-orbital bleeding. At 35min following injection, mice were sacrificed and whole blood, liver, spleen, lungs, kidneys, heart and brain were collected. The whole blood was then centrifuged and plasma collected.

Organs were imaged on the LiCor Odyssey imaging system (LI-COR Biosciences, Lincoln, NE) at 800 nm excitation. The integrated fluorescence intensity of the organs was normalized using the organ correction factor found by Christian et. al. (Christian 2009) and applied to all other measured intensities for all organs. The NIR intensity of the plasma was measured on the LiCor and calculated by fitting the slope of the linear dilution curve.

### 2.4.15 – Preparation of erythrocytes for injection

Blood from NSG mice were acquired by Cardiac Puncture, erythrocytes were separated from the rest of the blood component by centrifugation gradient to isolate the RBC pellet package. Samples were divided into two groups, they were labeled with a hydrophobic dye DiD and PKH 26 respectively and incubate for 20 min at room temperature (RT). Both samples were washed with PBS/ 0.4% BSA and then one of them was incubated with anti-mCD47 (mIAP) primary antibody for 45 minutes and both of them were opsonized with excess rabbit anti-mRBC prior to mixing cells together and injecting into the tail vein for 30 min at room temperature (RT). Cells were then washed with PBS/ 0.4% BSA and one quantified by light and fluorescent microscopy

### 2.4.16 – Measuring Beads and RBC in circulation

The total numbers of beads remaining in circulation were measured using flow cytometry with 10ul the samples collected from each mouse.

Beads, in whole blood sample (or serum), were labeled with 15μl of B6H12-FITC (BD Biosciences) against human-CD47 and with 1μl goat anti-rabbit F(ab')2 R-PE against rabbit anti-streptavidin (Sigma-Aldrich) for 30 min at room temperature. Beads were washed and resuspended in PBS for flow cytometry analysis.

Forward scatter, side scatter and fluorescence (FL1, FL2, FL3, FL4 channels in logarithmic mode) were acquired using a FACScan or FACSCalibur (BD Immunocytometry Systems). Data points from flow cytometry were plotted and the total number of beads in each 10ul sample was counted by the total number of events with the appropriately distinct forward and side scatter. These events also appeared positive for Opsonization and human-CD47.

### 2.4.17 – *In vivo* Blocking mouse-SIRPα

We pre-inject 4 NSG mice (30-120min and 24 hour before particle injections) with 100ug of CD172a (BD Biosciences) antibody. hCD47 nanoparticles were injected to each of the pre-injected mice and to 1 not pre-injected (control). At 35min following injection, mice were sacrificed and whole blood and spleen were collected.

The circulating particle ratio at 35 min was measured using flow cytometry. Forward scatter, side scatter and fluorescence (FL1, FL2, FL3, FL4 channels in logarithmic mode) were acquired using a FACScan or FACSCalibur (BD Immunocytometry Systems).

### 2.4.18 – Collagenase Digestion.

Spleens were chopped into pieces and placed into tubes containing 1 ml of collagenase/DNase solution [1 mg/ml type II collagenase (Worthington Biochemicals) and 0.1% DNase I (Sigma) in RPMI medium 1640 plus 10% FBS].

The suspension was pipetted intermittently for 20-30 min at 37℃. Cells were then washed, treated to remove red blood cells, and counted before staining for flow cytometry to immunostain for macrophages with F4/80 (Bioscience, Inc.).

Forward scatter, side scatter and fluorescence (FL1, FL2, FL3, FL4 channels in logarithmic mode) were acquired using a FACScan or FACSCalibur (BD Immunocytometry Systems).

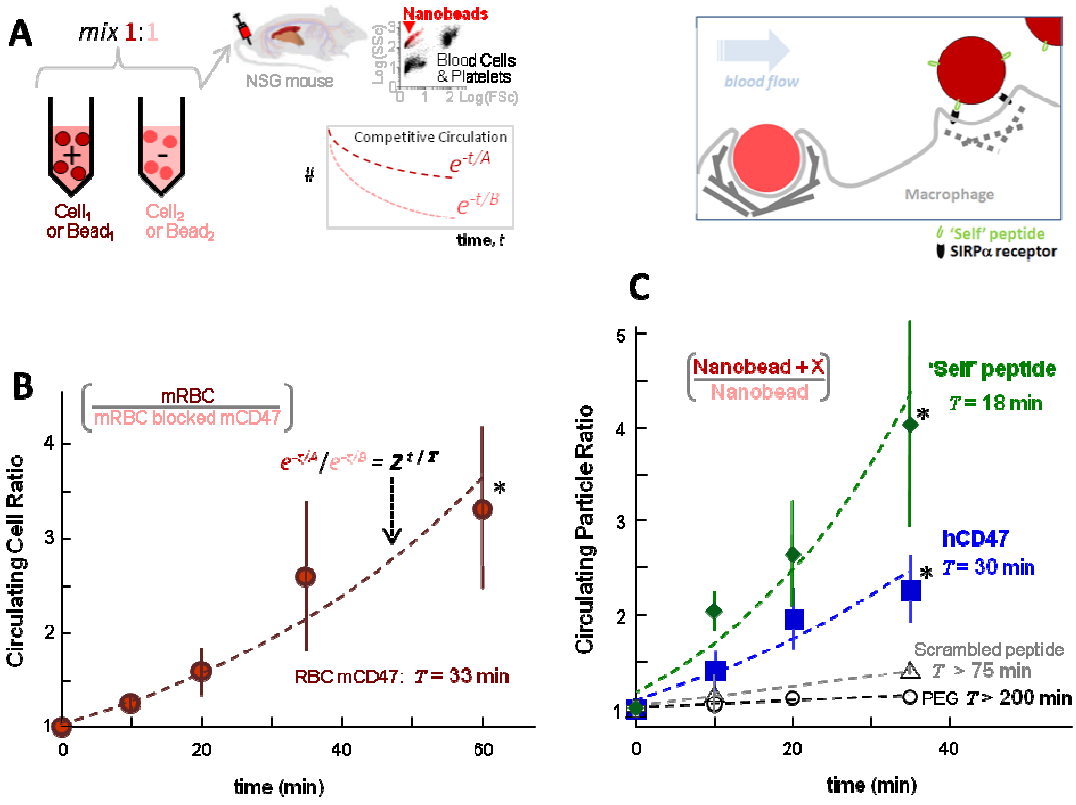


**Fig. 2.1.- "self"-peptide and human-CD47 prolong the circulation of nanobeads in NSG mice.**

**(A)** Competitive circulation experiment in which two colors of nanobeads or cells are mixed and injected into the same mouse after labeling with either red (PKH26) or a far-red (DiD) fluorophores. 50 μl of blood was periodically sampled, and flow cytometry analysis of decays in particle numbers are used to calculate the time-dependent *persistence ratio* in each mouse. **(B)** Circulation experiment in which mouse-RBC (mRBC) from NSG mice were CD47-blocked or not and also opsonized with excess anti-mRBC prior to mixing cells together and injecting into the tail vein (*n = 3 mice; $R^2$ = 0.93 for fit of means with indicated T*). **(C)** Upper sketch: nanobeads in blood flow being cleared by a splenic macrophage (left) or else recognized as "self" and let go (right). Circulation experiments used 160 nm polystyrene beads with covalently attached streptavidin incubated with biotinylated versions of: synthetic 'Self' peptide (n = 4; $R^2$ = 0.94 for fit of means), recombinant hCD47 (n = 6; $R^2$ = 0.92 for fit of means), or negative controls of either scrambled peptide (n = 3) or PEG (n = 5). Nanobeads were also opsonized with anti-streptavidin and then $10^7$ were injected. Flow cytometry quantitation was typically done on 100-10,000 particles at each time point, and typically included quantitation of both hCD47 and opsonin on the nanobeads. For hCD47 and 'Self' peptide, a separate fit for each mouse gives the indicated mean T ± SEM for each group, which is within 10% of the T obtained from fitting the group averages (dashed curves). Based on these analyses, an apparent difference between hCD47 and 'Self' peptide is not significant (p = 0.18), but nearly all datapoints do differ from PEG-nanobeads (* p < 0.05). All data are mean ±SEM.

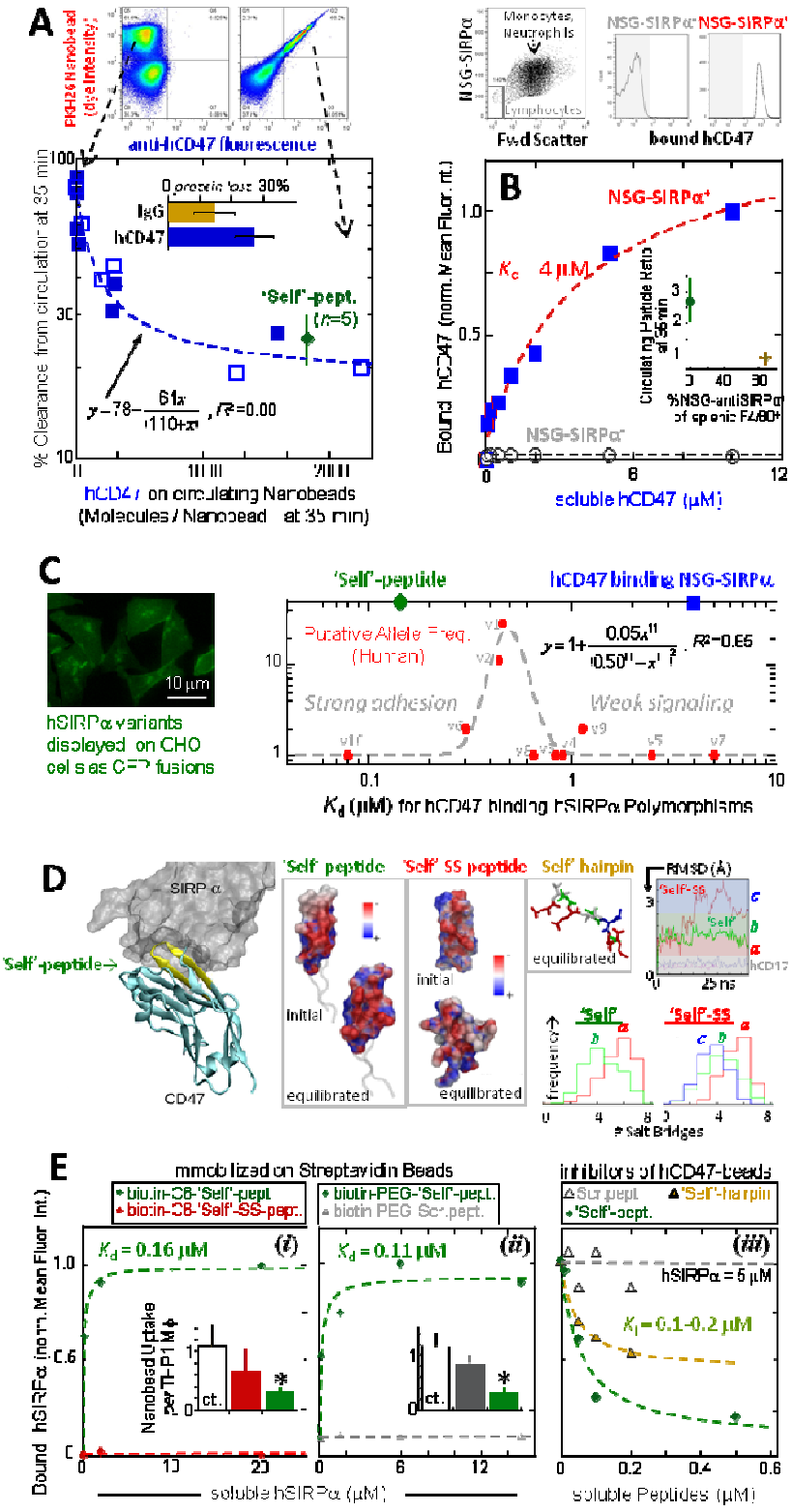
A
anti-hCD47 fluorescence
% Clearance from circulation at 35 min
0 protein loss 30%
IgG
hCD47
'Self'-pept.
(n=5)
hCD47 on circulating Nanobeads
(Molecules / Nanobead at 35 min)
Monocytes, Neutrophils
Lymphocytes
Fwd Scatter
NSG-SIRPα-
NSG-SIRPα+
bound hCD47
B
NSG-SIRPα+
Kd 4 μM
NSG-SIRPα-
Bound hCD47 (norm. Mean Fluor. Int.)
soluble hCD47 (μM)
Circulating Particle Ratio at 35 min
%NSG-antiSIRPα of specific FZ60+
C
10 μm
hSIRPα variants displayed on CHO cell surface GPI fusions
'Self'-peptide
hCD47 binding NSG-SIRPα
Putative Allele Freq. (Human)
Strong adhesion
Weak signaling
Kd (μM) for hCD47 binding hSIRPα Polymorphisms
D
SIRPα
'Self'-peptide
CD47
'Self' peptide
'Self' SS peptide
'Self' hairpin
initial
equilibrated
RMSD (Å)
'Self'
'Self'-SS
frequency
# Salt Bridges
E
immobilized on Streptavidin Beads
biotin-CB-'Self'-pept.
biotin-CB-'Self'-SS-pept.
biotin-PEG-'Self'-pept.
biotin PEG Scr.pept.
Kd = 0.16 μM
Kd = 0.11 μM
Bound hSIRPα (norm. Mean Fluor. Int.)
Nanobead Uptake per TI-P1 MΦ
ct.
soluble hSIRPα (μM)
inhibitors of hCD47-beads
Scr.pept.
'Self'-hairpin
'Self'-pept.
hSIRPα = 5 μM
Ki = 0.1-0.2 μM
soluble Peptides (μM)

**Fig. 2.2.- Persistence of hCD47- and "self"- nanobeads depends on hCD47 density, consistent with low affinity binding to NSG-mouse SIRPα relative to human-SIRPα variants.**

**(A)** The number of hCD47 molecules on the 160 nm beads at 35 min after injection was either measured in two color experiments (solid; n = 7 mice) or single color experiments (open; n = 6 mice), with an average of 30% protein lost in circulation (inset). 'Self' peptide levels are estimated to have a similar loss (n = 4 mice). Fluorescent nanobeads (PKH26+ in flow cytometry, upper plots) were confirmed by forward/side scatter, and fluorescent anti-hCD47 measured hCD47 levels (left plot is control nanobead sample, and right plot is hCD47 nanobead sample). The inhibition curve gives Ki = 110 molecules/nanobead. **(B)** Affinity of soluble hCD47 for fresh NSG neutrophils and monocytes, using flow cytometry analysis of Cy5-anti-Biotin. Lymphocytes are negative for SIRPα and do not bind soluble hCD47. In inset we show a blocking experiment for mSIRPα using anti-mouse SIRPα antibodies that block binding of mouse-SIRPα to hCD47. We pre-inject the antibody into 4 mice (30-120min before) and we didn't inject antibody in one of the mice. The circulating particle ratio at 35 min was measured and we also broke up the spleen and used flow cytometry to immunostain for macrophages with F4/80. **(C)**Ten reported variants of hSIRPα's N-terminal domain (Takenaka2007) were displayed on CHO cells to determine affinities for soluble hCD47 (**Fig. 2.S4**). The putative allele frequency is plotted *versus* the measured affinities, with the highest frequency at intermediate affinity. On this scale, the affinity of hCD47 for mSIRPα on NSG phagocytes (blue square) proves weak while the affinity of "self"-peptide for hSIRPα is strong (green diamond). The Lorentzian fit is inspired by other mechanobiological signaling processes and has the form: $y = 1+ 0.05x^{11}/(0.50^{11} + x^{11})^2$, $R^2 = 0.85$. **(D)** The co-crystal structure of hCD47 and hSIRPα (Hatherley 2008) identified the FG loop in hCD47 as one of two interaction sites, and so it formed the basis for design and simulation of several polypeptides (details, Fig. 2.S5). The upper right plot shows loop dimensions versus time in solution for hCD47, for the "self"-peptide, and for the disulfide containing "self"-SS-peptide, which tends to be larger (regime *c*). The lower histograms show the frequency of salt bridges formed between these two peptides and hSIRPα when docking various configurations from the size ranges *a-c*. **(E)** Affinities of peptides on beads for soluble hSIRPα based on flow cytometry measurements of beads (see Methods). Fits to saturation binding gave the indicated dissociation constants, $K_d$. Neither the "self"-SS-peptide nor the Scrambled-peptide exhibit any affinity for hSIRPα. The assays in (*iii*) use soluble versions of the peptides, lacking biotin, and show the unstructured "self"-hairpin is a weak inhibitor of the interaction. Bargraph insets in (*i,ii*) show *in vitro* phagocytosis assay results with the human THP1 cell line (see Methods), demonstrating that only the "self"-peptide (with C6 or PEG linkers) significantly inhibits phagocytic uptake ($p < 0.05$).

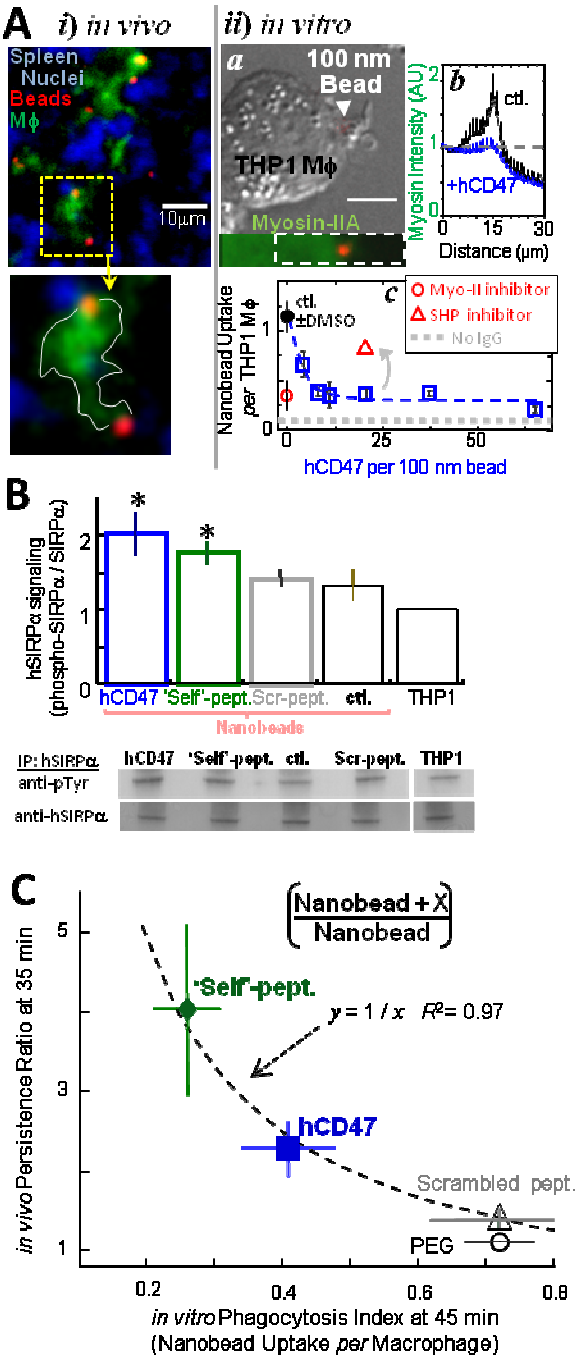
A
i) in vivo
Spleen
Nuclei
Beads
Mϕ
10μm
ii) in vitro
a
100 nm
Bead
THP1 Mϕ
Myosin-IIA
b
ctl.
+hCD47
Myosin Intensity (AU)
Distance (μm)
c
Myo-II inhibitor
SHP inhibitor
No IgG
ctl.
±DMSO
Nanobead Uptake per THP1 Mϕ
hCD47 per 100 nm bead
B
hSIRPα signaling
(phospho-SIRPα / SIRPα)
hCD47
'Self'-pept.
Scr-pept.
ctl.
THP1
Nanobeads
IP: hSIRPα
anti-pTyr
anti-hSIRPα
C
Nanobead + X
Nanobead
'Self'-pept.
y = 1 / x R²= 0.97
hCD47
Scrambled pept.
PEG
in vivo Persistence Ratio at 35 min
in vitro Phagocytosis Index at 45 min
(Nanobead Uptake per Macrophage)

**Fig. 2.3.- Phagocytosis of nanobeads is efficient and recruits Myosin-II, unless CD47 or "self"-peptide bind SIRPα and signal inhibition through SHP1.**

**(A)** Nanobead uptake in vivo in NSG mice and in vitro with human-derived THP1 macrophages. (i) Splenic macrophages co-localize with nanoparticles in situ. Spleens harvested at 35-40 min were frozen-sectioned, fixed and permeabilized for immunostaining green for macrophages (MΦ) and red with a secondary antibody against anti-streptavidin opsonized beads (goat anti-rabbit F(ab')2). Nuclei are stained blue with Hoechst dye. (ii) Phagocytosis of fluorescent 100 nm beads (red) by THP1 cells in vitro was assessed at 45 min by immunostaining cultures that were fixed (but not cell permeabilized) for non-ingested beads using secondary antibody against anti-streptavidin. Nonmuscle Myosin-IIA (a, lower panel) enriches near the nanoparticle unless hCD47 is on the bead (b, plot). Myosin-II's enrichment near the nanobead extends deeply into the cytoplasm (~5 μm) relative to bead size, suggestive of a diffuse signal that directs cytoskeletal assembly. Nanobeads with anti-streptavidin are readily engulfed at about 1 bead per cell (c), but uptake is inhibited by hCD47 and by inhibition of Myosin-IIA with blebbistatin (50 μM). Inhibition of SHP1, downstream of SIRPα, with NSC-87877 blocks the inhibition of uptake by hCD47. DMSO is the solvent for the drugs. **(B)** Phosphorylation of hSIRPα tyrosines in THP1 cells upon contact with opsonized nanobeads bearing hCD47 and 'Self' peptide. hSIRPα was immunoprecipitated from cell lysates and phosphotyrosine was immunoblotted for quantitation (n = 3; *$p < 0.05$). **(C)** Inverse correlation between in vivo persistence ratio at 35 min and in vitro inhibition of phagocytosis by hCD47 and 'Self' peptide at 45 min for 160 nm beads. All data are mean ±SEM.

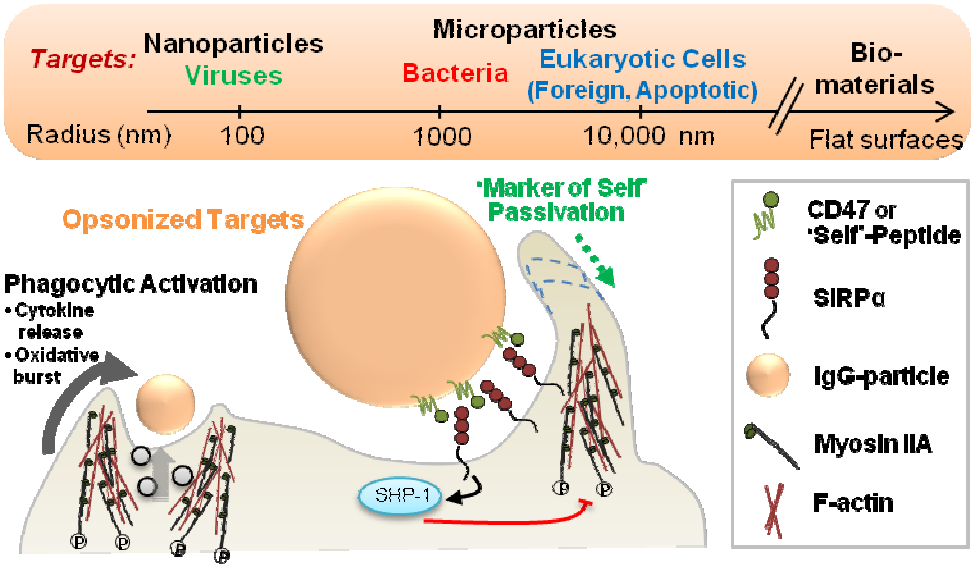


**Fig. 2.4.- Phagocytic activation can be passivated almost independent of curvature through signaling by hCD47 and a minimal "self"-peptide designed from the binding site with SIRPα.**

## Two-color RBC show for each color that mouse-CD47 prolongs Circulation.

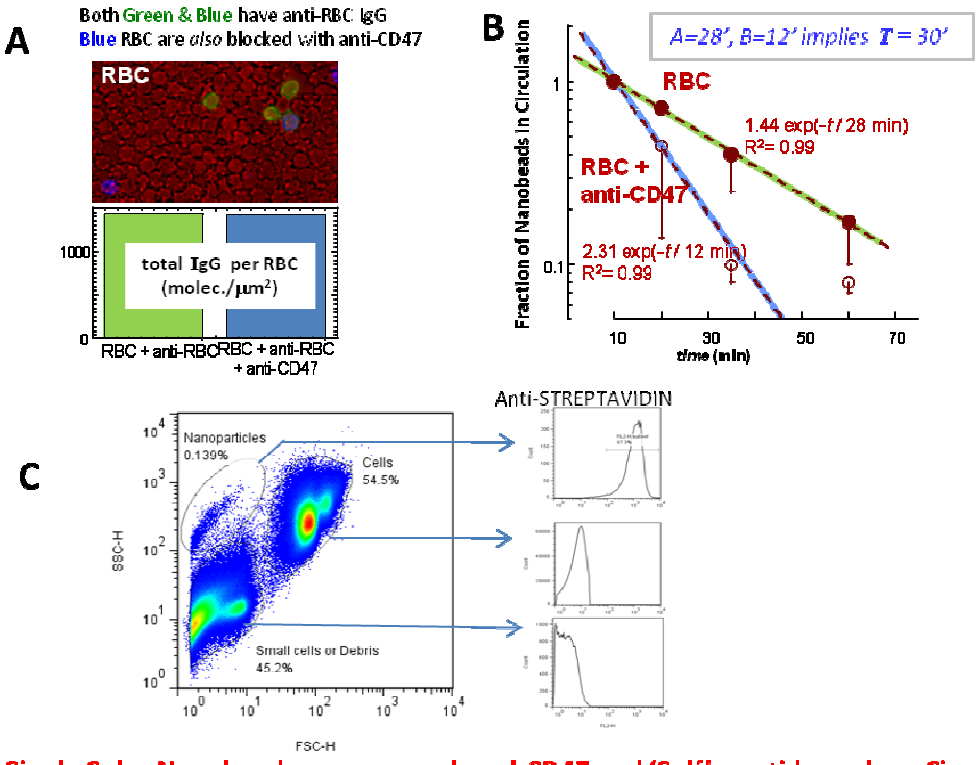


## D Single Color Nanobeads per mouse show hCD47 and 'Self'-peptide prolong Circulation.

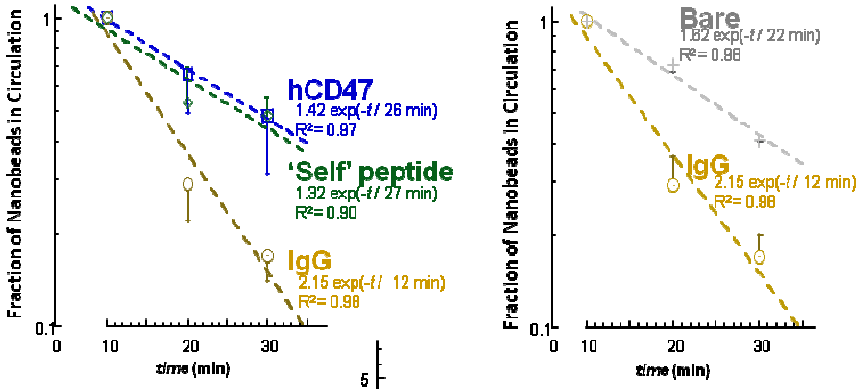


## E

αCD47 as opsonin,
*in vivo* testing

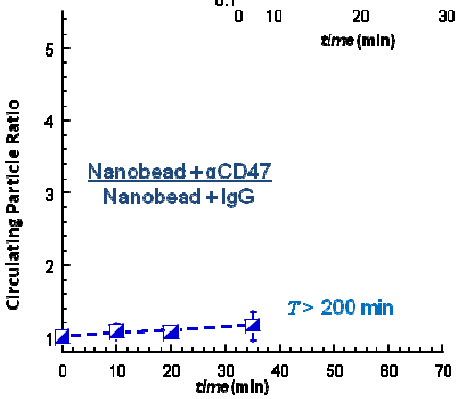

**Fig.2.S1.- Two-color RBC show for each color that mouse-CD47 prolongs Circulation, and Single Color Nanobeads show hCD47 and "self"-peptide prolong Circulation.**

**(A)** Representative images of blood samples taken at 10 min after injection of NSG mouse-RBC (mRBC) treated with anti-CD47 antibody (blue) or unblocked control mRBC (green). The opsonization level of the RBC was measured for each condition before injection, which showed approximately 2000 molecules/um$^2$ for both samples. **(B)** Two-color RBC experiment shows that mouse-CD47 prolongs circulation independent of fluorescence labeling. 50 µl of blood was periodically sampled, and flow cytometry analysis of the decays in particle numbers were used to calculate the circulation kinetics for each condition in each mouse. A doubling time similar to that in Fig.2.1B can be estimated from these results, and if it were extrapolated to one full day would yield $2^{24h/33min}$ (~10-trillion) more RBC with CD47 compared to every circulating *RBC without CD47*. This exceeds by ~100-fold the daily production of RBCs in humans and begins to suggest the potency of CD47 and/or co-factors on RBC. **(C)** Nanobeads in whole blood samples were identified using a unique methodology in flow cytometry for nanobeads in circulation . Forward and side scatter were used to separate nanoparticles from the rest of the blood components as well as by using anti-streptavidin antibody and the appropriate isotype controls (histograms) **(D)** Single Color Nanobeads show hCD47 and "self"-peptide prolong circulation. 50 µl of blood was periodically sampled from mice injected with one type of functionalized bead (hCD47, "self" peptide, or IgG control), and the circulation kinetics of the beads was measured by flow cytometry. Bare 320nm beads were cleared *in vivo* slower than IgG-opsonized but faster than beads functionalized with Opsonin+hCD47 and Opsonin+"self" peptide. **(E)** Any Targeting antibody will also opsonize nanoparticles and promote in vivo clearance. Since CD47 has been therapeutically targeted with antibodies, we attached biotinylated-(anti-hCD47) (see Methods) to the nanobeads and co-injected in mice with beads having anti-streptavidin (n = 3 mice). Periodic bleeds were analyzed by flow cytometry with quantitation of 100-1000 particles and verification of antibody attachment to the nanobeads. Beads are cleared equally for both antibodies.

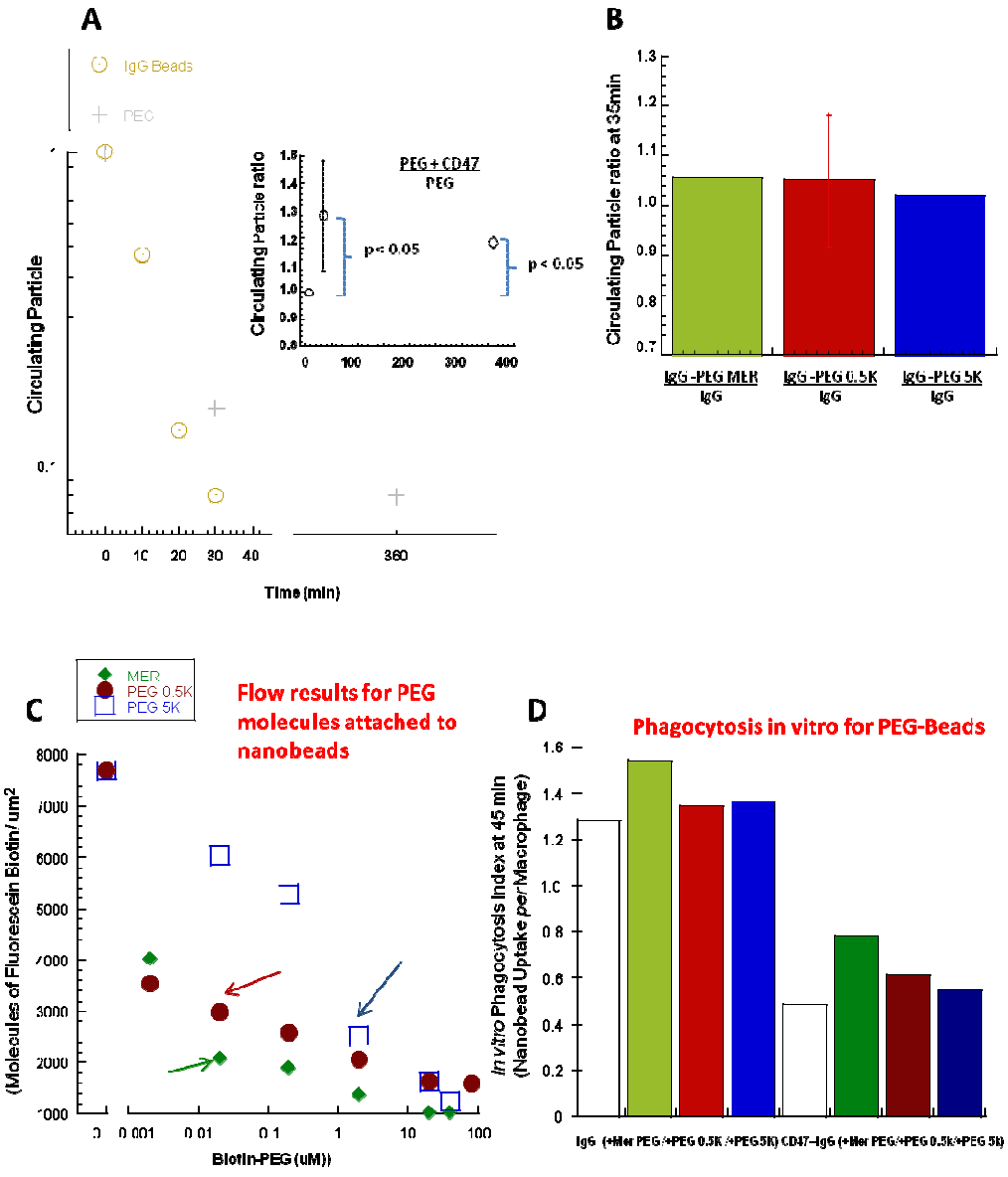


**Fig.2.S2.- IgG gives rapid clearance, while PEG (no IgG) gives long circulation and PEG + CD47 is better.**

**(A)** Single Color Nanobeads show PEG beads and hCD47-PEG beads prolong circulation. 50 µl of blood was periodically sampled from mice injected with one type of functionalized bead (hCD47 or IgG control), and the circulation kinetics of the beads was measured by flow cytometry. PEG 320nm beads were cleared *in vivo* slower than IgG-opsonized Beads but faster than beads functionalized with PEG+hCD47. **(B)** Circulation experiments used 160 nm polystyrene beads with covalently attached streptavidin (Spherotech) incubated with biotinylated versions of: PEG MER (n = 1), PEG 0.5K (n = 2), PEG 5K (n = 1). Beads were also opsonized with anti-streptavidin and then ~$10^7$ were injected. Flow cytometry quantitation was done on 100-1000 particles at 35min time point. Error bars are SEM; Characterization of beads size and surface charge were made with DLS and they didn't show any significant different between the particles. **(C)** Flow results for PEG molecules attached to nanobeads *in vitro*. Numbers of Fluorescein-Biotin molecules on the 160 nm beads were measured by flow cytometry at different concentration of Biotin-PEG attached to the beads first. The color arrows point to the max density used *in vivo* for each PEG size. **(D)** Phagocytosis *in vitro* for PEG-Beads. *in vitro* inhibition of phagocytosis by hCD47 at 45 min for 160 nm Pegylated beads.

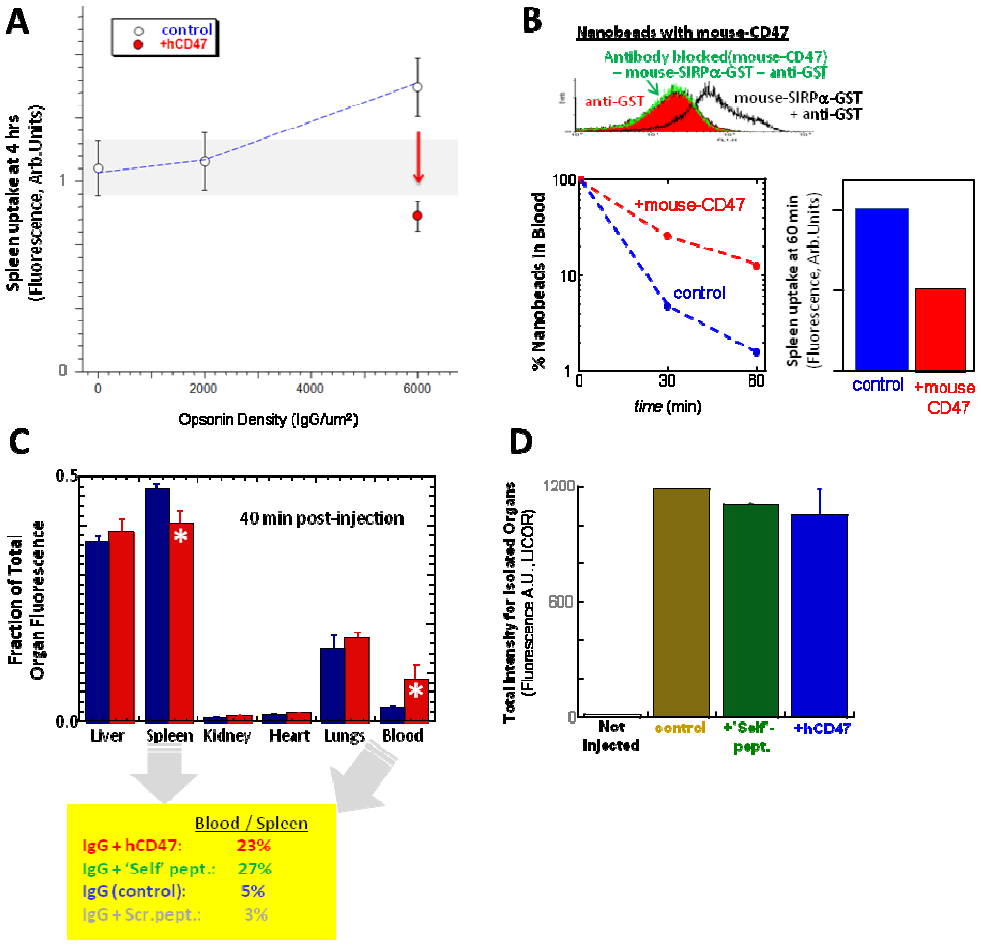


**Fig.2.S3.- Human and Mouse CD47 inhibit Splenic clearance based on imaging the Spleen and Tumor imaging is enhanced after second injection of hCD47-Nanobeads.**

**(A)** Human CD47 inhibits splenic clearance of highly opsonized (6000 molecules/$\mu m^2$) nanobeads in NSG mice. Accumulation of NIR-labeled nanobeads in the spleen was determined by total splenic NIR fluorescence intensity as measured by an Odyssey imaging system (LI-COR Biosciences) **(B)** Flow cytometry data shows binding of soluble mouse-SIRPα-GST to recombinant mouse CD47 attached to particles and also to nanoparticles with blocked mouseCD47 (mIAP301). Beads in circulation were collected 30 and 60 minutes after injection, and the concentration of beads opsonized with anti-streptavidin was compared to opsonized beads also coated with biotinylated mouse CD47. Spleens were harvested at 60 min after injection (*n*=3) and the number of particles were measured by splenic NIR fluorescence intensity **(C)** At 40 min post-injection of two colors of nanobeads, mice were sacrificed and whole blood, liver, spleen, lungs, kidneys, heart and brain were collected. NIR fluorescence intensity of each organ was measured and normalized for organ weight and optical density as well as for NIR signal resulting from particles in the blood volume of each organ. The NIR fluorescence intensity of the plasma was calculated by serial dilution in PBS. Plot showed results for n = 6 animals per group of control 160 nm polystyrene opsonized beads (blue bar) and similar beads functionalized with biotinylated hCD47 (red bar). All error bars are SEM, and (*) indicates $p < 0.05$. For Scrambled-peptide, measurements were more limited but clearly show rapid clearance from blood. **(D)** Normalized NIR fluorescence intensity for all organs in tumor-bearing mice measured by the Odyssey imaging system (n=2).

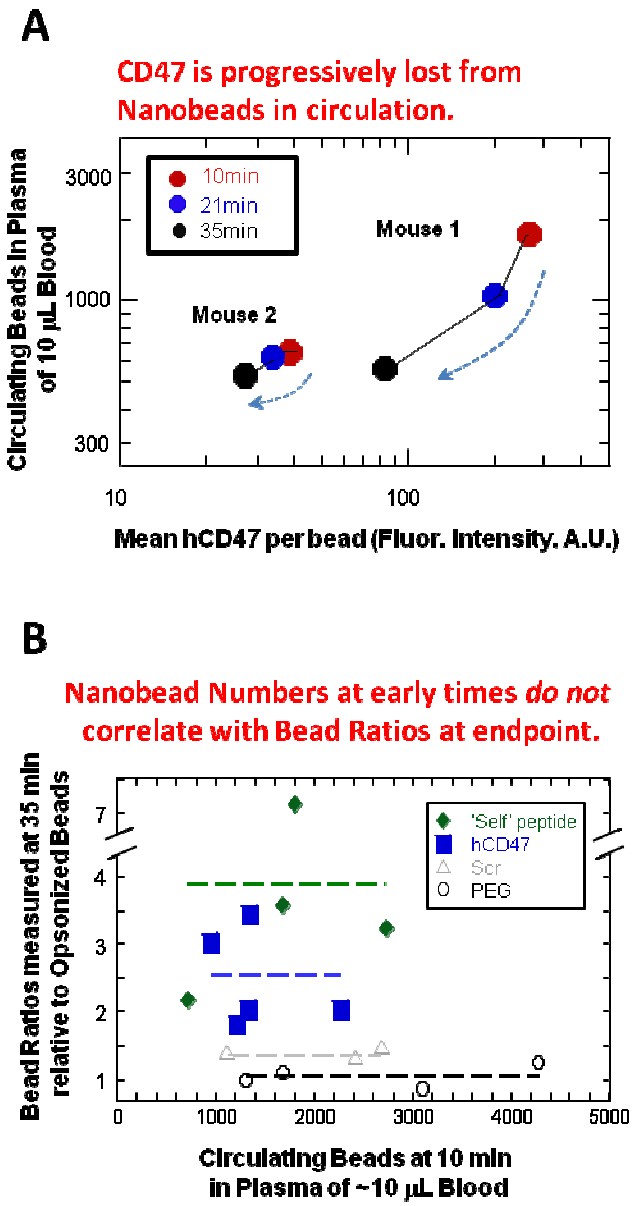


**Fig.2.S4.- CD47 is progressively lost from Nanobeads in circulation, and Nanobead Numbers at early times do not correlate with Bead Ratios at endpoint.**

**(A)** Increased surface density of hCD47 on the Nanobeads enhances the number of Nanobeads in circulation in single color bead experiments. Circulating Beads Numbers are proportional to the hCD47 concentration found on the surfaces of the beads measured by flow cytometry. Blood samples were taken at 10, 21 and 35min after single color beads injections. **(B)** In two color bead experiments, the number of beads at early timepoints does not correlate with the ratio at 35 min. In other words, PEG and Scrambled peptide fail to enhance persistence in circulation over a broad range of particle numbers, while 'Self' and hCD47 do work over a broad range of particle numbers but otherwise show no trend. These results suggest that the macrophages are not saturated by the beads in these experiments; if the macrophages were saturated, then the likely trend would be a decay in hCD47 beads toward a ratio of 1 because control beads would no longer be cleared. Dashed lines indicates means.

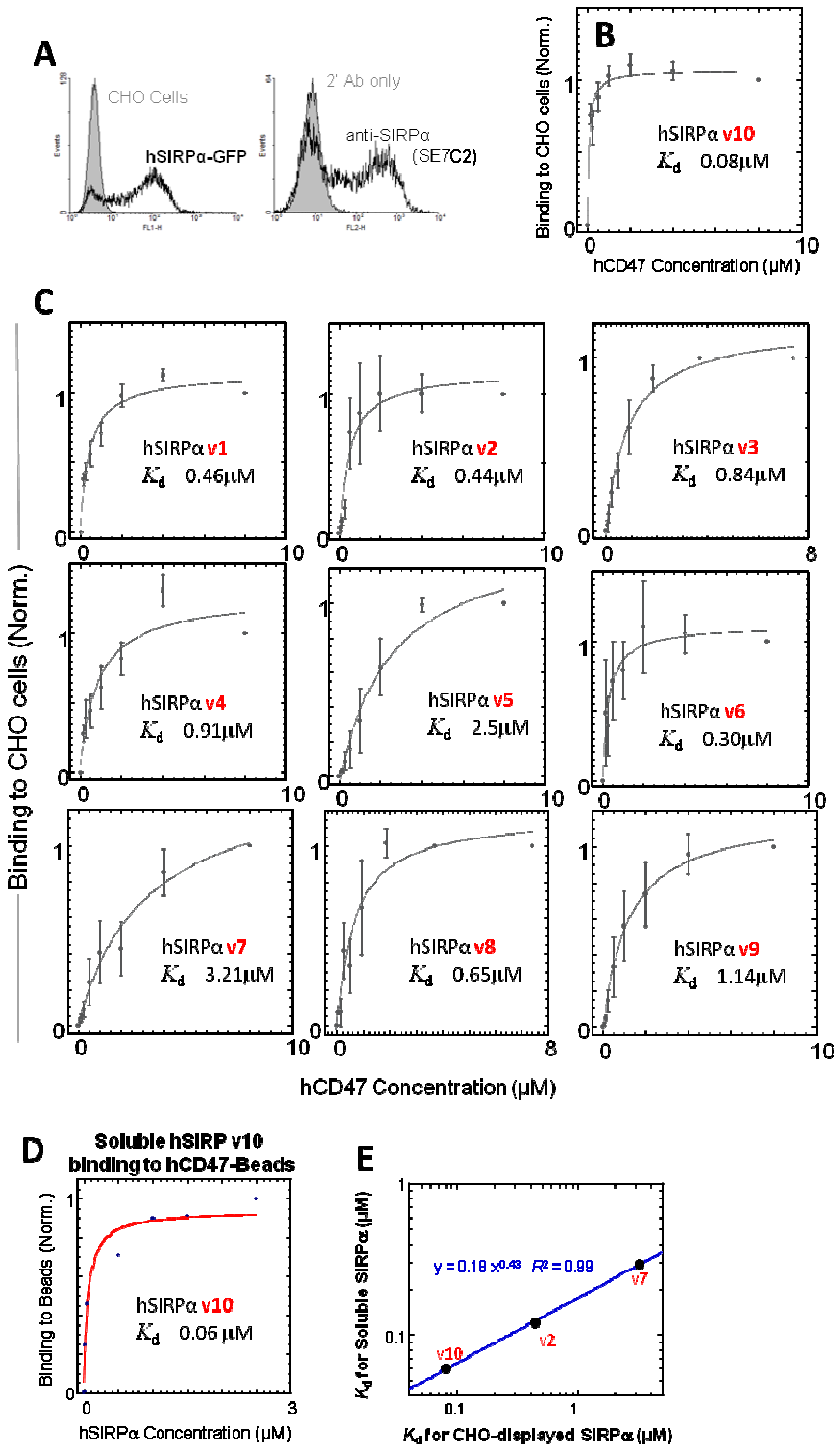


**Fig.2.S5.- hSIRPα variants exhibit different affinities for hCD47.**

**(A)** GFP-tagged full-length human SIRPα GFP (hSIRPα-GFP) was confirmed to be transiently expressed in CHO-K1 cells by GFP expression, and surface expression was confirmed with anti-SIRPα antibody by flow cytometry. **(B)** Affinities of surface-expressed hSIRPα variant 10 for soluble hCD47 was measured by flow cytometry. Saturation binding fits gave the indicated dissociation constants, $K_d$. **(C)** Human SIRPα polymorphisms variants 1-9 expressed on CHO cells with affinity binding to soluble hCD47 was based on flow cytometry. Saturation binding fits yield the dissociation constant, $K_d$ was summarized in the plot with binding curves repeated in triplicate ± standard deviation. **(D)** The binding affinity of hCD47 bound to the surface of beads to hSIRPα was measured using varying concentrations of soluble hSIRPα v10 to determine the dissociation constant, $K_d$. **(E)** Linear relationship between the $K_d$ obtained for surface-expressed hSIRPα polymorphisms variants 2,7 and 10 and soluble hCD47 and $K_d$ obtained for hCD47 attached to beads and soluble hSIRPα variants.

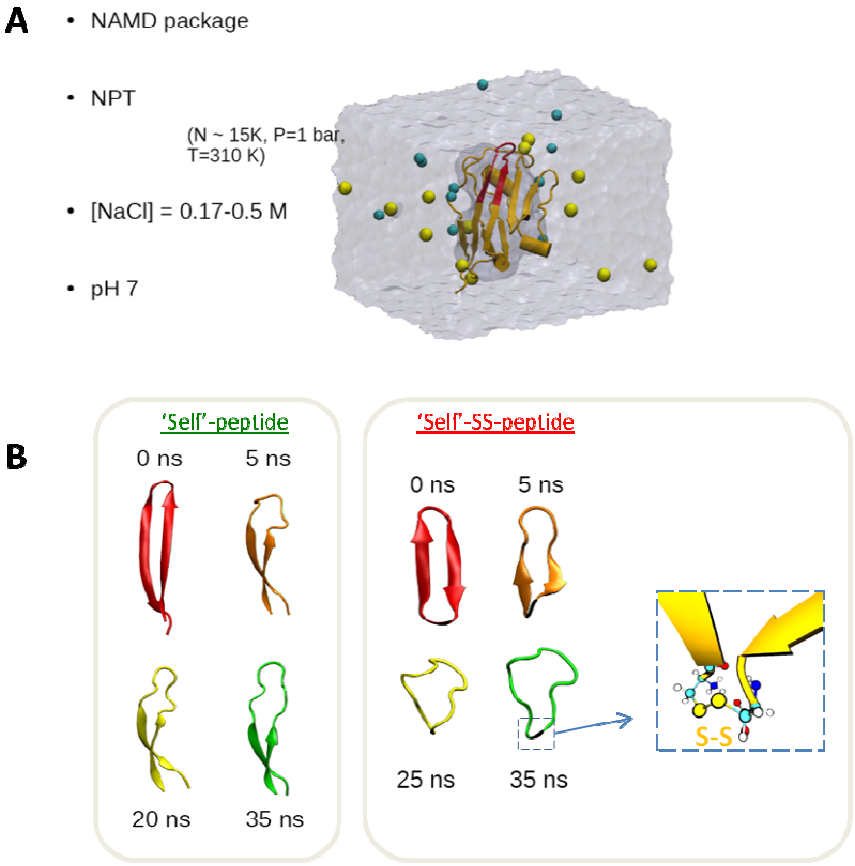


**Fig.2.S6.- Molecular Dynamics Simulations of Structures reveal Folding and Interactions.**

(**A**) Full atomistic molecular dynamics (MD) simulations were performed for over 50 ns with the hCD47-hSIRP$\alpha$ complex (PDB: 2JJS), with each component in water at the indicated solution conditions in constant particle isothermal-isobaric ensemble (NPT) constraints. Systems were equilibrated for over 5 ns followed by production runs for structural analysis. (**B**) The "self"-peptide has interstrand hydrogen bonds that increase the stability of the hairpin, while the "self"-SS-peptide has a mutation at T107C that promotes a disulfide bridge with C96 and induces a torque and splay in the circularized peptide. Both peptide structures are stable since unstable configurations tend to rearrange within 10 ns (Ivetac 2008). For electrostatic calculations of Fig. 2.3D we used Adaptive Poisson-Boltzmann Solver (APBS) (Baker 2001) as implemented in VMD (Humphrey 1996). (**C**) Peptide complexes with hSIRP$\alpha$ were obtained via computational docking. Structural heterogeneity of the peptide was taken into account by sampling of 100 representative configurations from a 100 ns long MD trajectory. Docking was performed using HADDOCK (Dominguez 2003), an algorithm able to bias the stochastic exploration of the configurational space via aptly defined distance restraints between sets of residues from the two complex constituents. The configurational space of the complex was sampled via a three-stage protocol: (i) Randomization of orientations and rigid body energy minimization; (ii) Semi-flexible simulated annealing in torsion angle space; (iii) Final refinement by MD simulations in Cartesian space with explicit solvent. For each conformation of the peptide, 2,000 structures of the complex were generated, and from these the best 200 were employed for further analysis. Salt bridges of Fig. 2.3E were calculated by identifying pairs of negatively and positively charged atoms within 4 Å, (Barlow 1983) without accounting for relative orientation.

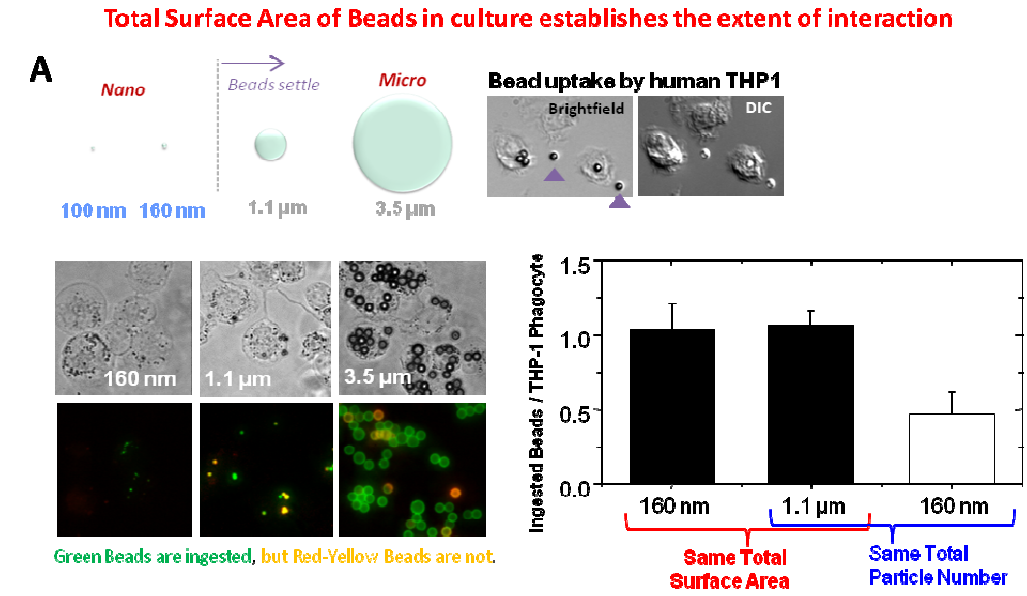
Total Surface Area of Beads in culture establishes the extent of interaction
A
Nano
Beads settle
Micro
Bead uptake by human THP1
Brightfield
DIC
100 nm 160 nm
1.1 µm
3.5 µm
160 nm
1.1 µm
3.5 µm
Green Beads are ingested, but Red-Yellow Beads are not.
Ingested Beads / THP-1 Phagocyte
1.5
1.0
0.5
0.0
160 nm
1.1 µm
160 nm
Same Total Surface Area
Same Total Particle Number

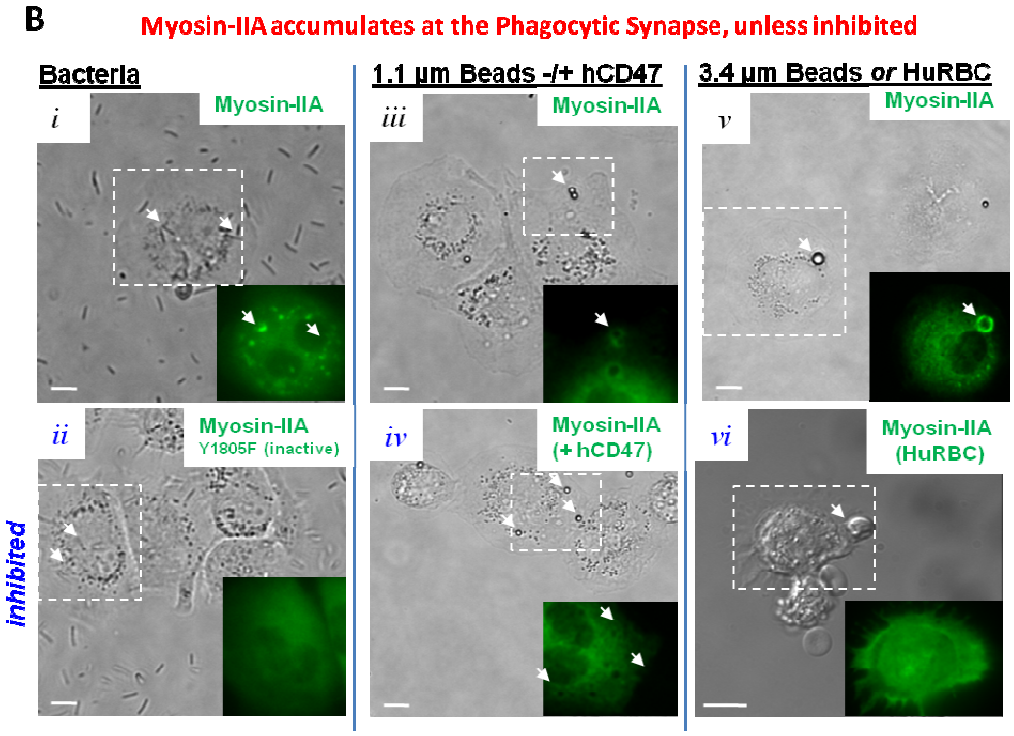
B
Myosin-IIA accumulates at the Phagocytic Synapse, unless inhibited
Bacteria
1.1 µm Beads -/+ hCD47
3.4 µm Beads or HuRBC
i
Myosin-IIA
iii
Myosin-IIA
v
Myosin-IIA
ii
Myosin-IIA
Y1805F (inactive)
iv
Myosin-IIA
(+ hCD47)
vi
Myosin-IIA
(HuRBC)
inhibited

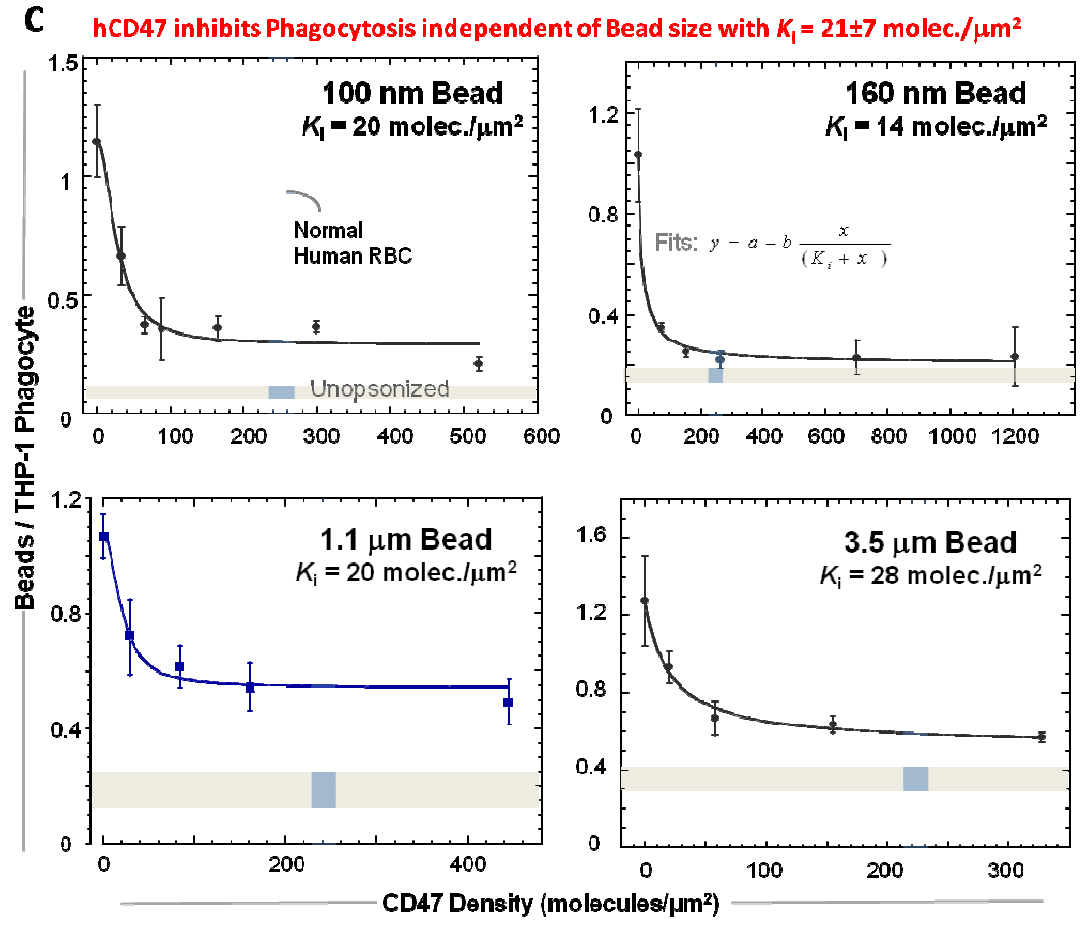
C
hCD47 inhibits Phagocytosis independent of Bead size with $K_i$ = 21±7 molec./μm²
100 nm Bead
$K_i$ = 20 molec./μm²
Normal
Human RBC
Unopsonized
160 nm Bead
$K_i$ = 14 molec./μm²
Fits: $y = a - b\frac{x}{(K_i + x)}$
1.1 μm Bead
$K_i$ = 20 molec./μm²
3.5 μm Bead
$K_i$ = 28 molec./μm²
Beads / THP-1 Phagocyte
CD47 Density (molecules/μm²)

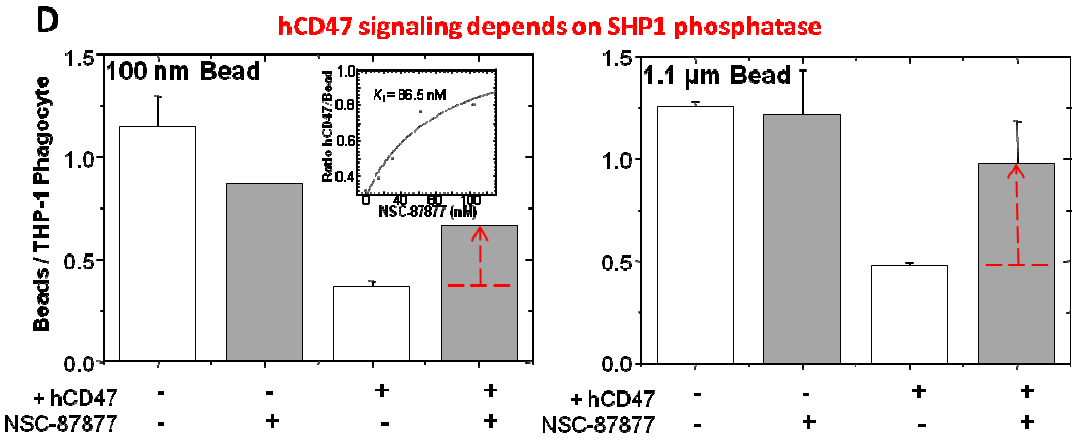
D
hCD47 signaling depends on SHP1 phosphatase
100 nm Bead
$K_i$ = 86.5 nM
Ratio hCD47/Bead
NSC-87877 (nM)
1.1 μm Bead
Beads / THP-1 Phagocyte
+ hCD47
NSC-87877

**Fig.2.S7.- The role of particle size, Myosin IIA, and SHP-1 in particle phagocytosis by macrophages**

**(A)** Nano to micron sized IgG-opsonized particles can be observed in phase contrast images (top) and fluorescent microscopy (bottom) to determine phagocytosed (green) versus non-phagocytosed particles (yellow) (*see materials and methods*). The number of IgG-opsonized particles per phagocyte was plotted for 160 nm and 1.1 μm at either a constant particle surface area or constant particle number, with 200 phagocytes counted (n=3, ± SD). **(B)** In the presences of bacteria, THP-1 phagocytes expressing (i) wild-type GFP-Myosin IIA (MYH9) show localization with arrows indicating points of contact in phase contrast and GFP image insets. (ii) A tyrosine mutation of GFP-MYH9 results in non-functional MyH9 and thus no GFP localization in the presence of bacteria. (iii) In THP-1 macrophages expressing wild-type GFP-MYH9, GFP signal localizes around 1.1 μm particles alone. (iv) hCD47 attached to the particle surface inhibits GFP-MYH9 localization around the particles (v) Larger 3.4 μm particles show GFP-MYH9 localization (inset). Scale bar 10 μm (vi) hRBC provide a hCD47 control for GFP-MYH9 localization in THP-1 cells. **(C)** Streptavidin beads were coated with varying concentrations of biotinylated hCD47 and anti-streptavidin IgG as the opsonin. Inhibition of phagocytosis is dependent on the density of human CD47 on beads but independent of particle sizes ranging from 100 nm to 3.5 μm. Phagocytosis inhibition occurs with an effective $K_i \approx 20$ molecules/$\mu m^2$ for particles from micro to nano-meter beads. The vertical blue bar is the normal density of CD47 found on normal human RBC (~250 CD47/$\mu m^2$) and the horizontal gray bar indicates the level of phagocytosis of unopsonized beads. **(D)** IgG-opsonized particles of radius 100 nm or 1.0 μm with or without hCD47 on the surface were incubated with THP-1 macrophages with an SHP-1 Inhibitor (NSC-87877) at 62.5 nM. The effects of SHP-1 inhibition were determined by the ratio of ingested particles per THP-1 phagocyte (*see Materials and Methods*). The numbers of particles ingested are shown based on 200 phagocytes counted ($n \geq 3$, ± SD). Inset shows the concentration dependence of NSC-87877 effect on particle uptake.

## 2.5 – References


1. D. W. Bartlett, H. Su, I.J. Hildebrandt, W.A. Weber, M.E. Davis, Impact of tumor-specific targeting on the biodistribution and efficacy of siRNA nanoparticles measured by multimodality in vivo imaging. *Proc Natl Acad Sci USA*. 104(39):15549-54 (2007).
2. A. L. Klibanov, K. Maruyama, A. M. Beckerleg, V. P. Torchilin, L. Huang, Activity of amphipathic poly(ethylene glycol) 5000 to prolong the circulation time of liposomes depends on the liposome size and is unfavorable for immunoliposome binding to target. *Biochim Biophys Acta.* 1062(2):142-8 (1991).
3. P. J. Photos , L. Bacakova , B. Discher, F. S. Bates, D. E. Discher, Polymer vesicles in vivo: correlations with PEG molecular weight. *J Control Release*. 90(3):323-34 (2003).
4. M. J. Turk, D. J. Waters, P. S. Low, Folate-conjugated liposomes preferentially target macrophages associated with ovarian carcinoma. *Cancer Lett*. 213(2):165-72 (2004).
5. R. Rossin, S. Muro, M. J. Welch, V. R. Muzykantov, D. P. Schuster, In vivo imaging of 64Cu-labeled polymer nanoparticles targeted to the lung endothelium. *J Nucl Med*. 49(1):103-11 (2008).
6. J. K. Armstrong *et al*., Antibody against poly(ethylene glycol) adversely affects PEG-asparaginase therapy in acute lymphoblastic leukemia patients. *Cancer.* 110 103-111 (2007).
7. P. A. Oldenborg *et al*., Role of CD47 as a marker of self on red blood cells. *Science.* 288(5473): 2051-4 (2000).
8. A. A. Bentley, J. C. Adams, The evolution of thrombospondins and their ligand-binding activities. *Mol Biol Evol*. 27(9):2187-97 (2010).
9. E. J. Brown, W. A. Frazier, Integrin-associated protein (CD47) and its ligands. *Trends Cell Biol*. 11(3):130-5 (2001).
10. L. J. Bruce *et al*., A band 3-based macrocomplex of integral and peripheral proteins in the RBC membrane. *Blood*. 101(10):4180-8 (2003).
11. I. Mouro-Chanteloup *et al*., Evidence that the red cell skeleton protein 4.2 interacts with the Rh membrane complex member CD47. *Blood.* 101(1):338-44 (2003).
12. S. Subramanian, R. Parthasarathy, S. Sen, E. T. Boder, D. E. Discher, Species- and cell type-specific interactions between CD47 and human SIRPalpha. *Blood.* 107(6): 2548-2556 (2006).
13. K. Takenaka et. Al, Polymorphism in SIRPα modulates engraftment of human hematopoietic stem cells. *Nature Immunology.* 8(12): 1313-23 (2007).
14. T. Strowig *et al*., Transgenic expression of human signal regulatory protein alpha in Rag2−/−γc −/− mice improves engraftment of human hematopoietic cells in humanized mice. *Proc Natl Acad Sci USA.* 108(32):13218-23 (2011).
15. R. K. Tsai, D. E. Discher, Inhibition of "self" engulfment through deactivation of myosin-II at the phagocytic synapse between human cells. *J Cell Biology.* 180(5): 989-1003 (2008).

16. D. Cox, S. Greenberg, Phagocytic signaling strategies: Fc(gamma)receptor-mediated phagocytosis as a model system. *Semin Immunol*. 13(6):339-45 (2001).
17. F. Turrini, F. Mannu, P. Arese, J. Yuan, P. S. Low, Characterization of the autologous antibodies that opsonize erythrocytes with clustered integral membrane proteins. *Blood.* 81: 3146 – 3152 (1993).
18. M. Lundqvist, J. Stigler, G. Elia, I. Lynch, T. Cedervall, K. A. Dawson, Nanoparticle size and surface properties determine the protein corona with possible implications for biological impacts. *Proc Natl Acad Sci USA*. 105(38):14265-70 (2008).
19. D. Wilflingseder *et al*., IgG opsonization of HIV impedes provirus formation in and infection of dendritic cells and subsequent long-term transfer to T cells. *J Immunol.* 178(12):7840-8 (2007).
20. A. M. Glodek *et al*. , Ligation of complement receptor 1 increases erythrocyte membrane deformability. *Blood.* 116(26):6063-71 (2010).
21. G. Deplaine *et al*., The sensing of poorly deformable red blood cells by the human spleen can be mimicked in vitro. *Blood*. 117(8):e88-95 (2010).
22. D. Hatherley, S. C. Graham, J. Turner, K. Harlos, D. I. Stuart, A. N. Barclay, Paired receptor specificity explained by structures of signal regulatory proteins alone and complexed with CD47. *Molecular Cell.* 31(2): 266-77 (2008).
23. S. Subramanian, E. T. Boder, D. E. Discher, Phylogenetic divergence of CD47 interactions with human signal regulatory protein alpha reveals locus of species specificity. Implications for the binding site. *J Biol Chem.* 282(3): 1805-18 (2007).
24. Y. Matsumura, H. Maeda, A new concept for macromolecular therapeutics in cancer chemotherapy: mechanism of tumoritropic accumulation of proteins and the antitumor agent smancs. *Cancer Research*. 46(12 Pt 1):6387-92 (1986).
25. H. Cabral *et al*., Accumulation of sub-100 nm polymeric micelles in poorly permeable tumours depends on size. *Nat Nanotechnol.* 6(12):815-23 (2011).
26. M. Seiffert et al., Human signal-regulatory protein is expressed on normal, but not on subsets of leukemic myeloid cells and mediates cellular adhesion involving its counterreceptor CD47. Blood. 94 : 3633 – 3643 (1999) .
27. T. Kuroishi et al., Biotin deficiency up-regulates TNF-alpha production in murine macrophages. J Leukoc Biol. 83(4):912-20. (2008).
28. H. Jeong Lee, W.M. Pardridge, Drug targeting to the brain using avidin-biotin technology in the mouse; (blood-brain barrier, monoclonal antibody, transferrin receptor Alzheimer's disease). J Drug Target 8(6):413-24. (2000).
29. W. Y. Lee et al., The role of cis dimerization of signal regulatory protein alpha (SIRPalpha) in binding to CD47. J Biol Chem. 285(49):37953-63 (2010).
30. J. A. Swanson, A. D. Hoppe, The coordination of signaling during Fc receptor-mediated phagocytosis. J Leukoc Biol. 76(6):1093-103 (2004).
31. T. Matozaki, Y. Murata, H. Okazawa, H. Ohnishi, Functions and molecular mechanisms of the CD47-SIRPα signalling pathway. Trends Cell Biol. 19(2):72-80 (2009).
32. S. J. Stachelek et al., The effect of CD47 modified polymer surfaces on inflammatory cell attachment and activation. *Biomaterials*. 32(19):4317-26 (2011).

33. S. B. Willingham *et al*., The CD47-signal regulatory protein alpha (SIRPa) interaction is a therapeutic target for human solid tumors. *Proc Natl Acad Sci USA.* doi/10.1073/pnas.1121623109 (2012).
34. D. Pan *et al*., Biodistribution and toxicity studies of VSVG-pseudotyped lentiviral vector after intravenous administration in mice with the observation of in vivo transduction of bone marrow. *Mol Ther.* 6(1):19-29 (2002).
35. C. M. Cameron, J. W. Barrett, M. Mann, A. Lucas, G. McFadden, Myxoma virus M128L is expressed as a cell surface CD47-like virulence factor that contributes to the downregulation of macrophage activation in vivo. *Virology.* 337(1):55-67 (2005).
36. A. Ivetac, M. S. Sansom, Molecular dynamics simulations and membrane protein structure quality. Eur Biophys J. 37(4):403-9 (2008).
37. N. A. Baker, D. Sept, S. Joseph, M. J. Holst, J. A. McCammon, Electrostatics of nanosystems: application to microtubules and the ribosome. Proc Natl Acad Sci U S A. 98(18):10037-41 (2001).
38. W. Humphrey, A. Dalke, K. Schulten, VMD: visual molecular dynamics. J Mol Graph. 14(1):33-8, 27-8 (1996).
39. C. Dominguez, R. Boelens, A. M. Bonvin, HADDOCK: a protein-protein docking approach based on biochemical and/or biophysical information. J Am Chem Soc. 125(7):1731-7 (2003).
40. D. J. Barlow, J. M. Thornton, Ion-pairs in proteins. J Mol Biol. 168(4):867-85 (1983).
41. D. A. Christian et al., Flexible filaments for in vivo imaging and delivery: persistent circulation of filomicelles opens the dosage window for sustained tumor shrinkage. Mol Pharm. 6(5):1343-52 (2009).

# CHAPTER 3 - Synthetic “self” peptide or hCD47 recombinant protein can enhance the effect of an anti-cancer drug

Pia L. Rodriguez, Takamasa Harada, Anthony Secreto and Dennis E. Discher

T. Harada helped with Imaging and Taxol loading studies and he also helped with the generation of the A549 tumors cells. A. Secreto helped with the mice injections, organs harvesting, mouse weight and tumor size measurements.

**Abstract**

Anti-phagocytic signals mediated by CD47–SIRPα interactions on cancer cells enable them to “hide” from innate immune system surveillance. CD47 is a critical regulator of innate immune surveillance, and is found in increased levels in various tumors. Monoclonal antibodies targeted to CD47 have been shown to lead to phagocytosis of cultured solid tumor cells *in vitro* and to prevent the metastasis of human tumor cells. Here, recombinant hCD47 or synthetic “self”-peptide was attached to virus-size nanoparticles for injection into NOD.SCID (NSG) mice-- which are known to exhibit unique compatibility with human cells—resulting in enhanced imaging of tumors with Near-Infrared nanobeads, increased tumor perfusion of the particles and a subsequent EPR effect. This indicates that the beads might be able to evade the immune system and thus be of potential biomedical application. The “self”-beads and hCD47-beads enhanced near-infrared imaging of human tumor xenografts by over tenfold. The hCD47 beads also led to statistically significant tumor shrinkage similar to that observed with beads carrying Cremophor® EL-paclitaxel (Taxol) treatments, but without the noted toxicity of Cremophor® EL. We successfully targeted human cancer cells with antibodies against CD47, where the “self”-peptide blocked phagocytic clearance from circulation and suppressed tumor growth within one day after injection. The antibody targeting approach revealed the importance and utility as

well as limitations of a human ‘Marker of “self”’ to improve drug delivery when bound to nanobeads along with a bioactive antibody against a therapeutic target.

### 3.1 – Introduction

The concept of tumor immune surveillance-- the identification and elimination of cancer cells by the immune system-- was first discussed over a century ago, and since then multiple immune system components have been implicated (Swann 2007). However, the role of macrophage phagocytosis in tumor pathogenesis has been relatively unexplored. Recent studies have demonstrated that tumors evade macrophage phagocytosis through the expression of anti-phagocytic signals, especially the ones mediated by antagonists of the CD47–SIRPα interaction against cancer cells (Chao 2011, Zhao 2011). CD47 is a critical regulator of innate immune surveillance in that monoclonal antibodies targeted to CD47 enable the phagocytosis of solid tumor cells *in vitro* and prevents the metastasis of human tumor cells (Willingham, 2012).

The increased expression of CD47 on many different human tumor types enables tumors to escape innate immune system surveillance through evasion of phagocytosis. This process occurs through binding of CD47 on tumor cells to SIRPα on phagocytes, thus promoting inhibition of phagocytosis and tumor survival (Chao 2012) and suggests the potential for targeting the CD47–SIRPα

pathway as a common therapy for human malignancies. CD47 on nanoparticles should likewise limit uptake by tumor-associated macrophages of nano-particle imaging agents and therapeutics and thus improve delivery to cancer cells. Here we demonstrate that nanobeads coated with “self” peptide or hCD47 injected intravenously into NSG mice-- which express a unique SIRPα strain compatible with human CD47—persist in circulation and exhibit enhanced perfusion, allowing for better imaging of tumors with nanobeads.

Anti-CD47 antibodies have demonstrated preclinical activity against many different human cancers both *in vitro* and in mouse xenotransplantation models (Majeti 2009). While monotherapies targeting CD47 were efficacious in several preclinical tumor models, combination strategies involving inhibition of the CD47–SIRPα pathway offer even greater therapeutic potential (Chao 2012). Concurrent administration of chemo-radiation therapy with anti-CD47 antibody is a combination strategy that may increase efficacy. However, this approach may also lead to increased toxicity as cell surface calreticulin is expressed on noncancerous cells undergoing apoptosis, a principle effect of chemo-radiation therapy (Gardai 2005, Obeid 2007). Anti-CD47 antibodies may facilitate elimination of tumor cells through a variety of mechanisms, but the role of CD47–SIRPα interactions in the context of antibody therapy against cancer, still need conclusive evidence. Here we describe a therapeutic application with “self”

peptide that it improves drug delivery when it's combined on nanobeads with bioactive antibody against a therapeutic target.

## 3.2 – Results

### 3.2.1 – "self"-Peptide enhances perfusion and imaging of tumors with nanoparticles

Prolonged circulation of hCD47-beads and "self"-beads is based on a delay of particle clearance by the spleen and liver, which rapidly accumulate nanobeads in whole body imaging of near-infrared fluorescent beads (**Fig. 3.1A**). Spleen and liver dominate biodistributions in the analysis of isolated organs in Chapter 2 and in many studies of others (e.g. Libanov 1991, Armstrong 2000, Photos 2003, Bartlett 2007, Rossin 2008). Recombinant mouse-CD47 gave results for circulation and splenic clearance similar to human-CD47 (**Fig. 2.S3B**), but hCD47 seemed more important to focus on due to known differences with mouse (Mouro-Chanteloup 2003, Subramanian 2006) and a lack of *in vivo* experiments on human-CD47. In particular, we hypothesized that persistent circulation of even a fraction of particles should enhance perfusion of other highly vascularized tissues such as a subcutaneous tumor.

Human-derived A549 lung epithelial cells were xenografted in the flanks of NSG mice, and the subsequent tumors were quantitatively imaged both in situ and ex vivo using Near-Infrared (NIR) fluorescent nanobeads. As early as 10

min after tail vein injection of nanoparticles, hCD47- and “self”-nanobeads gave mean tumor intensities 2-fold above those of non-injected mice while control beads gave background-level signal (**Fig. 3.1B**). With hCD47- and “self”-nanobeads, the fluorescence at every time point is significantly higher than control beads ($p < 0.05$), and the increase fits to first order kinetics ($T = 52$ min), consistent with enhanced perfusion that is limited by progressive clearance. Notably, at 40 min, both hCD47- and “self”-nanobeads give ~10-20 fold higher signals than controls. A second injection of hCD47-nanobeads after 2 hrs exhibits a similar increase in signal consistent with linearity (**Fig. 3.S1A, B**). An initial doubling time for tumor accumulation of particles can be estimated as $T_o = 12$ min from the first order fit (for $t << \tau$) and proves much shorter than control nanobeads ($T = 210$ min). Both doubling times are similar to those obtained in blood analysis for persistent circulation in chapter 2 (**Fig. 2.1C**), consistent with the hypothesis that enhanced tumor signal results from persistent circulation.

Tumors and other major organs in one experiment were subsequently excised and imaged in order to remove background from nearby tissue and minimize any uncertainty in the region-of-interest (**Fig. 3.1C**). The “self”-beads and hCD47-beads show 16- to 22-fold enhancement above the very low signals obtained with control beads, with no statistical difference between “self”-peptide and hCD47. The fraction of nanobeads in the blood within the tumor is small (**Fig. 3.1C, inset**), and so the majority of signal derives from beads that have

accumulated in the tumor, most likely by Enhanced Permeation and Retention (EPR) through the leaky vasculature that is characteristic of many solid tumors (Matsumura 1986, Cabral 2011). The NSG-mouse results are thus suggestive of active suppression of clearance through binding of both human-CD47 and the "self"-peptide to NSG-SIRPα on macrophages.

### 3.2.2 – Drug loading on the surface of nanobeads

We loaded nanobeads with Paclitaxel (Taxol), which is a common anti-cancer drug in wide clinical use against solid tumors as it induces cell death through the stabilization of microtubules (Kim 2004). The goal was to inject various paclitaxel formulations into the tumor-bearing mouse model that was used in the imaging studies of Fig (**3.1A**).

First, we tried using different concentrations of the organic solvent Tetrahydrofuran (THF) to make the particles swell and enable drug to be loaded into the polystyrene beads. **Fig 3.2A** shows the shape and size of 2.1um beads in a water solution and **Fig 3.2B** shows how the particles swell when in 20% THF. After swelling occurred, we eliminated the THF from solution and allowed particles to return to their original size. Panel C (**Fig 3.2C**) provides the polydispersions of polystyrene beads after THF treatment as measured by flow cytometry.

However, MTT Cell Proliferation Analysis for A549 cells after Paclitaxel drug was loaded into the beads revealed that the particles loaded with this drug weren't able to release the drug to target cells and didn't show any significance difference with plain beads. Therefore we decided to load the particles into polystyrene beads in water so the drug can be adsorbed into their surfaces be later released to cancer cells to induce cell death (**Fig 3.3**)

### 3.2.3 – "self"-Peptide and anti-hCD47 on the surface of nanobeads targets human cancer cells

Tumors were induced in mice by injection of human lung cancer derived A549 cells, and control mice with untreated tumors received Cremophor® EL, the castor oil-based clinical solubilizing agent that is most commonly used clinically. This emulsifier has its own dose-limiting side effect, namely cardiotoxicity and nephrotoxicity *in vivo* (Kim 2001, Gligorov 2004). We established the cytotoxic effects of these beads *in vitro* (**Fig 3.4A,B**) and we also established the safety of the beads along with Cremophor® EL formulations after tail vein injection (**Fig 3.4E**). Cremophor® EL is well known to cause allergic reactions, and the NSG mice developed tail lesions that were severe enough to require tail amputations in most mice, whereas the nanobeads did not exhibit such an effect (**Fig 3.4F**). The nanobeads thus had a toxicity advantage. The NSG mouse results thus reveal active suppression of clearance by both human-CD47 and 'Self' peptide, thereby enhancing both tumor imaging and drug delivery.

Efficacy was studied with two bead systems. First, we compared the non-treated mice and the Cremophor® EL-paclitaxel treated mice to the same beads from Chapter 2, which were loaded with drug instead of dye. All of the drug treatments suppressed tumor growth at day-4 and not earlier. However, the CD47 beads also showed statistically significant tumor shrinkage similar to the standard Cremophor® EL-paclitaxel (Taxol) treatments but without the noted toxicity of Cremophor® EL (**Fig. 3.4C**).

Secondly, we targeted human cancer cells with antibodies against CD47. We attached a biotinylated anti-hCD47 to the beads instead of the opsonizing antibody (anti-Avidin), and we then showed that the anti-CD47 beads bind to A549 cells *in vitro*, and any such targeting antibody still acts *in vivo* as an opsonin and promotes clearance. The “self”-peptide blocks this clearance and the anti-CD47 antibody cannot bind “self”-peptide. PEG was also attached to the beads although it provides no advantage for antibody-targeted beads. The anti-CD47 target beads with “self”-peptide suppressed tumor growth after just one day, and were statistically better than beads without “self”-peptide (**Fig 3.4D**).

Tax-loaded beads that displayed either recombinant hCD47 (**Fig 3.4C**) or Self-peptide plus PEG and anti-hCD47 targeting antibody (**Fig 3.4D**) consistently shrunk tumors more than beads lacking ‘Self’. The ‘Self’ beads also did as well or better than the standard paclitaxel nanocarrier Cremophor®. The NSG mouse

results thus reveal active suppression of clearance by both human-CD47 and 'Self' peptide, thereby enhancing both tumor imaging and drug delivery.

### 3.3 – Discussion

The understanding of the CD47-SIRPα interaction is beginning to suggest possible applications for disease, as blocking of CD47 on tumor cells allows for tumor-associated macrophages to attack the tumor (Willingham 2012). CD47 on nanoparticles should likewise limit uptake of nanoparticle imaging agents and therapeutics by tumor-associated macrophages and thus improve delivery to cancer cells. While SIRPα is abundant on macrophages and its key downstream phosphatase SHP1 is unique to hematopoietic lineages (such as macrophages), SIRPα is also expressed on other cell types. The A549 cancer cells used here (**Fig. 3.1**) indeed express low levels of SIRPα, but we find that our nanobeads (±hCD47) are not internalized by A549 cells *in vitro* compared to the THP1 cells used in chapter 2 (**Figs. 2.2E, 2.3**). Enhanced imaging of tumors with hCD47 and "self"-peptide on Near-Infrared nanobeads (**Fig. 3.1**) is therefore likely to result from increased tumor perfusion of the particles and the subsequent Enhanced Permeation and Retention (EPR) effect. It should be pointed out that a particle which stays in circulation will not guarantee delivery to a tumor site (Hong 1999).

We showed that “self” peptide improves delivery when combined on nanobeads with bioactive drug against a therapeutic target, consistent with previous results reported recently in the literature (Majeti 2009, Chao 2012, Zhao 2012, Willingham 2012). This is done in combination because chemotherapeutics are increasingly being combined with antibodies for tumor targeting. Many chemotherapeutics such as Taxol can kill tumor cells but will also permeate many non-tumor tissues where cytotoxic effects limit the dose that can be administered to patients.

Here we have shown that the drug treatments suppressed tumor growth at day 4 (**Fig. 3.4C**) and not earlier. However, the CD47 beads also showed statistically significant tumor shrinkage similar to the standard Cremophor® EL-paclitaxel (Taxol) treatments but without the noted toxicity of the Cremophor® EL excipient.

We also reported that targeting the human cancer cells with antibody against CD47 attached to the nanobeads coated with “self”-peptide was able to suppress tumor growth in NSG mice after just one day of injection, which was statistically better than beads without “self”-peptide. Even though Biotinylated anti-hCD47 antibody acts *in vivo* as an opsonin and promotes clearance, the “self”-peptide is able to block this clearance (the anti-CD47 antibody cannot bind “self”-peptide). The upper inset in (**Fig 3.4D)** shows soluble hSIRPα binding to Self-peptide on beads with anti-hCD47, which indicates that anti-hCD47 does not

inhibit Self-peptide activity or binding. PEG was also attached to the beads as a control, as it provides no advantage for antibody-targeted beads.

In this study, we have thus shown that nanobeads coated with “self” peptide and anti-CD47 antibody are a promising novel therapeutic target for cancer cells. Blocking CD47-SIRPα interaction promoted the phagocytosis of tumor cells and inhibited their growth. In order to draw further conclusions about the anti-cancer effects of these nanobeads, more drug doses and cytotoxic effects need to be evaluated. Still, it is a promising idea to combine a “self” peptide with targeting antibodies; perhaps a better delivery system such as filomicelles or toroidal polymers rather than polystyrene beads would be desirable as the study moves onto clinical stages.

## 3.4 – Materials and methods

### 3.4.1 – Chemicals

Dulbecco’s phosphate-buffered saline (DPBS) without $Ca^{2+}$ or $Mg^{2+}$ (Invitrogen) was supplemented with 1% BSA. Hoechst 33342 (Invitrogen, Carlsbad, CA) was used for DNA stains. The near-infrared lipophilic dye, DiR, was purchased from Invitrogen, Inc. and PKH26 Red Fluorescent Cell Linker Kit for General Cell Membrane Labeling from Sigma Aldrich. Chloroform, methanol, and hydrochloric acid were purchased from Fisher Scientific. N-Biotinyl-NH-(PEG)4-COOH was purchased from EMD Chemicals Inc., PEG Biotin, MW 550

was purchased from Nanocs Inc., and mPEG-Biotin, MW 5,000 from Laysan Bio Inc.

### 3.4.2 – Antibodies

The fluorescein-labeled antibody B6H12-FITC (BD Biosciences) and mIAP301-FITC (BD Biosciences) were used against human CD47 and mouse CD47 respectively. Opsonizing antibodies streptavidin coated polystyrene beads (Spherotech) included rabbit anti-streptavidin (Sigma-Aldrich), rabbit anti-streptavidin conjugated with FITC (Rockland Immunochemicals) and Biotin anti-human CD47 Antibody (BioLegend) were used as IgG opsonin. Secondary antibodies used for detecting opsonin levels and uningested beads included goat anti-rabbit FITC or goat anti-rabbit $F(ab')_2$ R-PE (Sigma-Aldrich). Primary antibody used to measure the level of PEG molecules bounded to streptavidin coated polystyrene beads was Biotin-4–fluorescein (Anaspec).

### 3.4.3 – Biodistribution Study with dye-labeled Beads

All mice were treated in accordance with approved IACUC protocols at the University of Pennsylvania. Near Infrared Fluorophore (NIRF)-labeled and unlabeled streptavidin coated polystyrene beads were injected into the tail veins of healthy Adult Immune-deficient (NSG) Mice (4-8 weeks). The range of injected beads was ~$10^7$ per ml, with some variability due to accuracy of locating the tail vein. Every 10 min, 50µl blood samples were collected by retro-orbital

bleeding. At 35min following injection, mice were sacrificed and whole blood, liver, spleen, lungs, kidneys, heart and brain were collected. The whole blood was then centrifuged and plasma collected.

Organs were imaged on the LiCor Odyssey imaging system (LI-COR Biosciences, Lincoln, NE) at 800 nm excitation. The integrated fluorescence intensity of the organs was normalized using the organ correction factor found by Christian et. al. (Christian 2009) and applied to all other measured intensities for all organs. The NIR intensity of the plasma was measured on the LiCor and calculated by fitting the slope of the linear dilution curve.

The fraction of total blood in the tumor must be estimated in order to determine the % of injected nanobeads within the Tumor blood (**Fig. 3.1C, inset**). The typical tumor weight is about 500 mg, which we approximate as 1 g, and assume the tumor has 10% blood volume like other highly vascularized tissues such as liver and spleen (Baxter 1994). One measurement reported tumors are ~2% blood by volume (Jain 1988), so the assume values of 10% and 1 g provide an overestimation of the amount of NIR intensity in the tumor provided by NIRF-labeled particles in the blood. This overestimation allows us to safely determine that particles functionalized with “self”-peptide or hCD47 have entered the tumor stroma.

### 3.4.4 – A549 anti-CD47 binding experiments.

In a first step, A549 cells were preincubated either with 15μl of CD47-B6H12-FITC at saturating levels (BD Biosciences) or with 10 μg/mL of Biotin anti-CD47 antibody (Biolegend) for 30 minutes on ice. The cells were then stained with Cy5 conjugated Affinity Purified Anti-Biotin goat (Rockland Immunochemicals). After washing twice, cells were analyzed on a flow cytometer.

### 3.4.5 – Biodistribution Study with Two Color-labeled Beads in Tumor-bearing NSG Mice

$10^6$ human lung carcinoma A549 cells suspended in PBS with 25% Matrigel (BD Bioscience) were injected subcutaneously into both flank sites of each NSG mouse. After about 5 weeks, the tumor-bearing mice received tail vein injection of the mixture of DiD and NIR dye-coated beads. Fluorescent intensity from both dyes in tumor areas was monitored at 10min, 40min, 90min and 120min, using IVIS Spectrum Imaging System (Caliper Life Sciences, Hopkinton, MA). After 120 min post-injection, the mice were sacrificed for harvesting tumors as well as organs (liver, spleen, lungs, kidneys, heart, brain). Tumors and organs were imaged on the LiCor Odyssey imaging system (LI-COR Biosciences, Lincoln, NE) at 800 nm excitation.

### 3.4.6 – Paclitaxel loading

$10^8$ polystyrene beads were suspended in 300 mL Milli-Q water. 5 mL of 4.5 mg/mL paclitaxel (LC Laboratories) in methanol was added to the beads to achieve 75 mg/mL concentration. After overnight incubation at room temperature and following spin-down, beads were re-suspended in PBS with 10-fold concentration. If necessary, beads surface was modified by attaching molecules.

### 3.4.7 – MTT Assay

5000 A549 cells were seeded on wells of 96-well plate, 24 hours prior to drug treatment. Cells were treated with series dilution of beads samples loaded with paclitaxel, starting from 7.5 mg/mL. After 24 hours incubation at 37°C with 5% CO2, cells were washed once with PBS and added with 100 mL growth medium and 20 mL of 5 mg/mL Thyazolyl Blue Tetrazolium Bromide (Sigma). After 4 hours incubation at 37°C with 5% CO2, purple crystal in the cells were solubilized by adding 100 mL DMSO. Absorbance was read at 560 nm.

### 3.4.8 – Checking body weight loss by paclitaxel-loaded beads treatment

NSG mice received intravenous (i.v.) injection of paclitaxel-loaded beads or Cremophor® EL (Sigma) at a dose of 7.5 mg/kg. To check weight loss by treatments, body weight of each mouse was measured right before and 24 hours after the injection.

### 3.4.9 – Tumor inhibition study

After a month of cancer cell inoculation, tumor-bearing mice were treated with 4 daily injections (i.v.) of paclitaxel-loaded beads at a dose of 7.5 mg/kg. Tumor size was measured on daily basis, giving an estimation of volume with

$$\text{Tumor volume} = \tfrac{1}{2} * (\text{major axis}) * (\text{minor axis})^2$$

As a positive control for tumor shrinkage, paclitaxel solubilized with Cremophor® EL was injected at 22 mg/kg.

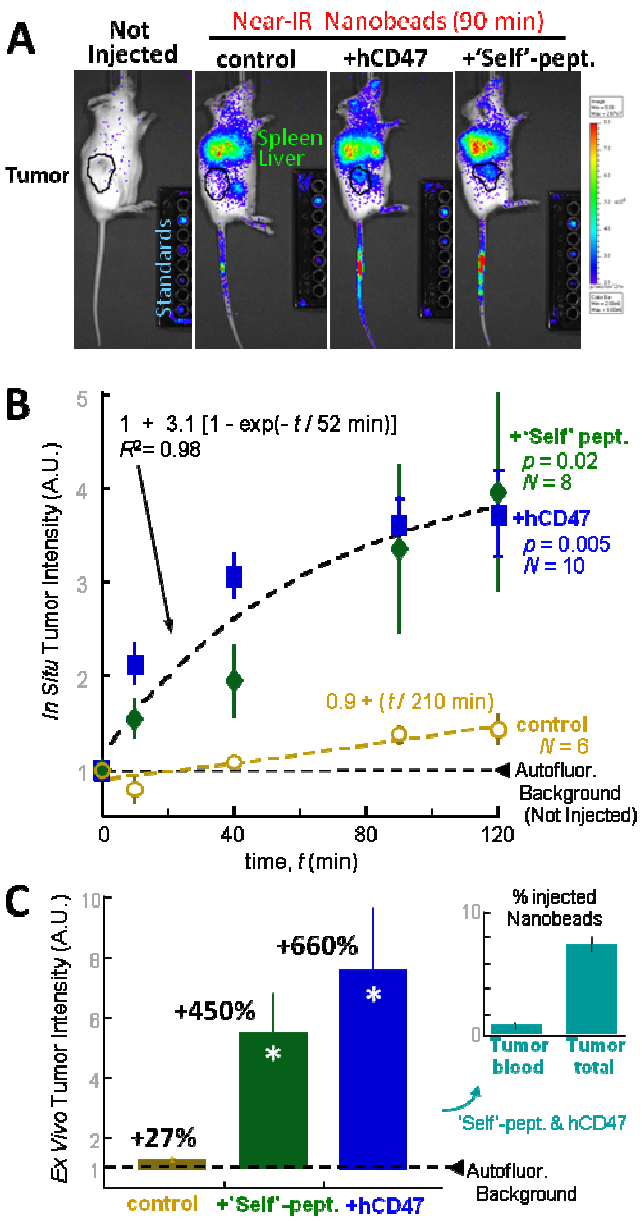


**Fig.3.1.- "self"-peptide and human-CD47 enhance tumor imaging by Near-Infrared particles.**

**(A)** NSG mice with flank tumors of A549 lung-derived cells (black circles) received tail vein injections of nanobead mixtures in which one bead type is labeled with DiR fluorophore. Images of live mice and calibration standards were taken with a Xenogen imager (IVIS Spectrum Imaging System, Caliper Life Sciences). Tumor-bearing mice have persistence ratios of particles in blood at 35 min similar to results in Fig.2.1C, even though many particles are seen in spleen and liver. **(B)** The tumor region was estimated in the brightfield image for quantitation of total fluorescence at each time point, and all results for "self"-peptide and hCD47 were combined in the fit. Results are cumulated from all tumors from three different sets of tumor-bearing mice. *N,* Number of tumors. **(C)** Tumors were harvested from one set of tumor-bearing mice for *ex vivo* quantitation by an Odyssey imaging system (LI-COR Biosciences). For control, $N = 2$; for "self"-peptide, $N = 4$; and for hCD47, $N = 6$ tumors. Inset bargraph shows the high percentage of nanobeads in the tumor compared to an upper bound (see Methods) for the nanobeads in the blood vessels within the tumors ($n = 2$).

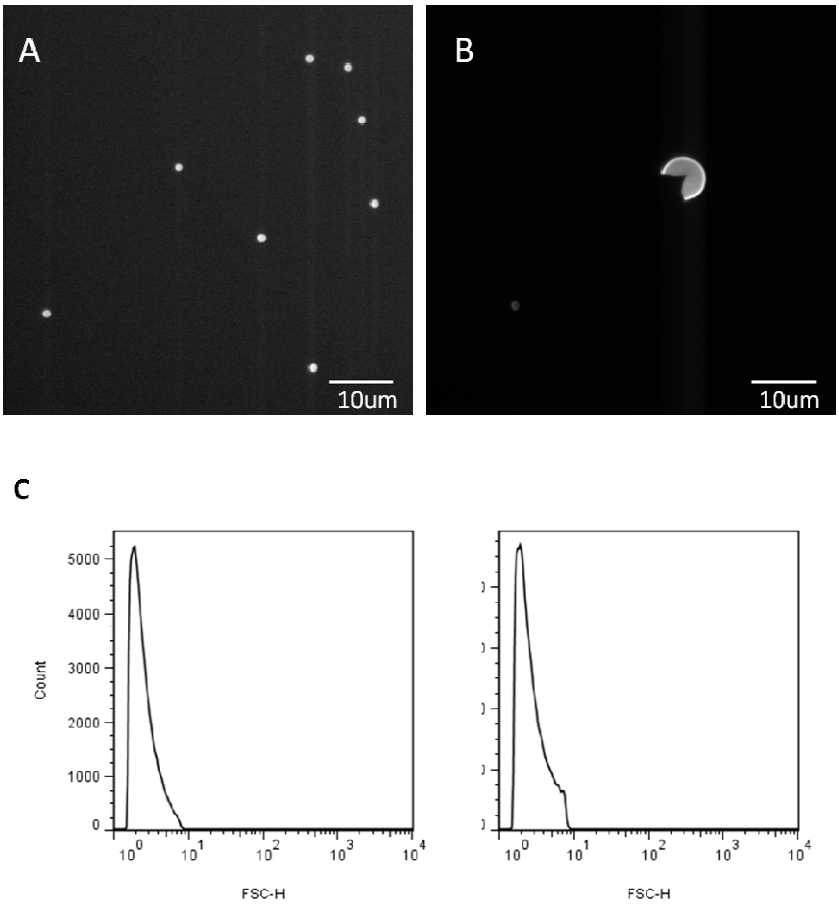


**Fig. 3.2.- Taxol drug loading in polystyrene beads.**

**(A)** Optical microscope images of 2.1µm polystyrene particles in water solution. **(B)** Optical microscope images of 2.1µm polystyrene particles in 80%water and 20%THF solution **(C)** Flow cytometry forward scatter plot for 2.1µm polystyrene particles in water (panel left) and after adding 20%THF to the water solution (panel right).

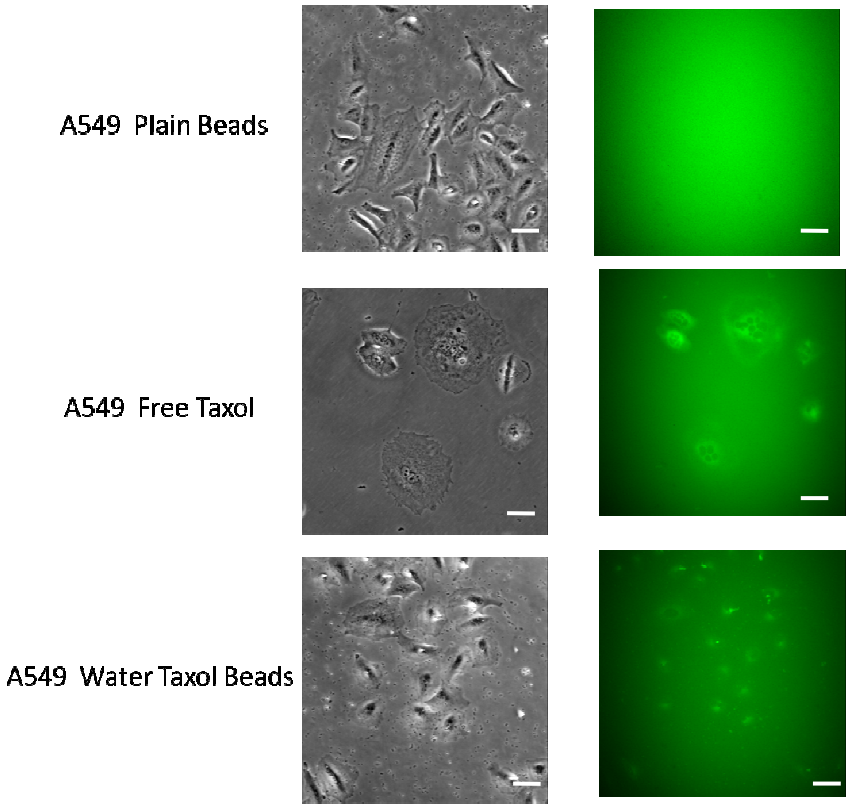


**Fig. 3.3.- Taxol drug loading in polystyrene beads added to A549 cells.**

Bright field images at the left side and fluorescence images of Green 488 paclitaxel at the right side are shown for A549 cells after 24 hours of for A549 cells after Paclitaxel drug was added. The upper representative picture is presented to illustrate the non toxicity effect of the particles in A549 cells. The middle and bottom pictures illustrate 2 different conditions for drug loading into A549 cells: In solution and loaded on the surface of polystyrene beads. Scale bar, 10um.

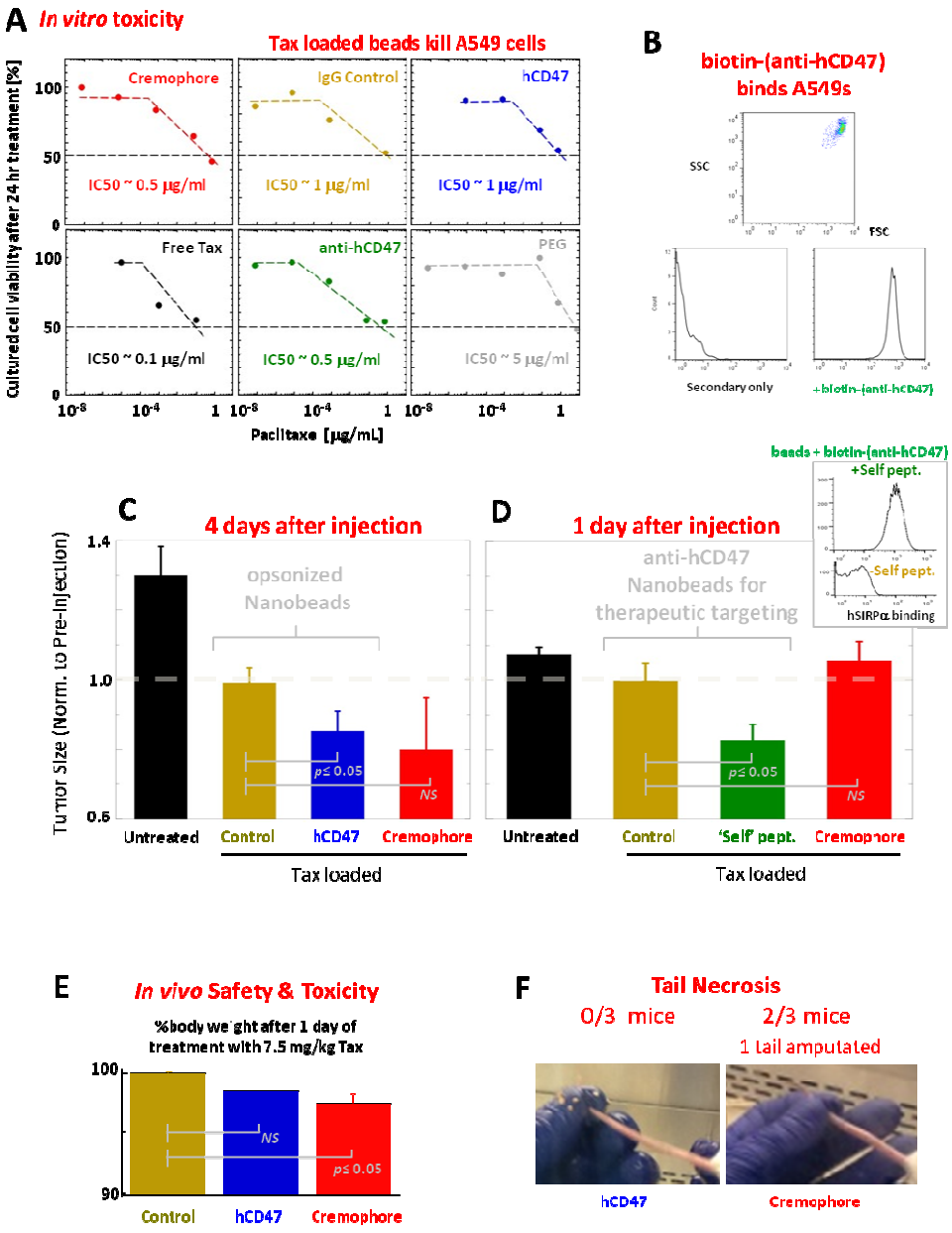


**Fig. 3.4.- Recombinant hCD47 protein or synthetic "Self"peptide can enhance the effect of an anti-cancer drug.**

**(A)** In vitro viability of A549 human lung cancer derived cells in the presence of various formulations with Paclitaxel (Tax), which is a common anti-cancer drug in wide clinical use against solid tumors including lung tumors. Cremophore is a standard clinical carrier of Tax. Nanobeads of the four rightmost panels are, clockwise: IgG control with anti-Streptavidin, IgG plus biotin-hCD47 per Fig. 1C and 2, PEG-biotin, and biotin-(anti-hCD47) (without anti-Streptavidin). Cell viability was measured by standard MTT assay to determine the 50% inhibition constant (IC50). **(B)** Targeting of A549 cells with biotin-(anti-hCD47). Upper panel shows the cancer cells by forward/side scatter, lower left panel shows non-specific binding of the secondary Ab Cy5-anti-Biotin, and the lower right panel shows the specific binding between cells and biotin-(anti-hCD47). **(C)** Tumor sizes 4 days after daily injections and normalized to initial A549 tumors. Control Tax-nanobeads have anti-Streptavidin IgG (per Fig. 2.1C) and hCD47 Tax-nanobeads also have this IgG; all beads were injected at the maximum drug load of 7.5 mg/kg Tax, whereas Tax-Cremophore was injected at 22 mg/kg. None of the drug treatments showed significant shrinkage until day-4. Tumor sizes were measured daily. (n ≥ 3 mice; ±SEM). **(D)** Small molecule therapeutics are increasingly being combined with targeting antibodies, and we hypothesized that adding Self-peptide would provide further advantage. Tumor sizes were measured 1 day after a single injection of targeted Control Tax-nanobeads (anti-hCD47 IgG + PEG) or targeted Self-peptide Tax-nanobeads (Self-pept. + anti-hCD47 IgG + PEG). CD47 is considered a therapeutic target on cancer cells, and chemotherapeutics are increasingly being combined with therapeutic antibodies as here. Note that Tax-Cremophore has no significant effect at day-1, whereas Self-peptide effectively shrinks the tumors. (n ≥ 3 mice; ±SEM). The upper inset shows soluble hSIRPα binding to Self-peptide on beads with anti-hCD47, which indicates that anti-hCD47 does not inhibit Self-peptide activity. **(E)** In vivo safety of 7.5 mg/kg Tax was assessed by measuring body weight changes 24 hr after injection (n = 3 mice each). All mice showed <10% body weight loss, which is the conventional maximum for a tolerable dose, but Tax-Cremophore alone gave a statistically significant loss of body weight. (F) As part of efficacy studies at a higher therapeutic dose of 22 mg/kg Tax-Cremophore, visibly necrotic tails near the site of injection (images) were evident in 2 of 3 mice injected with Tax-Cremophore, with 1 mouse requiring amputation of the tail based on standard of care criteria. Cremophor is well known to cause allergic reactions, but the higher dose was otherwise tolerated with weight losses <10% body weight. The hCD47 tax-nanobeads showed no significant loss of body weight and no tail necrosis. All data are mean ±SEM.

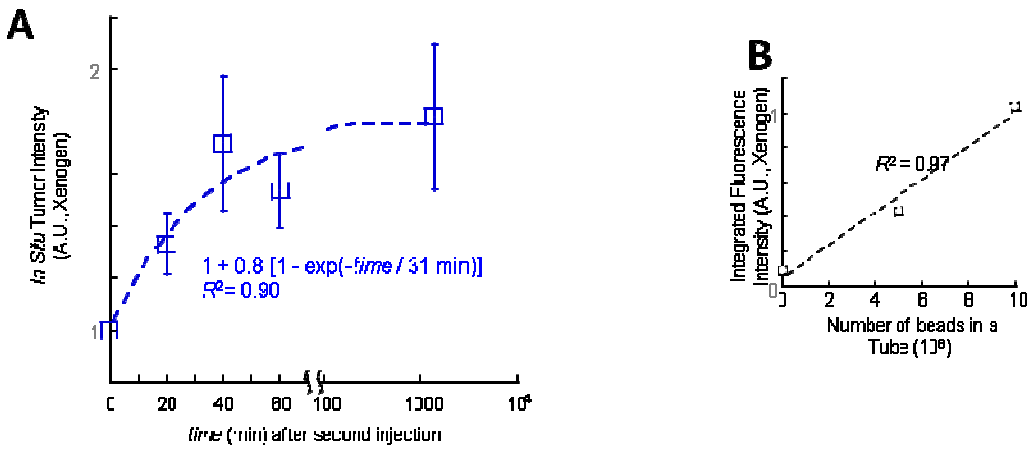


**Fig.3.S1.- Tumor imaging is enhanced after second injection of hCD47-Nanobeads.**

**(A)** Tumor imaging is enhanced after second injection of hCD47-Nanobeads at 120 min after first injection. **(B)** Calibration of fluorescence emission and number of beads using a Xenogen IVIS Spectrum Imaging System (Caliper Life Sciences, Hopkinton, MA).

## 3.5 – References


1. J.B. Swann, M.J. Smyth, Immune surveillance of tumors. J Clin Invest **117**:1137-1146 (2007).
2. M.P. Chao *et al*., Therapeutic antibody targeting of CD47 eliminates human acute lymphoblastic leukemia. Cancer Res **71**:1374-1384 (2011).
3. M.P. Chao, I.L. Weissman, R. Majeti, The CD47-SIRPα pathway in cancer immune evasion and potential therapeutic implications. Curr Opin Immunol **24**(2):225-32 (2012).
4. X. W. Zhao *et al*., CD47-signal regulatory protein-alpha (SIRPalpha) interactions form a barrier for antibody-mediated tumor cell destruction. Proc Natl Acad Sci U S A **108**:18342-18347 (2011).
5. R. Majeti *et al*., CD47 is an adverse prognostic factor and therapeutic antibody target on human acute myeloid leukemia stem cells. Cell **138**:286-299 (2009).
6. S.J. Gardai *et al*., Cell-surface calreticulin initiates clearance of viable or apoptotic cells through trans-activation of LRP on the phagocyte. Cell **123**:321-334 (2005).
7. M. Obeid *et al*., Calreticulin exposure dictates the immunogenicity of cancer cell death. Nat Med **13**:54-61 (2007).
8. D. W. Bartlett, H. Su, I.J. Hildebrandt, W.A. Weber, M.E. Davis, Impact of tumor-specific targeting on the biodistribution and efficacy of siRNA nanoparticles measured by multimodality in vivo imaging. *Proc Natl Acad Sci USA*. **104**(39):15549-54 (2007).
9. A. L. libanov, K. Maruyama, A. M. Beckerleg, V. P. Torchilin, L. Huang, Activity of amphipathic poly(ethylene glycol) 5000 to prolong the circulation time of liposomes depends on the liposome size and is unfavorable for immunoliposome binding to target. *Biochim Biophys Acta.* **1062**(2):142-8 (1991).
10. P. J. Photos , L. Bacakova , B. Discher, F. S. Bates, D. E. Discher, Polymer vesicles in vivo: correlations with PEG molecular weight. *J Control Release*. **90**(3):323-34 (2003).
11. M. J. Turk, D. J. Waters, P. S. Low, Folate-conjugated liposomes preferentially target macrophages associated with ovarian carcinoma. *Cancer Lett*. **213**(2):165-72 (2004).
12. R. Rossin, S. Muro, M. J. Welch, V. R. Muzykantov, D. P. Schuster, In vivo imaging of 64Cu-labeled polymer nanoparticles targeted to the lung endothelium. *J Nucl Med*. **49**(1):103-11 (2008).
13. I. Mouro-Chanteloup *et al*., Evidence that the red cell skeleton protein 4.2 interacts with the Rh membrane complex member CD47. *Blood.* **101**(1):338-44 (2003).
14. S. Subramanian, R. Parthasarathy, S. Sen, E. T. Boder, D. E. Discher, Species- and cell type-specific interactions between CD47 and human SIRPalpha. *Blood.* **107**(6): 2548-2556 (2006).
15. Y. Matsumura, H. Maeda, A new concept for macromolecular therapeutics in cancer chemotherapy: mechanism of tumoritropic accumulation of proteins and the antitumor agent smancs. *Cancer Research*. **46**(12 Pt 1):6387-92 (1986).

16. H. Cabral *et al*., Accumulation of sub-100 nm polymeric micelles in poorly permeable tumours depends on size. *Nat Nanotechnol.* **6**(12):815-23 (2011).
17. T.Y. Kim et al., Phase I and pharmacokinetic study of Genexol-PM, a cremophor-free, polymeric micelle-formulated
paclitaxel, in patients with advanced malignancies. Clinical Cancer Research **10**:3708–3716.( 2004)
18. J. Gligorov, J.P. Lotz. Preclinical pharmacology of the taxanes: Implications of the differences. Oncologist **9**:3–8. (2004).
19. S.C. Kim et al., In vivo evaluation of polymeric micellar paclitaxel formulation: toxicity and efficacy. Journal of Controlled Release **72**:191– 202. (2001)
20. S. B. Willingham et al., The CD47-signal regulatory protein alpha (SIRPa) interaction is a therapeutic target for human solid tumors. Proc Natl Acad Sci USA. doi/10.1073/pnas.1121623109 (2012).
21. D. A. Christian et al., Flexible filaments for in vivo imaging and delivery: persistent circulation of filomicelles opens the dosage window for sustained tumor shrinkage. Mol Pharm. **6**(5):1343-52 (2009).
22. L. T. Baxter, H. Zhu, D. G. Mackensen, R. K. Jain, Physiologically based pharmacokinetic model for specific and nonspecific monoclonal antibodies and fragments in normal tissues and human tumor xenografts in nude mice. Cancer Res.**54**(6):1517-28 (1994).
23. R. K. Jain, Determinants of tumor blood flow: a review. Cancer Res. **48**(10):2641-58 (1988).

# CHAPTER 4 – Modeling the implications of SIRPα binding to CD47 *in cis* (on the same cell surface) on SIRPα's ability to bind to CD47 *in trans* (on target cells)

Pia L. Rodriguez, Richard K. Tsai, Diego Pantano and Dennis E. Discher

Dr. Tsai provided the generation of the lentivirus knockdown on CD47, the expression studies in CHO cells and helped with sheep phagocytosis. Also he provided general discussion of the subject. Dr. Pantano provided the Normal mode analysis of SIRPα.

**Abstract**

A large number of membrane proteins possess extracellular domains that interact with extracellular domains of other membrane proteins, transducing important signals to cells. Such interactions can occur either *in cis* (both proteins on the same cell's surface) or *in trans* (proteins embedded in membranes of different cells.) These two possibilities raise important questions about the differences between signaling that occurs *in cis* vs. *in trans*. Many cells express not only the ubiquitous 'Marker of Self' protein CD47 but also some level of its counter-receptor SIRPα (CD172). Here we show that CD47-SIRPα interactions occur not only *in trans* in cell-cell adhesion, but also in *cis*, modulating downstream signals. Activation is clearly increased with CD47-SIRPα interactions *in trans*, resulting in the inhibition of phagocytosis of any CD47-displaying target. Knocking down CD47 on macrophages decreases the level of basal signaling, increases binding of soluble CD47, and enhances phagocytosis of opsonized targets above wild-type cells. When multiple knockdowns are performed, the effective Kd for binding in trans is shown to depend linearly on *cis* CD47 on the macrophage, consistent with the simplest mathematical modeling for *cis* vs. *trans* competition. *Cis* interactions might be unavoidable with this system and others studied, but it is also possible that by lowering the threshold at which activation exceeds inhibition, *cis* interactions may optimize discrimination *in trans*.

## 4.1 – Introduction

Macrophages like other innate immune cells have the ability to clear foreign and apoptotic cells. The recognition of these foreign or host cells is induced through direct recognition by conserved receptors such as complement and Fc receptors that lead to clearance by phagocytosis (Tenner, Robinson et al. 1995; Ravetch 1997). Recognition of foreign cells may occur through antigen recognition, resulting in IgG opsonization (Ravetch and Clynes 1998) that is not limited to foreign cells, but autologous cells as well (Turrini, Mannu et al. 1993). Binding of macrophage Fcγ-R to IgG opsonin on a target cell leads to extension of pseudopodia, creating a phagocytic synapse that "zipper" around the target with increasing activation signal (Swanson and Baer 1995). However when host cells express CD47 and IgG-opsonized they are recognized by receptors transmitting both activating and inhibitory signals to the macrophage. The inhibitory signal is occurs when self cells express CD47 that bind to the immune inhibitory receptor, SIRPα (Seiffert, Cant et al. 1999). The integration of these signal inputs determines whether the target cells will undergo clearance.

This ubiquitously expressed protein CD47 protein is an Ig superfamily member that interacts specifically with SIRPα found on macrophages (Jiang, Lagenaur et al. 1999; Seiffert, Cant et al. 1999; Vernon-Wilson, Kee et al. 2000). This receptor-ligand interaction signals self in macrophages, enabling

selective phagocytosis of foreign cells or particles. Phosphorylation of the immune-receptor tyrosine-based inhibitory motif (ITIM) in the cytoplasmic domain of SIRPα upon ligation with CD47 leads to the recruitment of SHP-1 and deactivation of phagocytosis (Vernon-Wilson, Kee et al. 2000; Seiffert, Brossart et al. 2001). The loss of CD47 protein in red blood cells (RBCs) and apoptotic cells results in the susceptibility of these self cells to clearance by macrophages (Oldenborg, Zheleznyak et al. 2000; Anniss and Sparrow 2002; Krieser and White 2002; Gardai, McPhillips et al. 2005).

The receptor SIRPα is composed of three IgSF domains while CD47 contains only a single IgSF domain with a disulfide link between one of the loops between the transmembrane regions (Tsai, 2008), which may be required for optimal binding of SIRPα (Rebres, Vaz et al. 2001). The crystal structure of SIRPα-CD47 complex indicates that the loops of SIRPα are highly flexible, and that CD47 binds at the N-terminal ligand-binding domain of SIRPα (Hatherley, Graham et al. 2008). CD47 has a high specificity to SIRPα. The regions of the mammalian brain in which CD47 is particularly abundant overlap substantially with those enriched in SIRPα (Mi, Z.P. et al. 2000, Ohnishi, H. et al. 2005). The similar expression patterns of SIRPα and CD47 in the brain indicate that the transinteraction of the two proteins mediates intercellular signaling in a bidirectional manner. By contrast, SIRPα is barely detectable in red blood cells (RBCs) or in T or B lymphocytes, whereas CD47 is expressed in a variety of

hematopoietic cells (Adams, S. et al. 1998, Veillette, A. et al. 1998, Seiffert, M. et al. 1999, Seiffert, M. et al. 2001, Brown, E.J. and Frazier, W.A. 2001). CD47 or SIRPα might thus mediate unidirectional signalling in the hematopoietic or immune systems. For instance, the binding of CD47 on RBCs (in which minimal expression of SIRPα exists) to SIRPα of macrophages regulates phagocytosis by macrophages in a unidirectional manner (Matozaki, Murata et al. 2009). CD47 binding to SIRPα is relatively low affinity, and is less important for cell-cell adhesion (Hatherley, Harlos et al. 2007; Subramanian, Boder et al. 2007). The lower affinity interaction of CD47-SIRPα allows for rapid interaction on the macrophage surface from intracellular (cis) to intercellular (trans) binding to target cells.

Expression of both SIRPα and CD47 on the surface of macrophages raises the possibility that these proteins interact on the same macrophage surface (in cis). If so, this would have implications for SIRPα's ability to bind to CD47 on target cells (in trans) (Doucey, Scarpellino et al. 2004). To explore the possibility that SIRPα and CD47 can interact in cis, we used a CHO cell display system. CHO cells expressing human SIRPα were co-expressed with or without human CD47. We demonstrated that the binding excluded simultaneous cis and trans interaction due to a specific binding site in the SIRPα receptor (Hatherley, Harlos et al. 2007). The functional implication of cis interaction was demonstrated with CD47 knockdown macrophages that indicated higher level of phagocytosis

of IgG-opsonized sheep RBCs. This was a consequent of the loss of the inhibitory signal associated with CD47-SIRPα interaction via cis. However this had no effect on the phagocytosis of IgG-opsonized human RBCs. From our earlier studies with human macrophages, the phagocytic synapse extended but eventually retracted. This delayed retraction occurs due to the competitive binding of SIRPα with CD47 from cis on macrophage surface to trans on target cells.

## 4.2 – Results

### 4.2.1– Expression profiles of CD47 and SIRPα in human cells

CD47 expressed on the surface of self cells prevents elimination of these cells by binding to the inhibitory receptor SIRPα on the surface of phagocytes. Once it is activated, SIRPα inhibits pro-phagocytic signals from Fc and complement receptors, resulting in inhibition of phagocytosis (de Almeida 2009). In agreement with previous reports (Brown and Frazier 2001), flow cytometry analysis revealed that all cells (both professional and non-professional phagocytes) express CD47 (**Fig. 4.S1 and 4.S2**). The level of CD47 expression was high in red blood cells compared to other eukaryotic cells explored based on total CD47 expression. Mature RBCs express high copies of CD47 protein on the surface because they are unable to further express CD47 after erythropoiesis (Furusawa, Yanai et al. 1998) unlike other eukaryotic cells. As RBCs age the

level of CD47 proteins are reduced that eventually lead to clearance (Anniss and Sparrow 2002). However we have previously reported that only 10-20% CD47 density of normal human RBC (hRBC) is necessary to inhibit uptake by human macrophages (Tsai and Discher 2008). In each of the cell types explored, the number of CD47 molecules was above the necessary minimum of ~20 CD47 molecules/μm2. In contrast to CD47, we found that SIRPα expression was restricted to phagocytes, including human THP-1 macrophages, peripheral blood monocytes (PBMC) and, in lower levels, human mesenchymal stem cells (MSC). One interesting observation was that human hematopoietic stem cells displayed SIRPα expression that was very similar to the one found in THP-1 macrophages, but only after being cultured and induced with granulocyte colony-stimulating factor (G-CSF) for 7 days (**Fig. 4.1A**). The expression of SIRPα on MSC is in agreement with other studies (Vogel, Grunebach et al. 2003) suggesting that these cells express Fcγ-R and exhibit low phagocytic capabilities (Charriere, Cousin et al. 2006). THP-1 macrophages and MSC had a ratio of 3.2 and 10.9 CD47 to SIRPα molecules respectively (**Fig. 4.1**). This was calculated based on flow cytometry analysis using antibodies against CD47 and SIRPα to obtain the ratio in unpermeabilized live cells. In both cell types the total level of CD47 was observed to be higher than total level of SIRPα suggesting that macrophages can signal self when in contact with other macrophages.

To address the molecular basis of the reduced inhibition through SIRPα in the presence of CD47, we sought to explore the phosphorylation signal that associates with CD47-SIRPα ligation. SIRPα interaction by trans with targets presenting CD47 (**Fig. 4.2A**) triggers SIRPα's immunorecptor tyrosine-based inhibiting motif (ITIM) activation (Kharitonenkov, Chen et al. 1997) and subsequent SHP-1 phosphatase induction (Brown and Frazier 2001; Latour, Tanaka et al. 2001), ultimately leading to the inhibition of phagocytosis. Previous studies showed an inherent endogenous SIRPα phosphorylation in macrophages alone without the presence of IgG-opsonized targets (Oldenborg, Zheleznyak et al. 2000; Ide, Wang et al. 2007; Tsai and Discher 2008) which may be attributed to the cis interaction on macrophages that we observed in our studies above.

### 4.2.2 – Reduced SIRPα function and foreign cell phagocytosis

In order to directly assess the function of the cis interaction on macrophages, CD47 expression was suppressed using RNA interference. The expression of CD47 was reduced to levels ranging from 13% to 50% wild-type levels (**Fig. 4.S3A**) while the levels of SIRPα on these macrophages remained unchanged.

As observed in the CHO cell system, the level of soluble hSIRPα trans interaction was reduced (**Fig. 4.6C**) we sought to explore the difference in binding affinity in THP-1 macrophages at physiological levels of CD47 and SIRPα

as opposed to the extreme overexpressions of CD47 co-expression with SIRPα on CHO cells. The macrophages tested demonstrated a moderate affinity and saturable interaction of hSIRPα for CD47 in wild-type and the two CD47 blocking antibody (**Fig. 4.3A**). The binding affinity in wild-type (WT) THP-1 macrophages was 1.6 μM with increasing binding affinity to 0.26 μM in cells with blocking anti-hCD47 antibody B6H12 (clone with high specificity to hCD47 protein) and the binding affinity remain the same in the case of blocking anti-hCD47 antibody 2D3 used as a negative control due to its low specificity to hCD47. The binding affinity increased to 0.26 μM in cells with ~13% wild-type CD47 levels (CD47′ THP-1 cells) and to 0.87 μM in cells with ~48% wild-type CD47 levels (**Fig. 4.3B**). A linear relationship was observed in relation to CD47 expression level and the measured dissociation constant, Kd where the reduction or elimination of the cis interaction between CD47 and SIRPα led to a higher binding affinity with soluble hCD47 (**Fig. 4.3C**). The reduction of CD47-SIRPα cis interaction led to a linear decrease in tyrosine phosphorylation (**Fig. 4.4B**). These results suggest that CD47-SIRPα may affect the efficiency of macrophages to differentiate non-self and self because of the inherent phosphorylation signal associated with cis interaction.

In order to understand the role of CD47-SIRPα cis interaction in phagocytosis, IgG-opsonized sheep and human red blood cells (RBCs) were used as targets for THP-1 macrophage WT and CD47′ THP-1 cells.

Phagocytosis by THP-1 macrophages was studied by imaging in differential interference contrast (DIC) microscopy and quantified by the number of ingested RBCs per macrophage. The internalization of sheep RBC was seen to increase by 20% with CD47′ THP-1 cells compared to wild-type macrophages, but human RBC targets showed no statistical difference ($p = 0.12$) (**Fig. 4.5A**). We used two CD47 suppression vectors that showed no difference in phagocytosis of human RBCs compared to WT THP-1 macrophages. In order to assess that lentiviral KD did not impact THP-1 macrophages phagocytic capabilities, a mock knockdown was performed that showed IgG-opsonized ShRBC had comparable level of phagocytosis to THP-1 WT and knockdown (KD) controls (**Fig. 4.S5**).

RBCs are common targets used in phagocytosis studies, but RBC membranes are complex. We therefore tested whether particles with or without CD47 had similar trends as observed with the RBC targets. The extracellular immunoglobulin-like domains of human CD47 (hCD47) was recombinantly expressed and attached to streptavidin-coated particles (2.1 μm). To study phagocytosis, beads were IgG-opsonized by pre-treatment with anti-streptavidin to induce FcγR-mediated phagocytosis (Tsai and Discher 2008). As with our RBC studies (**Fig. 4.5A**), a ~50% higher level of phagocytosis of uncoated beads was observed in 13% WT CD47 compared to WT THP-1 (**Fig. 5B**). Particles coated with hCD47 at the lower limit necessary for inhibition (~24 CD47 molecules/μm2) showed no difference in phagocytosis. The results from both the

RBC and particle targets showed an increase in phagocytosis of non-self targets due to lower cis interaction.

In order to determine if CD47 and SIRPα indeed interact in cis, we sought to explore the extreme case by overexpressing both proteins in a model CHO display system where expression levels can be controlled (Subramanian, Boder et al. 2007). We first compared the effect of CD47 on protein localization on the surface. CHO cells co-expressed with human SIRPα showed a reduced level of antibody binding compared to hCD47-GFP expression alone (**Fig. 4.6A**). The level of anti-hCD47 antibody bound was drastically reduced in cells co-expressing hCD47-GFP and hSIRPα across the different levels of hCD47-GFP expression suggesting a competitive interaction (**Fig. 4.6B**). Similar to the observations with anti-hCD47 antibody hSIRPα bound signal was reduced to near background levels in CHO cells co-expressing hCD47 and hSIRPα (**Fig. 4.6C**).

### 4.2.3 – SIRPα and CD47 physically associated in cis

In order to determine if CD47 and SIRPα indeed interact in cis, we sought to explore the extreme case by overexpressing both proteins in a model CHO display system where expression levels can be controlled (Subramanian, Boder et al. 2007). We first compared the effect of CD47 on protein localization on the surface. Fluorescent microscopy images of unpermeabilized CHO cells

expressing hCD47-GFP showed localization of anti-hCD47 antibody labeling and soluble human SIRPα (hSIRPα) confirmed pool of hCD47-GFP was properly displayed on the surface and functional (**Fig. 4.6**). In order to rule out the possibility that the co-expression of hSIRPα was masking the epitope for the CD47 antibody (clone 2D3), a number of additional antibodies were used each recognizing different epitopes of human CD47 confirmed the above results of reduced binding (**Fig. 4.S6B**). Poor multimeric binding to SIRPα in the presence of CD47 may be the due to steric hindrance as a result of direct or indirect association within the plane of the same membrane (in cis).

### 4.3– Describing a model for the competitive binding between CD47-SIRPα *in cis* and *in trans* interactions

In order to understand the competitive binding occurring during the interaction of SIRPα and CD47 in cis or in trans, we developed an equilibrium model (**Fig. 4.3**). We assumed that the two CD47 ligands—denoted as trans ($C_t$) or cis ($C_c$)-- could only occupy a single site on the macrophages SIRPα ($S_v$) (Rebres, Kajihara et al. 2005; Takenaka, Prasolava et al. 2007). Binding constant for cis and trans interactions was defined as $K_c$ and $K_t$ respectively. We began calculating the fractional occupation of the site, θ by trans-CD47 (Eq. 1.1).

$$\theta = \frac{K_t C_t}{1 + K_c C_c + K_t C_t} \qquad \text{(Eq. 4.1)}$$

The free receptor SIRPα and ligand concentration CD47 was related to the chemical equilibrium through the dissociation constant, $K_d$ ($k_{off}/k_{on}$) while the chemical potential was simultaneously related with the fraction occupation site (Eq. 1.2) (Hill 1985).

$$K_d = \frac{1 + K_c C_c}{K_t} \qquad \text{(Eq. 4.2)}$$

This model validates the experimental results that the affinity binding constant had a linear behavior (**Fig. 4.3C**) and confirms that the effective affinity of trans-CD47 ($C_t$) for free SIRPα ($S_v$) is a function of cis-CD47 ($C_c$) concentration. The accessibility of SIRPα to soluble CD47 in trans was shown to have a slower binding with an association constant kon of 0.65min-1 in WT compared to 0.36 min-1 in CD47′ THP-1 cells (**Fig. 4.S4**).

## 4.4 – Discussion

In this study we have shown that the signal regulatory protein (SIRPα) found on macrophages binds to CD47 ligand expressed on target self cells but is

also constitutively associated with CD47 in the plane of the macrophages membrane (cis interaction). It has been well characterized that the self signal of SIRPα and CD47 inhibits macrophages in mouse (Oldenborg, Zheleznyak et al. 2000; Gardai, McPhillips et al. 2005) and humans (Tsai and Discher 2008) through a trans interaction. We proposed that the cis interaction exists and restricts the extent to which SIRPα inhibits macrophage phagocytosis of non-self cells lacking CD47.

We addressed the importance of CD47 in cis on macrophages due to the necessity of the protein to function as a marker of self on all cells. Two types of THP-1 macrophages, wild-type and 13% WT CD47 showed equal phagocytic activity against self targets human RBCs and hCD47 coated particles. In contrast, phagocytosis was increased by 25-50% for foreign or uncoated "CD47-null" particles in THP-1 cells with reduced cis interaction (**Fig. 4.3**). In order to rule out the possibility of knockdown effect on THP-1 phagocytosis capabilities, SIRPα expression was confirmed for all knockdowns by flow cytometry and a mock lentiviral KD was shown to have comparable phagocytosis capabilities to WT THP-1 Cells (**Fig. 4.S5**). This suggests that the cis interaction of CD47-SIRPα may negatively inhibit macrophages regardless of targets due to the inherent signal.

Phagocytosis initiated by the activation of Fcγ-R on macrophages through binding to IgG-opsonized targets leads to the phosphorylation of the

immune-tyrosine activation motif (ITAM) (Cambier 1995; Lowry, Duchemin et al. 1998). Alternatively an inhibition signal exists with self cells expressing CD47 that interaction with the receptor SIRPα that results in the inhibition of phagocytosis. The CD47-SIRPα interaction has been shown to be species-specific (Subramanian, Parthasarathy et al. 2006) and normal macrophages have been shown to engulf “self” cells at lower frequency than typical targets – foreign and apoptotic cells or particles. Self cells signal inhibition through CD47-SIRPα interaction in trans results in the recruitment of the SHP-1 phosphatase, but inherent phosphorylation has been shown to exist in macrophages that may suggest the inefficiency of recognizing non-self and self cells as demonstrated by with Sheep RBCs with human THP-1 macrophages (**Fig. 4.5A**). However when CD47 coated particles or RBCs interact with SIRPα of the same species, this results in increased phosphorylation that reaches a saturating level dependent on CD47 density (Vernon-Wilson, Kee et al. 2000; Liu, Soto et al. 2005).

SIRPα affinity to CD47 is relatively low affinity interaction with a $K_d$ of 1.6 μM that allows for rapid exchange of CD47-SIRPα binding from an intracellular cis to a intercellular trans interaction (**Fig. 4.3**). Further confirmation of the competitive binding was demonstrated through measurement of the association constant, kon showing a slower rate for wild-type macrophages suggesting the availability of the CD47 to interact by trans was occupied by CD47 in cis (**Fig. 4.S4**). The basal level of SIRPα activation suggests the

threshold difference needed for inhibition may be local. Soluble CD47 in solution with foreign sheep RBC did not have a significant effect in inhibiting phagocytosis (data not shown), but a local concentration of SIRPα and CD47 clustering at the phagocytic synapse may be necessary to signal self. When human macrophage attempts to engulf its targets through pseudopod extension it verifies the presence of CD47 as in normal human RBCs. This spurs the macrophage to stop mid-swallow, shifting from an intracellular cis to an accumulated intercellular trans signal (Tsai and Discher 2008). The observed delayed retraction of human RBCs may serve as a function for microbe clearance through CR1 receptor found on RBCs where microbe would be removed during macrophage contact (Ghiran, Glodek et al. 2008).

Normal THP-1 macrophages have a higher ratio of CD47 to SIRPα by a 3-to-1 ratio but in our highest CD47 knockdown the ratio dropped to 0.5-to-1 resulting in more SIRPα than CD47. That led to a decrease in SIRPα phosphorylation levels that fit linear to the extent of CD47 expression (**Fig. 4.4B**). This elimination of phosphorylation by cis interaction led to a better discrimination of foreign and self cells with a 25-50% increase in phagocytosis of IgG-opsonized ShRBC and uncoated particles. It is interesting to note that the reduction of cis interaction in THP-1 macrophages did not significantly affect HuRBC and hCD47 coated particles.

Our finding raises the question of how SIRPα is able to bind with CD47 both in cis and trans interaction at the binding site. A past crystallographic study showed that the CD47/SIRPα complex binds near the N-terminal ligand binding domain of SIRPα (Hatherley, Graham et al. 2008). SIRPα and other members of the SIRP family have three IgSF domains while CD47 contains only a single IgSF domain; this suggest that SIRPα may have some flexibility in the structure as the binding site is near the N-terminus as it was shown with the computed flexibility model (**Fig. 4.2**). However the structure of CD47 is unique because of the disulfide link between the IgSF domain and one of the loops between the transmembrane regions was shown to be required for optimal binding of SIRPα (Rebres, Vaz et al. 2001).

In order to account for our findings, our model suggests that SIRPα inhibits phagocytosis through CD47 and SIRPα by trans while foreign target cells are not able to signal self leading to activation Fcγ-R by IgG-opsonization. In wild-type macrophages both cis and trans CD47-SIRPα interaction co-exists with the presences of a basal level of inhibitory signal rega**rdless of self or foreign cells.** The importance of CD47 and SIRPα by cis appears to partially affect phagocytosis of foreign particles, but it is important for macrophages to maintain their own display of the “marker of self” signal, CD47 to prevent phagocytic clearance by other macrophages.

## 4.5– Materials and Methods

### 4.5.1 – Chemicals

Dulbecco's phosphate-buffered saline (DPBS) without Ca2+ or Mg2+ (Invitrogen) was supplemented with either 1% BSA or 1% BSA and 0.05% Tween 20 (Sigma-Aldrich).

### 4.5.2 – Antibodies

The anti-human CD47 antibody B6H12 (BD Biosciences), clone 2D3 (EMD Biosciences), clone 6H9 a gift from Dr. M. Telen (Duke University) was used for detection of human CD47 on macrophages or CHO cells expressing full length human CD47. Quantification of CD47 and SIRPα was performed using B6H12-FITC and anti-SIRPα (SE7C2) (Santa Cruz Biotech) respectively. Human SIRPαex (this laboratory) used for experiments comparing binding affinities between species. Opsonizing antibodies against sheep RBCs included rabbit anti-sheep RBCs (Sigma-Aldrich) and antibodies against streptavidin coated polystyrene beads (Spherotech) included rabbit anti-streptavidin (Sigma-Aldrich) and rabbit anti-streptavidin conjugated with FITC (Rockland Immunochemicals) was used as IgG opsonin in phagocytosis assays. Secondary antibodies used for detecting opsonin levels and uningested beads included goat anti-rabbit FITC or goat anti-rabbit F(ab')2 R-PE (Sigma-Aldrich). Secondary antibodies used for

detecting SIRPαex binding included anti-GST Alexa 488 (Invitrogen). Cytokine G-CSF was purchased from R&D Systems.

### 4.5.3 – Cells culture and transfection

COS-1, CHO-K1, A549, THP-1 cells (American Type Culture Collection) and Human mesenchymal stem cells (MSCs; Osiris Therapeutics) were respectively maintained in DMEM, MEMα, F-12, RPMI 1640, and DMEM low glucose media (Invitrogen) supplemented with 10% heat inactivated FBS (Sigma-Aldrich). Cells were detached using 0.25% Trypsin/0.5mM EDTA (Invitrogen) for passaging. Differentiation of THP-1 cells was achieved in 100 ng/mL phorbol myristate acetate (PMA) (Sigma-Aldrich) for 2 days and confirmed by attachment of these cells to tissue-culture plastic. Peripheral blood monocytes from human donors were obtained through the Human Immunology Core (University of Pennsylvania). Human blood was obtained from finger pricks of healthy donors. Blood from other species was obtained from Covance and washed 3x in PBS plus 0.4% BSA. Human Hematopoietic Stem Cells were obtained from Fresh purified bone marrow (BM)-derived humanCD34+ cells from Lonza. All experiments were performed in hematopoietic stem cell (HSC) expansion media (StemLine-II; Sigma) and supplemented with 1× antibiotics and G-CSF (100 ng/mL) for 7 day for cultured cells.

### 4.5.4 – Expression of human CD47-GFP and SIRPα

Human CD47 (hCD47; isoform 2 (Reinhold, Lindberg et al. 1995)) were PCR amplified, digested with XhoI & BamHI (New England Biolabs) and ligated to similarly digested vector, pEGFP-N3 (Clontech laboratories). CHO cells were plated at 1 x 105 cells/cm2 a day prior to transfection. On the day of transfection, medium was replaced with 2 mL Opti-MEM I (Invitrogen) per 25 cm2 surface area and 10-15 µL Lipofectamine 2000 and 5 µg plasmid DNA were diluted in 0.25 mL Opti-MEM I separately and 5 min later mixed and incubated for a minimum of 20 min at 25℃. Lipid-DNA complexes in a total volume of 0.5 mL Opti-MEM I was added to the flasks and incubated for 4-6 hrs and then replaced with fresh growth medium. Transfected cells were harvested using DPBS supplemented with 2 mM EDTA (Invitrogen) 1-2 days post-transfection for analysis. Full-length human SIRPα was expressed in CHO cells similar to human CD47-GFP above.

### 4.5.5 – Soluble human SIRPα production

COS-1 cells were transfected with pcDNA3-based vector (Seiffert, Cant et al. 1999) encoding a human SIRPα extracellular domain fused to GST using Lipofectamine 2000 (Invitrogen). Secreted SIRPα1-GST (referred as hSIRPαex) was affinity-purified using Glutathione Sepharose 4B (Amersham Biosciences) and dialyzed against PBS (Invitrogen). The protein was stored at -20℃ with or without addition of 10% v/v glycerol (Fisher Scientific).

### 4.5.6 – Production of recombinant human CD47

Plasmid encoding the extracellular domain of human CD47, mouse CD47 were PCR amplified, digested with XbaI & SalI (New England Biolabs) and ligated to similarly digested vector, pEF-BOS-XB (Vernon-Wilson 2000), which results in an in-frame fusion of CD4d3+4-biotin at the c-terminus of the extracellular domain of CD47. The above vector containing the extracellular domain of CD47 was transfected into CHO(-K1) cells using Lipofectamine 2000 (Invitrogen). Secreted CD47-CD4d3+4 was concentrated using a 10K MWCO Amicon (Millipore) and biotinylated at the c-terminus using a biotin-protein ligase (Avidity, LLC) and dialyzed against PBS (Invitrogen). The protein was affinity-purified using a monomeric avidin (Promega) and dialyzed against PBS.

### 4.5.7– Measurement of human SIRPα and CD47 on cells

Human RBCs, THP-1 cells, A549, peripheral blood monocytes, human mesenchymal stem cells were labeled with 15µl of B6H12-FITC at saturating levels (BD Biosciences) against human CD47 for 30 min at room temperature. Cells were washed and resuspended in PBS for flow cytometry analysis. Anti-human CD47 measurements and detections were performed using B6H12 antibody. Saturating concentration of anti-SIRPα or anti-human CD47 antibodies were used as similarly described for the above cells.

### 4.5.8 – Lentiviral knockdown of CD47 in THP-1 cells

ShRNA lentiviral supernatants to CD47 purchased from Sigma-Aldrich were targeting CD47 (TRC#: TRCN0000007836, TRCN0000007837) resulted in 50-87% knockdown, respectively. Further details of these clones are available from Sigma-Aldrich website. Target THP-1 cells were infected with lentiviral supernatants at a multiplicity of infection (MOI) of 10 in the presence of 80 µg/mL Polybrene (hexadimethrine bromide) (Sigma-Aldrich) and remained in culture for 24 hours at 37℃ and replaced with fresh RPMI 1640 + 10% FBS. Cells with integrated viral sequence were selected using puromycin (Sigma-Aldrich) at 2 µg/ml and then passaged with continuous puromycin selection. The degree of CD47 silencing was regularly monitored by flow cytometry and Western blotting with 1:200 anti-SIRP□ (SE7C2) (Santa Cruz Biotech). Control cell cultures were generated with control lentiviruses in parallel.

### 4.5.9 – Binding isotherm for soluble hSIRPα for THP-1 and knockdowns

The binding isotherm of soluble hSIRPα was performed for THP-1 wild-type and CD47 knockdowns as noted over a range of concentration using flow cytometry. Forward scatter, side scatter and fluorescence (FL1, FL2, FL3, FL4 channels in logarithmic mode) were acquired using a FACScan or FACSCalibur (BD Immunocytometry Systems). Data points from flow cytometry were plotted and fitted to obtain the $K_d$ values as shown.

### 4.5.10 – Kinetics Measurements

Rates of association (kon) of SIRPα with soluble hCD47 were measured at room temperature. Mixtures of 8uM,4uM and 2uM soluble hCD47 with 15□l of B6H12-FITC against human CD47 at saturating levels (BD Biosciences) were preequilibrated for 3 hours to produce the primary complex. After mixing, aliquots were periodically withdrawn and added to the human THP-1 cells, then washed and diluted in PBS (1:30) to measure the hCD47 and SIRPα binding using flow cytometry. Forward scatter, side scatter and fluorescence (FL1, FL2, FL3, FL4 channels in logarithmic mode) were acquired for at least 104 events using a FACScan or FACSCalibur (BD Immunocytometry Systems). Data points from flow cytometry were plotted and fitted to obtain the Kon values as shown.

### 4.5.11 – Phagocytosis Assay

For phagocytosis assays, macrophages were plated in 4cm2 Lab-Tek II Chambered Coverglass (Nalge Nunc International) at 1 x 105/4cm2. Streptavidin polystyrene beads or RBC were added to macrophages at a ratio of 20:1 and allowed to incubate at 37˚C for 45 min. Non-phagocytosed beads or RBCs were washed with PBS. Cells were fixed with 5% formaldehyde (Fischer Scientific) for 5 min, followed by immediate replacement with PBS. For differentiation of non-internalized beads, beads were labeled with a primary antibody, rabbit anti-streptavidin (Sigma) at 1:1,000 in PBS for 20 min at 25℃. A second antibody, anti-rabbit R-PE (Sigma) was added at 1:1,000 in PBS to the cells and incubated

for an additional 20 min at 25℃. Cells were then w ashed with PBS/ 0.4% BSA and then quantified by light and fluorescent microscopy. At least 200 cells were scored per well and experiments were repeated at least three times. Assays using RBCs as targets, lysis of uningested RBC was performed by adding deionized H2O for 60s, followed by immediate replacement with PBS/0.4% BSA and fixing with 5% formaldehyde for 5 min.

For stimulated phagocytosis assays, beads with or without CD47 were incubated with rabbit anti-streptavidin serum and for sheep and human RBCs with rabbit anti-sheep RBC, and rabbit anti-human RBC respectively as the opsonin. Beads or RBCs were opsonized at the respective concentration for 30 min at RT. Opsonized beads and RBCs were washed 2x and resuspended in 50 µl of PBS/0.4% BSA. Phagocytes were washed with PBS and uningested RBCs were lysed and uningested beads were labeled as described above.

**4.5.12 – Immunoprecipitation and Western blotting**

Human Phagocytes, THP-1 wild-type and CD47 knockdowns ($2x10^6$) were cultured and differentiated in 6-well plates for 48 hours after PMA differentiation. Human CD47 was attached to 2.1µm diameter beads at specific densities as described above and added at a bead to cell ratio of 20:1 for 10 minutes. Following the incubation time, the cells were washed with ice-cold PBS and then lysed on ice in 300 µl of lysis buffer (50 mM Tris-HCl (pH 7.4), 150 mM NaCl,

1mM EDTA, 1% NP-40, 1% protease inhibitor cocktail [Sigma-Aldrich] and 2mM activated sodium orthovanadate). For immunoprecipitation, whole lysate was mixed with 1:200 anti-SIRPα (SE7C2) antibody (Santa Cruz Biotechnology, Inc.) with Protein G agarose (Pierce) at 4˚C overnight. Precipitated proteins was placed in 4-12% SDS-PAGE in MOPS buffer (Invitrogen), transferred to PVDF membrane, blocked and labeled via phosphotryosine IgG HRP-conjugated (Cell Signaling) and anti-SIRPα (C-20) (Santa Cruz Biotechnology, Inc.) as primary antibodies and anti-goat-HRP (Amersham). All Westerns were run in duplicate, along with an additional blot for actin to ensure constant protein load among samples.

### 4.5.13 – Fluorescent labeling of transfected CHO with soluble SIRPα and CD47 antibodies

Five microliters of soluble SIRPμ (final concentration ~1 μM); 5 μl of 2 mg/ml AlexaFlour 647 rabbit anti-GST; 40 μl DPBS, 1% BSA; and 2.5 x $10^6$ CHO cells were mixed and incubated at room temperature for at least 30 min. Cells were pelleted and resuspended in 1 ml cold DPBS and analyzed immediately. For antibody labeling, saturating levels of anti-CD47 antibody in 50 μl of DPBS, 1% BSA and 2.5 x $10^6$ CHO cells were mixed together and incubated as above. Cells were washed in 0.5 ml of DPBS, 1% BSA and then resuspended in 50 μl of DPBS, 1% BSA containing 5 μl of secondary antibody (2 mg/ml). After incubate

for 30 min at room temperature, cells were washed once in 0.5 ml of DPBS and resuspended in 1 ml of DPBS, 1% BSA and used immediately for imaging.

### 4.5.14 – Quantification of fluorescent intensity

Images were acquired with an inverted microscope (Olympus; IX71) with a 60x (oil, 1.4 NA) objective using a Cascade CCD camera (Photometrics, Tuscon, AZ). Image acquisition was performed with Image Pro software (Media Cybernetics, Silver Spring, MD). All subsequent image analysis was done using ImageJ.

### 4.5.15 – Normal Mode Analysis of SIRPα structure

To gain insight about the degree of flexibility and mobility of the Signal-regulatory protein α (SIRPα) we employed Normal Mode Analysis technique. For this purpose we used the α-carbon backbone of the recently published crystal structure for SIRP-α1 as model (PDB: 2WNG). Our first goal was to detect the presence of hinges. This is a challenging problem when only one structure is known and several algorithms and techniques have been developed to tackle it. (Thorpe et al. 2001; Wells et al. 2005; Flores et al. 2006; Flores et al. 2008). Our approximation will use the Gaussian Network Model which assumes that all the residue fluctuation around their equilibrium coordinates are gaussian. (Bahar et al. 1997; Haliloglu et al. 1997). This method has been tested to be suitable to determine structural displacements and consequently backbone motional

correlations. By virtue of these correlations, the different domains in the protein are determined as well as the location of the hinges. (Kundu et al. 2004; Haibo et al. 2007)The normal modes have been obtained using a $r_{cutof\ f}$ = 15Å and the correlations between them were computed using the following expression:

$$C_{ij} = \frac{\left\langle \Delta r_i \cdot \Delta r_j \right\rangle}{\sqrt{\left\langle \Delta r_i^{\,2} \right\rangle \left\langle \Delta r_j^{\,2} \right\rangle}}, \qquad \text{(Eq. 4.3)}$$

where $\Delta r_i$ is the total displacement of the α-carbon of the i-th residue from its equilibrium position due to the first n normal modes, and

$$\left\langle \Delta r_i \cdot \Delta r_j \right\rangle = \sum_{k=1}^{n} \frac{\kappa_B T}{\omega_\kappa^2} \frac{L_{ik} L_{jk}}{\sqrt{m_i m_j}}, \qquad \text{(Eq. 4.4)}$$

where $\omega_\kappa^2$ is the frequency of the k-th normal mode and $L_{ik}$ is the displacement of the α-carbon of residue i due to normal mode k.

The result of this correlation for the first two lowest frequency modes is shown in (**Fig. 4.2**). It is possible to distinguish three different regions that correspond very accurately with the three domains present in the crystal structure. The regions along the diagonal which values close to zero, i.e. regions with reduced mobilities, are expected to behave as hinges. (Flores et al. 2008) In this way we can determine that the regions limited by residues 113-117 and 220-222 will act as hinges. The spatial location of these residues can be seen in (**Fig. 4.2B**) depicted in space filling representation. Since we were also interested in

having a spatial description of the normal modes we needed to make use of the Anisotropic Network Model (ANM). (Hinsen et al. 1999)

We used this method because albeit being less realistic than GNM, it is the only possible model when assessing of directions of the motions is needed. (Cui and Bahar 2006) **Fig. 4.2C** shows the global dynamics of SIRP-α as predicted by three out of the first six modes. It is important to remark that the almost cylindrical shape of the protein in the crystal structure yields normal modes that are very close in energy and that describe almost the same movement but in a different plane. In this way we have that the modes 1 and 2, 3 and 5, as well as 4 and 6 can be represented by **Fig. 4.2C**. The remarkable aspect of these movements is that in all of them, the residues previously predicted as hinges seem to have that role, separating domains which move as rigid bodies and this dynamical domain overlap almost perfectly with the structural domains.

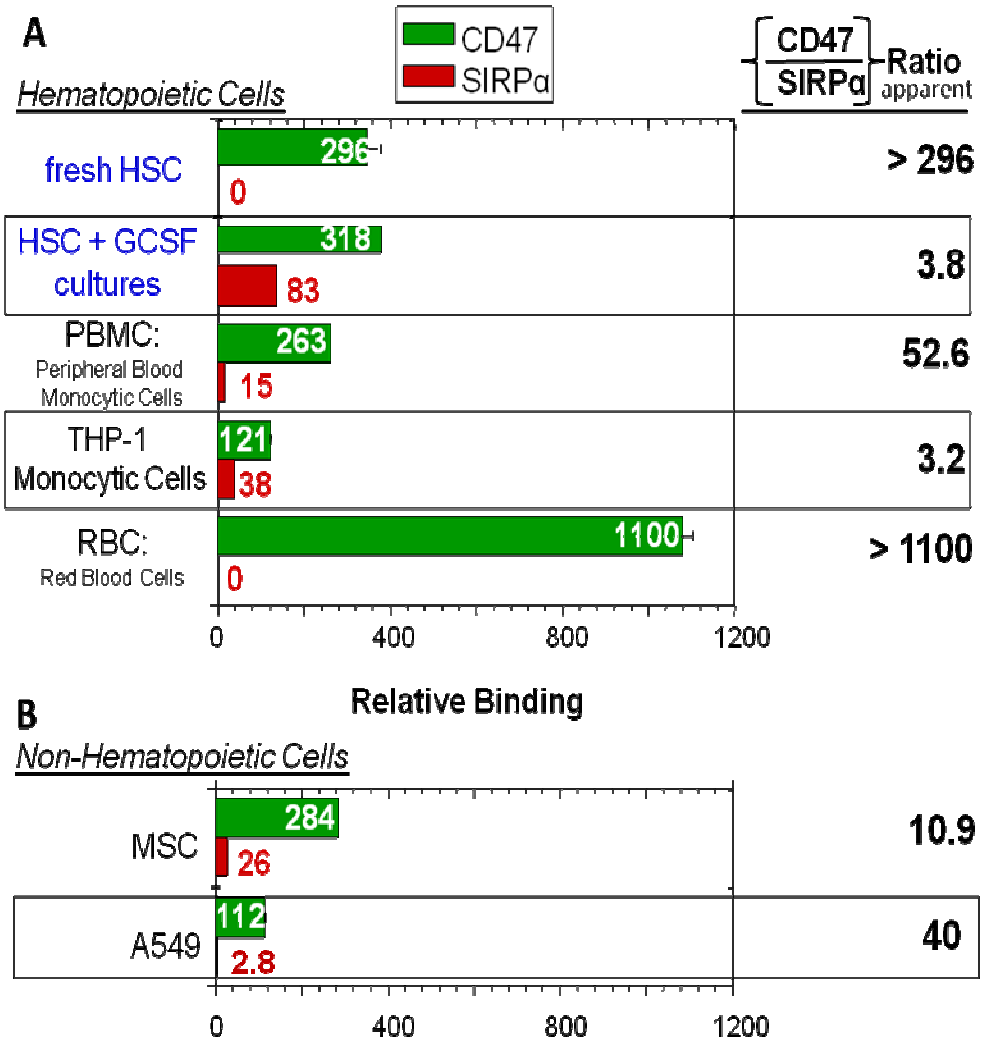


**Fig. 4.1.- Surface Expression of CD47 and SIRPα**

**(A)** Expression profiles of human cells from different hematopoietic cells show relative number of CD47 and SIRPα surface expression taken from flow cytometry using antibodies against the specific ligands (n=3). **(B)** The ratio of CD47 to SIRPα of Non-professional phagocytes, Mesenchymal Stem Cells (passage 4, n=2) and Human lung adenocarcinoma, was determine from flow cytometry data using RBC as a control (n=4). Avg. ± SEM for all results.

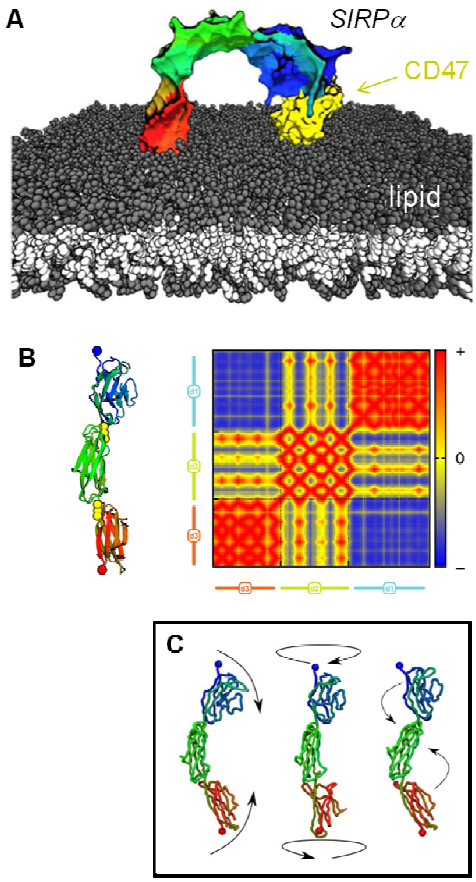


**Fig. 4.2.- Cis interactions between SIRPα and CD47 seem consistent with computed flexibility of SIRPα.**

**(A)** Membrane snapshot showing computed deformation of the extracellular region of SIRPα together with the CD47 structure (represented in yellow, extracted from pdb code 2jjs). **(B)** Crystal structure of the extracellular region of SIRP-a in ribbon representation: blue (C terminal - d1 domain), green (d2 domain), red (N terminal - d3 domain). In yellow space filling representation the residues C-a carbons from Arg-114, Ala-115, Lys-116, Arg-220, Val-221 and Phe-222 which are estimated to act as hinges. Plot is the covariance matrix of the C-a atoms in 2WNG based on the lowest 10 normal modes obtained by GNM **(C)** The first three distinct normal modes obtained by ANM. From left to right: mode 1 (mode 2 is similar but in a perpedicular plane), mode 3 (mode 5 invert rotations), mode4 (mode 6 is similar but in a perpendicular plane). In all modes the protein behaves as a set of three rigid bodies that can rotate and bend around the hinges.

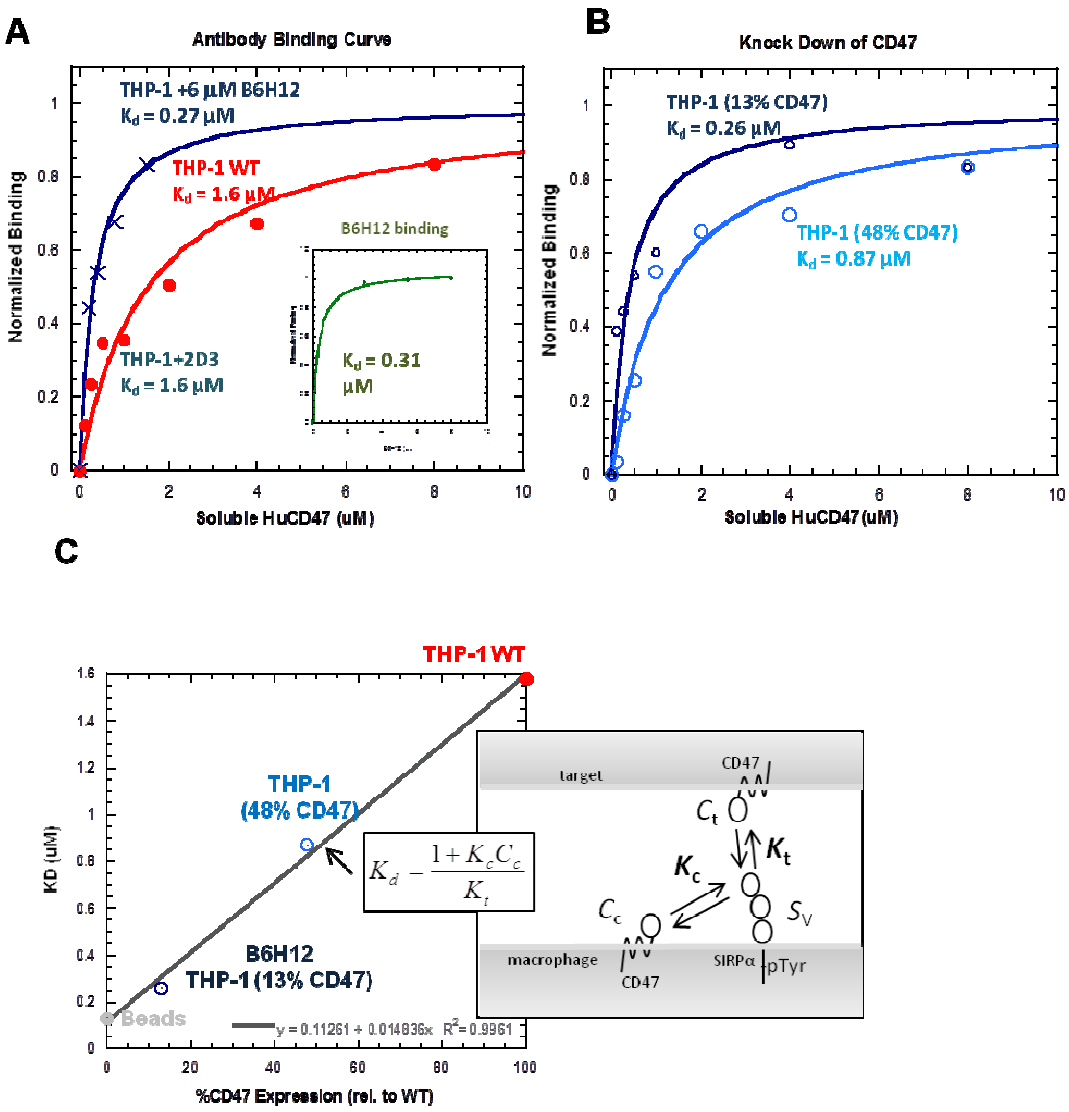


**Fig. 4.3.- CD47-SIRPα Cis intereaction effect on binding of soluble human-SIRPα on THP-1 Macrophages**

**(A)** Affinity of CD47 on THP-1 macrophages wild-type, CD47 knockdowns with antibodies against CD47 (Clones 2D3 and B6H12) at saturation levels binding to soluble hSIRPα based on flow cytometry. Saturation binding fit gave the indicated dissociation constant, Kd. **(B)** Affinity of CD47 on THP-1 macrophages wild-type, CD47 knockdowns with 48% and 13% CD47 wild-type levels binding to soluble hSIRPα based on flow cytometry. Saturation binding fit gave the indicated dissociation constant, Kd. Since this is a 3D binding constant relevant to binding in a narrow membrane gap between two cells, it is equivalent to Kd ≈ 1 molecule/[10 nm x (10 mm)2], which is the concentration of free SIRPα that would half-saturate CD47 on a surface. **(C)** Dissociation constant was plotted as a function of percentage of wild-type CD47 expression and plotted on a linear scale ($R^2$ = 0.99). Competitive binding model for cis/trans interaction of CD47-SIRPα

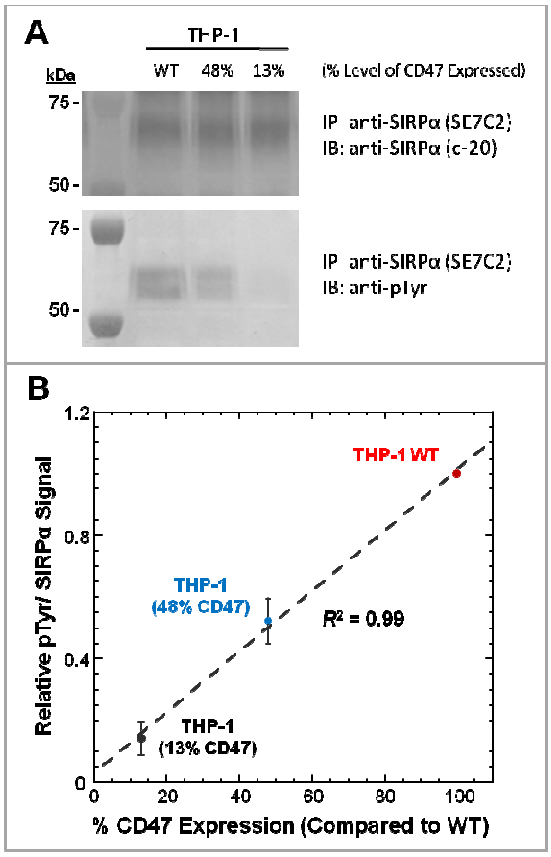


**Fig. 4.4.- CD47 expression levels on THP-1 depends on pTyr Signaling**

**(A)** CD47 was knockdown by lentivirus to various efficiency in THP-1 macrophages. From macrophage lysates, SIRPα was immunoprecipitated with anti-SIRPα (SE7C2 clone) and immunoblotted for phospho-tyrosine and total SIRPα (C-20 clone) for normalization. **(B)** Quantification of the immunoblotted data was plotted as a function of the % of wild-type CD47 expression levels and the fit of the data gave a linear relationship ($R^2$=0.99) that depends on the CD47-SIRPα Cis interaction without the presences of targets.

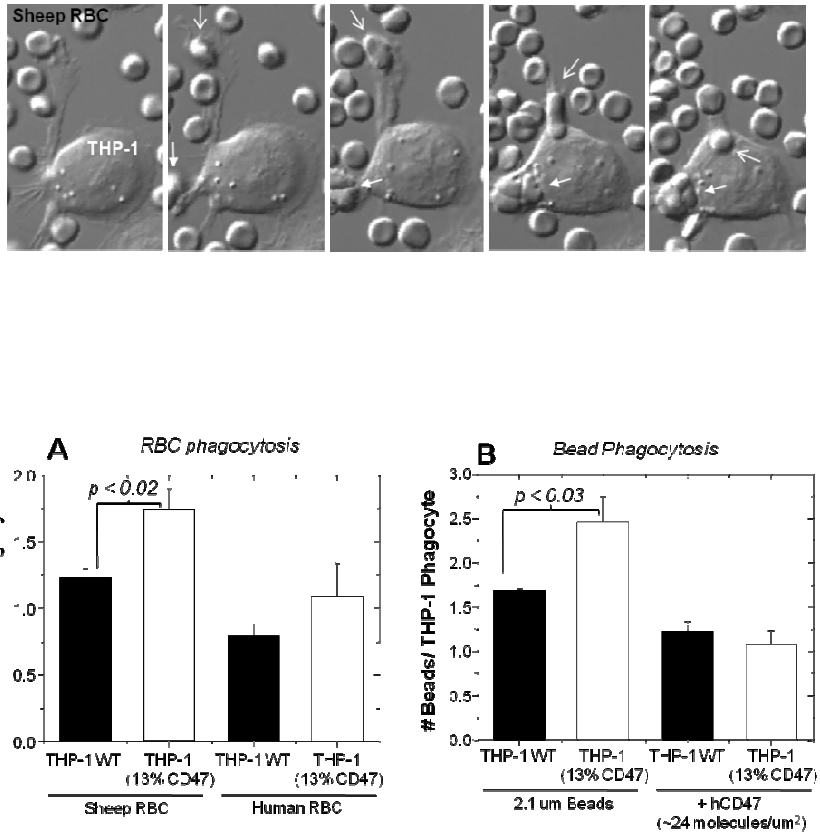


**Fig. 4.5- Reduction of CD47-SIRPα Cis Effect on phagocytosis in THP-1 Macrophages**

**(A)** IgG-opsonized sheep RBC (ShRBC) and human RBC (HuRBC) or **(B)** IgG-opsonized 2.1 μm particles with or without hCD47 targets were used for phagocytosis studies with wild-type (black bar) and 13% CD47 levels of wild-type (white bar) THP-1 macrophages. The ratio of ingested particles per phagocytes shown are based on randomly selected phase contrast microscopy images with 200 phagocytes counted (n ≥ 3, ± SD).

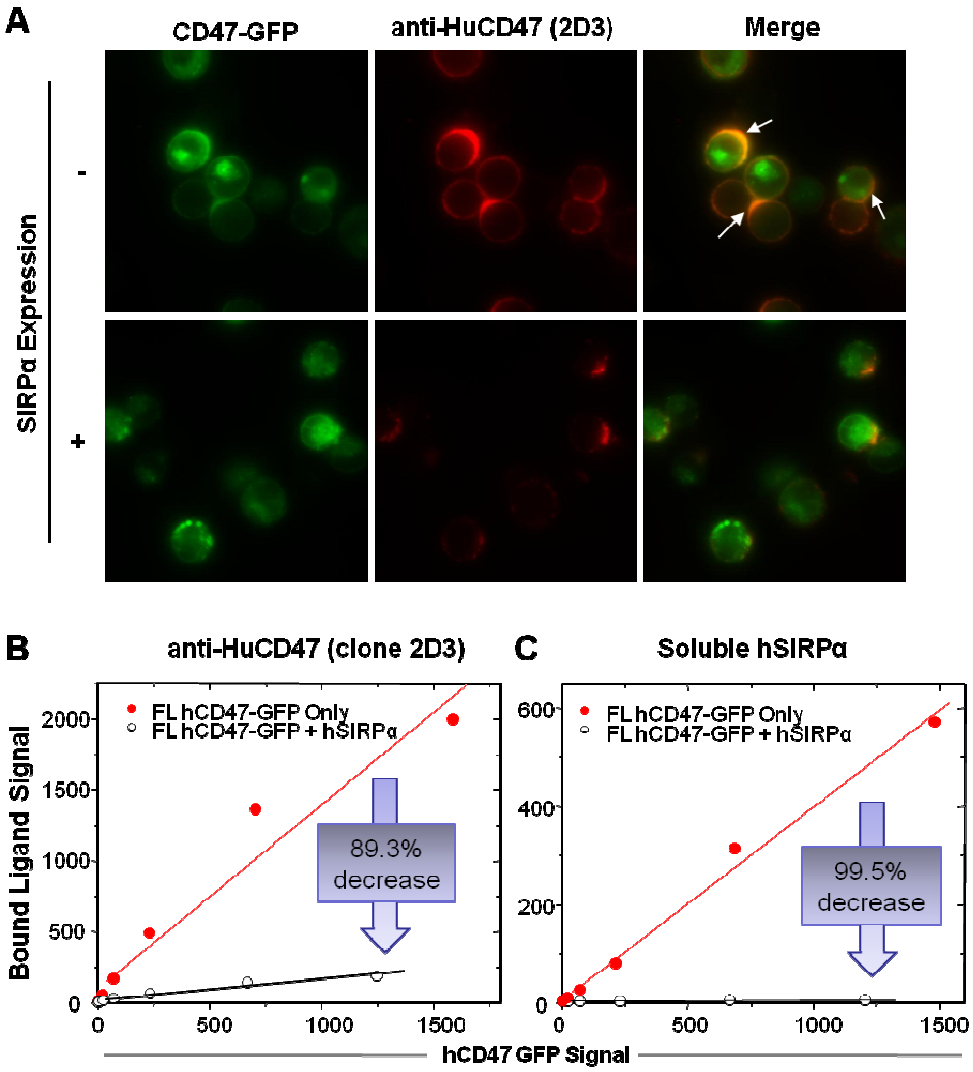


**Fig. 4.6- CD47-SIRPα Trans Interaction Reduced by Cis**

**(A)** CHO cells expressing human CD47-GFP were labeled with anti-Human CD47 (clone 2D3), detected using AlexaFluor 647 secondary antibody, showing that the fusion is targeted to the membrane and the Ig domain is accessible to antibodies and co-localized (white arrows), but not present with cells co-expressing full length human SIRPα. CHO cells expressing hCD47-GFP with or without hSIRPα were labeled with **(B)** anti-HuCD47 (clone 2D3) or **(C)** soluble hSIRPα were analyzed by flow cytometry. The flow cytometry log-log data is replotted on linear scales to determine binding slopes as a function of hCD47 GFP Signal to the respective bound ligand signal.

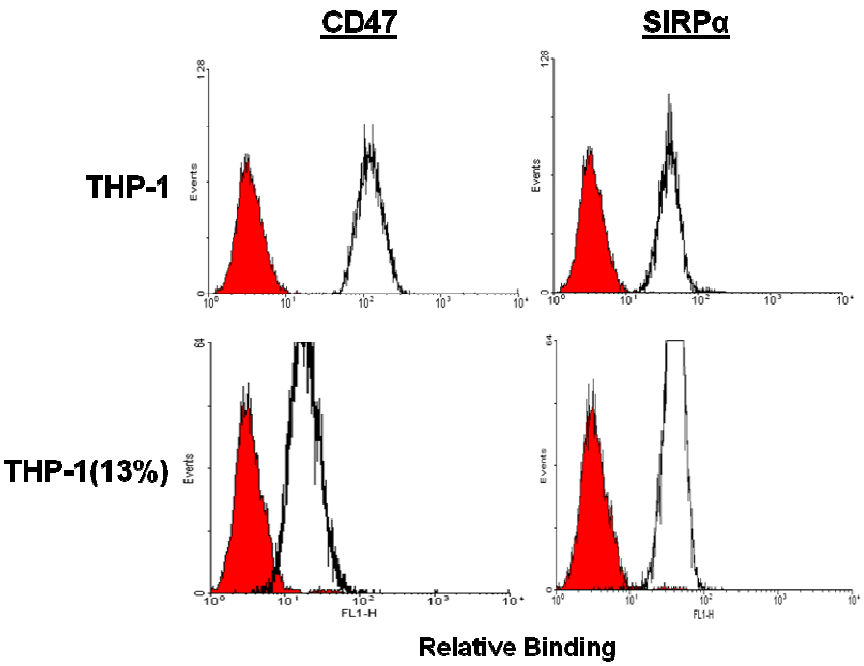


**Fig. 4.S1.- Professional Phagocyte CD47-SIRPα expression**

Flow cytometry data shows binding of anti-CD47 antibody, B6H12 binding difference, but no difference in binding of anti-SIRPα antibody, SE7C2 in THP-1 wild-type and cells expressing 13% wild-type CD47 levels.

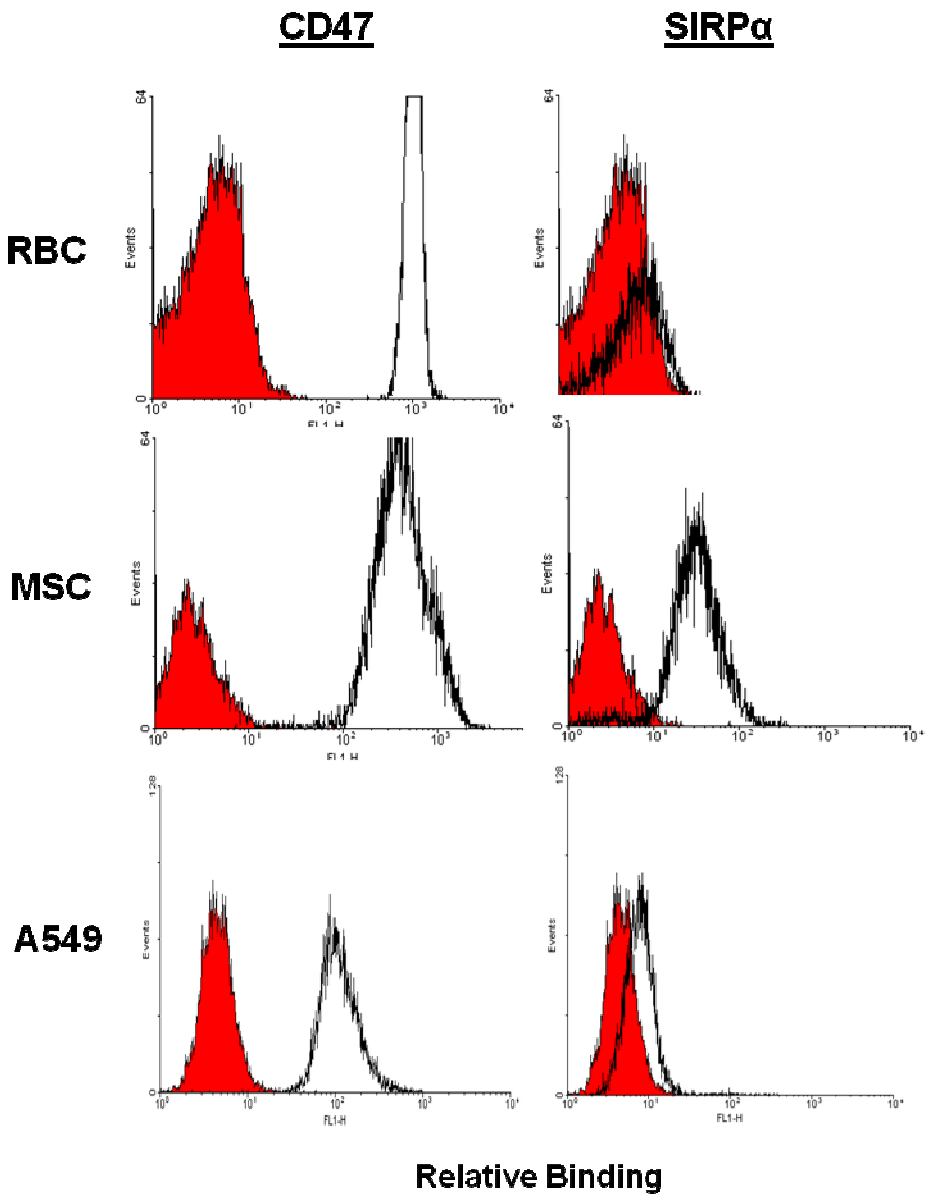


**Fig. 4.S2.- Non-professional phagocyte CD47-SIRPα expression**

Flow cytometry data shows binding of anti-CD47 antibody, B6H12 and anti-SIRPα antibody, SE7C2 show different levels of either CD47 or SIRPα profiles for non-professional phagocytes (e.g. red blood cells (RBC), Mesenchymal stem cells (MSC), and lung carcinoma epithelial cells (A549).

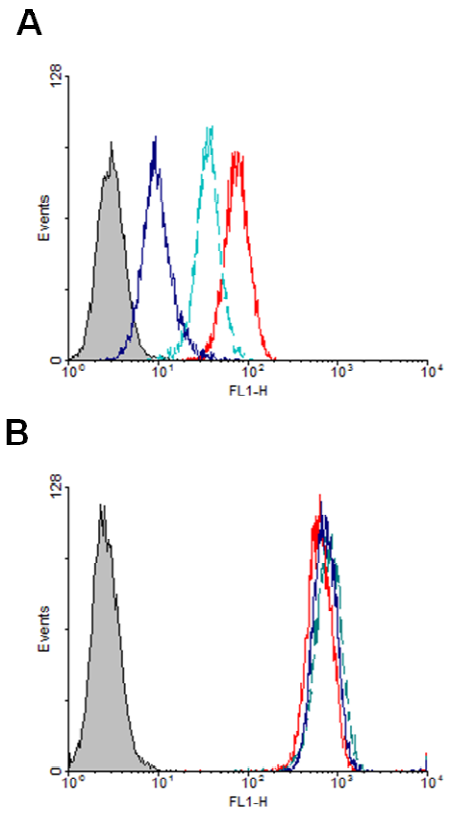


**Fig. 4.S3.- CD47 Knockdown in THP-1 Phagoctyes**

**(A)** CD47 knockdown in THP-1 macrophages was detected with anti-human CD47 (FITC) showing the extent of CD47 knockdown efficiency using different lentiviral ShRNA targets against CD47 and **(B)** SIRPα expression levels was detected using anti-SIRPα (SE7C2) for each of the CD47 knockdown THP-1 macrophages using flow cytometry

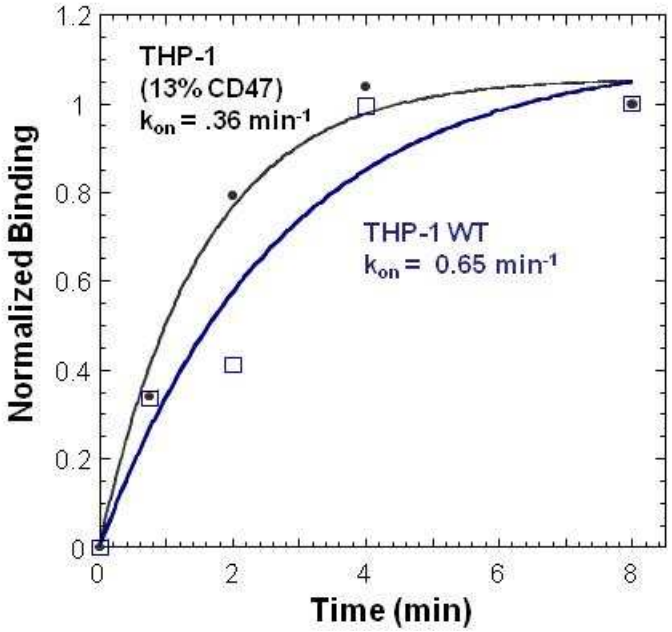


**Fig. 4.S4.- Association rate of CD47 in trans**

Association rate of CD47 binding via trans in wild-type macrophages show a slower binding rate compared to 13% CD47 wild-type levels based on flow cytometry . Saturation association binding fit gave the indicated constant, $k_{on}$.

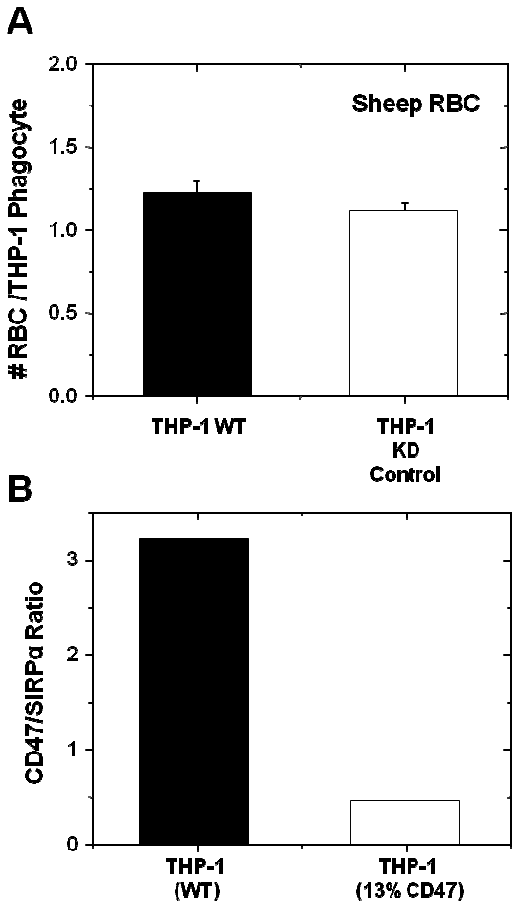


**Fig. 4.S5.- Effect of mock lentivirus knockdown on phagocytosis**

**(A)** IgG-opsonized Sheep RBC were incubated with wild-type and mock shRNA lentivirus knockdown THP-1 macrophages and allowed to phagocytose as described in Materials and Methods. Phagocytosis of Sheep RBC was measured as the ratio of ingested RBC per phagocytes with 200 phagocytes counted (n≥3, ±SD). **(B)** THP-1 wild-type cells have higher ratio of CD47-to-SIRP while knockdowns with 13% wild-type CD47 the number of SIRPα molecule dominate based on flow cytometry results

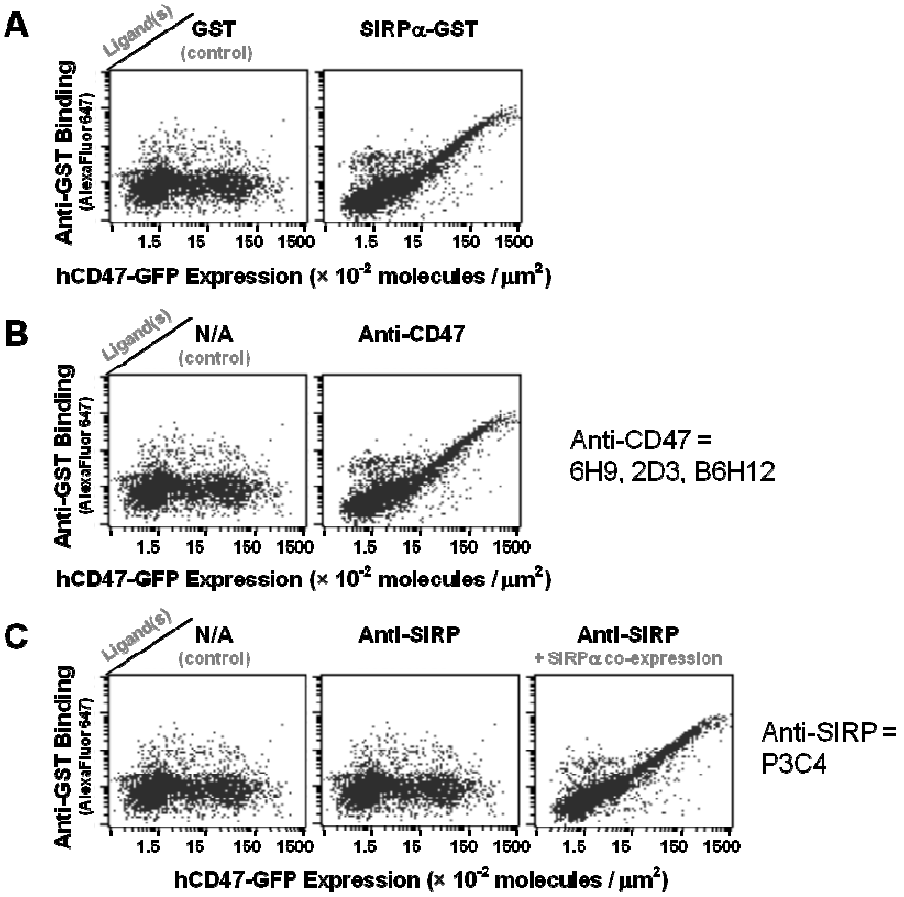


**Fig. 4.S6.- CHO Expression System of CD47 and SIRPα**

Flow cytometry data of CHO cells expressing CD47-GFP only detected with binding with **(A)** soluble SIRPα-GST or **(B)** antibodies against CD47 (Clones 6H9, 2D3, and B6H12). **(C)** CHO expression of CD47-GFP and SIRPα was confirmed by GFP and anti-SIRPα antibody, P3C4.

## 4.6 – References


1. Adams, S., L. J. Van der Laan, et al. (1998). "Signal-regulatory protein is selectively expressed by myeloid and neuronal cells". J. Immunol. 161, 1853–1859.
2. Anniss, A. M. and R. L. Sparrow (2002). "Expression of CD47 (integrin-associated protein) decreases on red blood cells during storage." Transfus Apher Sci 27(3): 233-8.
3. Arase, H., E. S. Mocarski, et al. (2002). "Direct recognition of cytomegalovirus by activating and inhibitory NK cell receptors." Science 296(5571): 1323-6.
4. Bahar, I., A. R. Atilgan, et al. (1997). "Direct evaluation of thermal fluctuations in proteins using a single-parameter harmonic potential". Fold Des. 2(3): 173–81.
5. Bauer, S., V. Groh, et al. (1999). "Activation of NK cells and T cells by NKG2D, a receptor for stress-inducible MICA." Science 285(5428): 727-9.
6. Brown, E. J. and W. A. Frazier (2001). "Integrin-associated protein (CD47) and its ligands." Trends Cell Biol. 11(3): 130-5.
7. Cambier, J. C. (1995). "Antigen and Fc receptor signaling. The awesome power of the immunoreceptor tyrosine-based activation motif (ITAM)." J Immunol 155(7): 3281-5.
8. Cui, Q., I.E., Bahar (2006). Normal Mode Analysis. Theory and Applications to Biological and Chemical Systems; Taylor & Francis Group, LLC, London, UK.
9. Charriere, G. M., B. Cousin, et al. (2006). "Macrophage characteristics of stem cells revealed by transcriptome profiling." Exp Cell Res 312(17): 3205-14.
10. Doucey, M. A., L. Scarpellino, et al. (2004). "Cis association of Ly49A with MHC class I restricts natural killer cell inhibition." Nat Immunol 5(3): 328-36.
11. Flores, S., N. Echols, et al (2006). "The Database of Macromolecular Motions: new features added at the decade mark." M. Nucleic Acids Res 34,D296–301.
12. Flores S. C, K.S. Keating, et al (2008). "HingeMaster: normal mode hinge prediction approach and integration of complementary predictors." Proteins. 73(2):299-319.
13. Furusawa, T., N. Yanai, et al. (1998). "Integrin-associated protein (IAP, also termed CD47) is involved in stroma-supported erythropoiesis." J Biochem 123(1): 101-6.
14. Gardai, S. J., K. A. McPhillips, et al. (2005). "Cell-Surface Calreticulin Initiates Clearance of Viable or Apoptotic Cells through trans-Activation of LRP on the Phagocyte." Cell 123(2): 321.
15. Ghiran, I., A. M. Glodek, et al. (2008). "Ligation of erythrocyte CR1 induces its clustering in complex with scaffolding protein FAP-1." Blood 112(8): 3465-73.
16. Haliloglu, T., I. Bahar, et al. (1997). "Gaussian dynamics of folded proteins". Phys. Rev. Lett. 79: 3090–3093.
17. Hatherley, D., S. C. Graham, et al. (2008). "Paired receptor specificity explained by structures of signal regulatory proteins alone and complexed with CD47." Mol Cell 31(2): 266-77.

18. Hatherley, D., K. Harlos, et al. (2007). "The structure of the macrophage signal regulatory protein alpha (SIRPalpha) inhibitory receptor reveals a binding face reminiscent of that used by T cell receptors." J Biol Chem 282(19): 14567-75.
19. Hill, T. L. (1985). Cooperativity theory in biochemistry : steady-state and equilibrium systems. New York, Springer-Verlag.
20. Hinsen K. , A. Thomas A, et al. (1999). "Analysis of domain motions in large proteins." Proteins. 34(3):369-82.
21. Ide, K., H. Wang, et al. (2007). "Role for CD47-SIRPalpha signaling in xenograft rejection by macrophages." Proc Natl Acad Sci U S A 104(12): 5062-6.
22. Jiang, P., C. F. Lagenaur, et al. (1999). "Integrin-associated protein is a ligand for the P84 neural adhesion molecule." J Biol Chem 274(2): 559-62.
23. Kharitonenkov, A., Z. Chen, et al. (1997). "A family of proteins that inhibit signalling through tyrosine kinase receptors." Nature 386(6621): 181-6.
24. Krieser, R. J. and K. White (2002). "Engulfment mechanism of apoptotic cells." Curr Opin Cell Biol 14(6): 734-8.
25. Kundu S., D.C. Sorensen, et al. (2004). "Automatic domain decomposition of proteins by a Gaussian Network Model." Proteins. 57(4):725-33.
26. Lanier, L. L. (2005). "NK cell recognition." Annu Rev Immunol 23: 225-74.
27. Latour, S., H. Tanaka, et al. (2001). "Bidirectional negative regulation of human T and dendritic cells by CD47 and its cognate receptor signal-regulator protein-alpha: down-regulation of IL-12 responsiveness and inhibition of dendritic cell activation." J Immunol 167(5): 2547-54.
28. Liu, S. Q., P. K. Alkema, et al. (2005). "Negative regulation of monocyte adhesion to arterial elastic laminae by signal regulatory protein alpha and Src homology 2 domain-containing protein-tyrosine phosphatase-1." J Biol Chem 280(47): 39294-301.
29. Liu, Y., I. Soto, et al. (2005). "SIRPbeta1 is expressed as a disulfide-linked homodimer in leukocytes and positively regulates neutrophil transepithelial migration." J Biol Chem 280(43): 36132-40.
30. Ljunggren, H. G. and K. Karre (1990). "In search of the 'missing self': MHC molecules and NK cell recognition." Immunol Today 11(7): 237-44.
31. Lowry, M. B., A. M. Duchemin, et al. (1998). "Functional separation of pseudopod extension and particle internalization during Fc gamma receptor-mediated phagocytosis." J Exp Med 187(2): 161-76.
32. Matozaki, T., Y. Murata, et al. (2009). "Functions and molecular mechanisms of the CD47-SIRPα signalling pathway". Trends Cell Biol. 19(2):72-80.
33. Mi, Z.P., P. Jiang, et al. (2000). "Expression of a synapse-associated membrane protein, P84/SHPS-1, and its ligand, IAP/CD47, in mouse retina". J. Comp. Neurol. 416, 335–344.
34. Ohnishi, H., Y. Kaneko, et al. (2005). "Differential localization of Src homology 2 domain-containing protein tyrosine phosphatase substrate-1 and CD47 and its molecular mechanisms in cultured hippocampal neurons". J. Neurosci. 25, 2702–2711.
35. Oldenborg, P. A., A. Zheleznyak, et al. (2000). "Role of CD47 as a marker of self on red blood cells." Science. 288(5473): 2051-4.
36. Ravetch, J. V. (1997). "Fc receptors." Curr Opin Immunol 9(1): 121-5.

37. Ravetch, J. V. and R. A. Clynes (1998). "Divergent roles for Fc receptors and complement in vivo." Annu Rev Immunol 16: 421-32.
38. Rebres, R. A., K. Kajihara, et al. (2005). "Novel CD47-dependent intercellular adhesion modulates cell migration." J Cell Physiol. 205(2): 182-93.
39. Rebres, R. A., L. E. Vaz, et al. (2001). "Normal ligand binding and signaling by CD47 (integrin-associated protein) requires a long range disulfide bond between the extracellular and membrane-spanning domains." J Biol Chem 276(37): 34607-16.
40. Reinhold, M. I., F. P. Lindberg, et al. (1995). "In vivo expression of alternatively spliced forms of integrin-associated protein (CD47)." J Cell Sci 108 ( Pt 11): 3419-25.
41. Seiffert, M., P. Brossart, et al. (2001). "Signal-regulatory protein alpha (SIRPalpha) but not SIRPbeta is involved in T-cell activation, binds to CD47 with high affinity, and is expressed on immature CD34(+)CD38(-) hematopoietic cells." Blood 97(9): 2741-9.
42. Seiffert, M., C. Cant, et al. (1999). "Human signal-regulatory protein is expressed on normal, but not on subsets of leukemic myeloid cells and mediates cellular adhesion involving its counterreceptor CD47." Blood 94(11): 3633-43.
43. Subramanian, S., E. T. Boder, et al. (2007). "Phylogenetic divergence of CD47 interactions with human signal regulatory protein alpha reveals locus of species specificity. Implications for the binding site." J Biol Chem 282(3): 1805-18.
44. Subramanian, S., R. Parthasarathy, et al. (2006). "Species- and cell type-specific interactions between CD47 and human SIRP{alpha}." Blood 107(6): 2548-2556.
45. Swanson, J. A. and S. C. Baer (1995). "Phagocytosis by zippers and triggers." Trends Cell Biol 5(3): 89-93.
46. Takenaka, K., T. K. Prasolava, et al. (2007). "Polymorphism in Sirpa modulates engraftment of human hematopoietic stem cells." Nat Immunol 8(12): 1313-23.
47. Tenner, A. J., S. L. Robinson, et al. (1995). "Mannose binding protein (MBP) enhances mononuclear phagocyte function via a receptor that contains the 126,000 M(r) component of the C1q receptor." Immunity 3(4): 485-93.
48. Thorpe, M. F.; M. Lei, et al. (2001). "Protein flexibility and dynamics using constraint theory." J Mol Graph Model, 19 :60–9.
49. Tsai, R. K. and D. E. Discher (2008). "Inhibition of "self" engulfment through deactivation of myosin-II at the phagocytic synapse between human cells." J Cell Biol 180(5): 989-1003.
50. Turrini, F., F. Mannu, et al. (1993). "Characterization of the autologous antibodies that opsonize erythrocytes with clustered integral membrane proteins." Blood 81(11): 3146-52.
51. Veillette, A., E., Thibaudeau, et al. (1998). "High expression of inhibitory receptor SHPS-1 and its association with protein-tyrosine phosphatase SHP-1 in macrophages". J. Biol. Chem. 273, 22719–22728
52. Vernon-Wilson, E. F., W. J. Kee, et al. (2000). "CD47 is a ligand for rat macrophage membrane signal regulatory protein SIRP (OX41) and human SIRPalpha 1." Eur J Immunol. 30(8): 2130-7.

53. Vogel, W., F. Grunebach, et al. (2003). "Heterogeneity among human bone marrow-derived mesenchymal stem cells and neural progenitor cells." Haematologica 88(2): 126-33.
54. Wells, S., S., Menor, et al. (2005). "Constrained geometric simulation of diffusive motion in proteins". Phys Biol. 2(4):S127-36.
55. Yu H., L. Ma L, et al. (2007)." Mechanochemical coupling in the myosin motor domain. II. Analysis of critical residues." PLoS Comput Biol. 3(2):e23.

# CHAPTER 5 – The Role of “Self signal” on Neutrophil attachment-migration on a surface and phagocytosis of synthetic microbeads.

Pia L. Rodriguez, Luke Witherspoon and Dennis E. Discher

L. Witherspoon helped with the phagocytosis and migration measurement.

**Abstract**

The ability of a cell to distinguish foreign cells from “self” cells is required for a healthy, functioning immune system. One mechanism through which cells appear able to differentiate between “self” and foreign cells is through the surface protein CD47. In previous chapters we have shown that synthetic beads labeled with CD47are able to remain in circulation far longer than unlabeled ones. One drawback to CD47 labeling is that it may be species-specific: one individual’s CD47 interacting with their own receptor Sirpα may not prevent an immune response in another individual. This chapter will specifically characterize the interaction of different neutrophil hSirpα with the “self” peptide and with hCD47 in an attempt to determine the effects of this surface interaction on cell attachment, and the transmigration and phagocytosis of synthetic microbeads.

## 5.1 – Introduction

The ability of a cell to identify foreign cells from “self” cells is a requirement for a healthy, functioning immune system. Without such a mechanism in place, our immune system, and the cells that compose it, would inappropriately attack normal tissues. Tissue or medical device rejection in implantations is a constant concern, and patients are placed on immunosuppressive therapy to prevent immune rejection of these foreign entities.

One mechanism through which cells appear able to differentiate between "self" and foreign is through the surface cellular ligand CD47 (Tsai 2010). CD47-SIRPα interactions mediate the ability of CD47 to function as a marker for macrophages to suppress phagocytosis (Matozaki 2009). CD47 has also been implicated in cell migration, (Lindberg 1996), axon extension (Miyashita 2004), and T cell co stimulation (Reinhold 1997). Furthermore, immuno-depletion of either CD47 or SIRPα leads to an impairment of neutrophil ability to migrate over cell mono-layers (Parkos 1996, Liu 2002). However, recent studies of the role of CD47 expression on normal or leukemic hematopoietic stem and progenitor cells, which are also physiologically migrating, does not support a role for CD47 in the migration phase of mobilization (Jaiswal 2009).

Neutrophils are the most abundant white blood cell in mammals and are an essential part of the innate immune response. They are typically present in the bloodstream, and are among the first cells to be recruited to sites of inflammation as a result of infection (Smith 1994). Neutrophils play a central role in host defense by migrating to the site of infection. Neutrophils mature in the bone marrow before entering circulation, where they remain for 4-10 hours before exiting to tissue pools where they survive for another1 to 2 days (Smith 1994). Although estimates vary, neutrophils are produced in healthy human bone marrow at a rate of 1011 cells per day, although infection can drastically increase (10x) the number of neutrophils produced (Cannistra 1988). At sites of

inflammation they congregate and adhere to extracellular matrix (ECM) components such as laminin and fibronectin (Cronstein 1993). As part of the innate immune response neutrophils then phagocytose pathogens. Neutrophils, as with all phagocytic immune cells, are strongly influenced to phagocytose by the presence of opsonins, such as antibodies, highlighting the cooperative nature of the innate and adaptive immune responses (Smith 1994).

The mechanism through which receptor-ligand signaling interactions at the neutrophil surface can regulate transmigration and ultimately inflammatory diseases remains poorly understood. CD47 has been shown to regulate the rate of neutrophil transmigration in mice infected with bacteria as well as across cell monolayers and matrix (Cooper 1995, Parkos 1996, Chin 2009). In addition, CD47 has been implicated in multiple cellular functions in addition to its role as marker of 'self' (Oldenborg 2000), such as platelet activation (Chumg 1997), macrophage multinucleation (Han 2000), immune cell apoptosis (Pettersen 1999), and dendritic cell maturation (Demeure 2000). However, CD47 signaling pathways in transmigration have not been clearly elucidated. Furthermore, the identification of the contribution of the CD47-SIRPα pathway to inflammatory cell attachment to different surfaces remains unclear. Recent studies have suggested that polyurethane slabs coated with hCD47 inhibit polymer oxidation in vivo (Stachelek 2011), indicating that this 'Marker of Self' could passivate the inflammatory response.

## 5.2 – Results

### 5.2.1 – Effect of “self”-peptide on Phagocytosis by Neutrophils

For all assays the target number of observed neutrophils was 200, and each sample was examined until this number had been reached or the entire sample had been examined. To ensure no “double” counting could occur the samples were searched in a grid pattern that ensured no field of view was visited twice. Following imaging, each photo of a neutrophil was made into a composite image of all three fields using ImageJ Software and the number of microbeads that were phagocytized were counted to generate a phagocytized microbead:neutrophil ratio, representative image shown in **Fig. 5.S1**. Neutrophils had originally been kept in 10% FBS in non-HEPES $CO_2$ independent media, but this led to relatively low levels of phagocytosis. To attempt to increase phagocytosis the media was changed to 50% FBS in non-HEPES $CO_2$ independent media. This led to a 2.4 fold increase in phagocytosis over neutrophils tested in 10% serum **(Fig. 5.S2)**

We found that in 50% FBS in non-HEPES $CO_2$ independent media there was no difference in phagocytosis of peptide-beads as compared to control beads after 1 hour (**Fig. 5.1**), (student’s t-test, $p>0.05$). Further experiments will be necessary to rule out the effect that “self” peptide had on phagocytosis in neutrophils.

### 5.2.2 – Effect of Sirpα polymorphism in Neutrophil attachment and migration on glass surfaces.

Similar to our hypothesis that CD47-labeled microbeads may decrease the phagocytosis response, we wanted to evaluate neutrophils' ability to migrate and adhere to CD47 labeled substrates. This assay had to be designed to allow for neutrophils to access to both CD47 labeled substrate (CD47 + BSA), as well as control (BSA-only) labeled substrate (**Fig. 5.2**).

### 5.2.3 – Analysis of Migration Abilities

First we characterized how the neutrophils responded to BSA substrates before we could evaluate whether or not CD47 labeling changed this response. When neutrophils were present on the BSA substrate they appeared to adhere strongly and generally stopped moving significantly after 5 minutes of exposure to the BSA substrate. When a scratch was made on the slide, the neutrophils in the affected area were unable to adhere within such a timeframe and began to float, similarly to the RBCs still present in the solution.

### 5.2.4 – Effect of Neutrophils from diverse geographic populations in attachment and migration on CD47-Labeled Substrate

Although neutrophils had no response to CD47 labeled synthetic beads, we observed a very distinct response to CD47 labeled substrates. Neutrophils rarely attached to these surfaces, and if they did attach they migrated less and

often detached from the surface. This was very encouraging, as reduced attachment of neutrophils would be a desirable effect of CD47 labeling on xenographic transplants (Zehr 1994). It is unclear why neutrophils would behave differently between CD47 labeled substrates and synthetic beads.

Using both commercially available HL60 neutrophils as well as primary donor neutrophils, Stachelek et al demonstrated that CD47 labeling reduced neutrophil attachment in fluid flow experiments (Stachelek 2011). The observations from our study thus provide further evidence that neutrophils show reduced attachment and migratory response to CD47-labeled substrates. The differences we observed between some donors may be attributed to polymorphisms in SIRPα observed across different geographic populations (Takenaka 2007).

Indeed, donors of European descent were the most CD47-responsive, while donors of Indian descent possessed the only neutrophils observed to be able to move on CD47 surfaces (non significant differences between BSA and CD47/BSA surface), suggesting polymorphisms in SIRPα may affect CD47 responsiveness (**Table 5.1**).

Although our observations of reduced migration on CD47 surfaces were similar to those of Stachelek et al, our study differed somewhat in respect to their observations of what occurs when neutrophils were blocked for either CD47 or

SIRPα. We found that when CD47 was blocked, our donor neutrophils behaved identically to our control neutrophils, whereas Stachelek et al found CD47-blocked neutrophils to have reduced activity and binding efficiency to most surfaces (Stachelek 2011). Perhaps the difference can be explained by their use of HL60 neutrophils for this experiment, compared to our use of primary non-cancerous donor neutrophils.

### 5.3 – Discussion

Three different approaches to neutrophil isolation were evaluated before ultimately settling on one method for analysis. One of the best characterized means for extraction of neutrophils is through the protocol published by Oh et al, which uses commercially available separation media and centrifugation to separate blood into distinct bands (Oh 2008). This protocol requires high volumes, which meant we would need to obtain blood from a blood depository. Therefore we decided to pursue a protocol (detailed in materials and methods) based on blood obtained from a finger prick. This protocol yields a lower purity of neutrophils, but is easier to plan and more cost effective, allowing us to run several assays over the course of a day.

Although the effect of “Self” markers in neutrophil phagocytosis and transmigration remains unclear, we have provided insight on the different effects that human SIRPα polymorphisms could have on Neutrophil behavior on

synthetic surfaces coated with recombinant hCD47. These surfaces mimic neutrophil flow through vessel walls before attachment and spreading into endothelial cells, infection sites, synthetic polymer slabs or biomaterials.

From the 10 Sirpα polymorphisms we identified using HapMap data (www.hapmap.org) along with the structural analysis of the paired SIRPα-CD47 protein (Hatherley 2008), we discovered in Chapter 2 that there are two SIRPα variants (5 and 7) with approximately 20-40 fold reduced binding affinity to hCD47. It seems very plausible that macrophages expressing SIRPα variants 5 and 7 would not recognize “self” cells expressing hCD47, and would therefore be prone to clearing “self” cells. Our results in Table 5.1 demonstrate that, assuming comparable hSIRPα expression on all cells tested, neutrophils from donors who are most likely to express variant 7 based on their geographic origin do not strongly bind to hCD47, and their surface attachment and spreading is unaffected by the presence of our recombinant protein.

## 5.4 – Materials and Methods

### 5.4.1 – Neutrophil Extraction

A reusable needle pen (BD Biosciences) was used with disposable 30 gauge needles (BD Biosciences). The pen was completely sterilized after each use with 70% ethanol wipes and allowed to dry. The donor’s index finger was cleaned with 70% ethanol and allowed to dry. Following this sterilization,

constricting pressure was applied around the donor's finger to condense blood into the tip of the finger. Blood was extracted with a 200µl pipette and placed into a solution of 0.5M EDTA (Gibco)/ 1x DPBS solution (Gibco) in a 0.5ml Eppendorf tube. Blood was extracted until the injection site stopped bleeding, which generally yielded ~200µl of blood. The blood sample was then spun in a centrifuge (Spectrafuge 24D) at 5000 rpm for 5 minutes. The upper plasma/PBS layer was then removed and 500µl of RBC lysis buffer (Sigma) was added. Cells were allowed to lyse for 5 minutes. The cells were then centrifuged for 3 minutes at 3000rpm. The supernatant from this tube was then removed and allowed to continue lysing until the solution appeared see-through (5-7 minutes) in a 37℃ incubator. This tube underwent a subsequent centrifugation step (5 minutes at 5000rpm) to pellet the neutrophils. The pellet was then re-suspended in 50µl 50% FBS (Gibco) / non-HEPES CO2 independent media (Gibco) and placed in an incubator at 37℃.

### 5.4.2 – Neutrophil Phagocytosis Assay

To analyze neutrophil phagocytosis 2.1 µm opsonized (IgG) microbeads (Spherotech) were blocked by washing 3 times in a 1% BSA – 1 x DPBS solution, followed by centrifugation for 6 minutes at 10,000 rpm. The ratio used was approximately 20:1 microbeads to neutrophils.

Following blocking, beads were incubated in a 6 µg/ml solution of conjugated anti-streptavidin (Rockland) in PBS for 30 minutes and then spun down for six minutes at 10,000 rpm and re-suspended in 1 x PBS. Opsonin (IgG )+, CD47- peptide-labeled beads were then incubated with 2uM of CD47 derived peptide in PBS overnight at room temperature and then spun down for 5 minutes at 7,000 rpm and re-suspended in 1 x PBS. Following CD47-peptide labeling the beads were incubated in with anti-streptavidin (Rockland) in PBS for 30 minutes and then spin down for 5 minutes at 7000 rpm and resuspended in 1 x PBS. Extracted neutrophils were then placed in 2-chambered plates (Labtech) and 50% FBS / non-HEPES CO2 independent media were added. The cells were then placed in an incubator (37℃) for 1 hour. Afte r 1 hour had elapsed following microbead addition, the cells were fixed in 0.4% formaldehyde for 10 minutes at room temperature.

The cells were then placed into a 1.5ml Eppendorf tube and centrifuged at 5000rpm for 5 minutes. The supernatant was removed and the pellet was resuspended in 500ul PBS.

The cells were then incubated for 20 minutes at room temperature with anti-rabbit secondary IgG antibody (Thermo Scientific). Cells were then imaged and analyzed in the bright field, FITC, and TRITC spectrums. Each sample well was searched for any neutrophils that were present and each was imaged first in bright field, then in FITC to see if any microbeads had been phagocytized, and

then finally in TRITC to analyze secondary antibody staining. Since only non-phagocytosed microbeads could be bound by secondary antibody, this presented a good mechanism to ensure microbeads observed to be attached to or inside of a neutrophil had indeed been phagocytized and internalized. The number of phagocytosed microbeads was counted to calculate a phagocytosed microbead: neutrophil ratio.

### 5.4.3 – Migration Assays

Slides were coated with a 1% BSA solution. We then added an aliquot of neutrophils in suspension to these slides and took sequential images to track their migration ability.

### 5.4.4 – Neutrophil Imaging

Images were acquired with an inverted microscope (IX71; Olympus) with a 60x (oil, 1.4 NA) objective using a Cascade CCD camera (Photometrics). Image acquisition was performed with Image Pro software (Media Cybernetics, Inc.). Time-lapse imaging was performed using a heated stage (Ibidi GmbH) at 37° C in non-HEPES CO2 independent media. Image acquisition was performed with Image Pro software (Media Cybernetics, Inc.). All subsequent image analysis was done using ImageJ.

In the migration assay, randomly selected cells were followed from their center of mass from time zero up to 45 minutes in 3-minute increments.The total

migration distance was obtained by adding the measured distances between the center of mass of each selected neutrophil in the field of view

### 5.4.5 – CD47 Substrate

One side of a BSA coated slide was labeled with 2uM of full length CD47 in PBS and allowed to dry (we followed Stachelek et al.'s recommendation on the amount of hCD47 needed to observe an effect on neutrophil response, >16 ng CD47/cm2). Using the same neutrophil extraction procedure, 10µl of the neutrophil solution was pipetted onto the center of the CD47 slide. A cover slip (Fisher brand) was then put on the slide, and sealed with nail polish. Cells were then imaged for 45 minutes. No cell death was observed in this time frame due to nail polish toxicity.

### 5.4.6 – Protein Blocking Experiments

For protein blocking experiments anti-CD47 (BD Biosciences,B6H12), or anti-SIRPα (Santa Cruz, SE7C2) were used. Antibodies were allowed to incubate with neutrophils in media at room temperature for 30 minutes. Blocking by antibodies was confirmed through fluorescence microscopy where imaged neutrophils were examined for appropriate fluorescent signals.

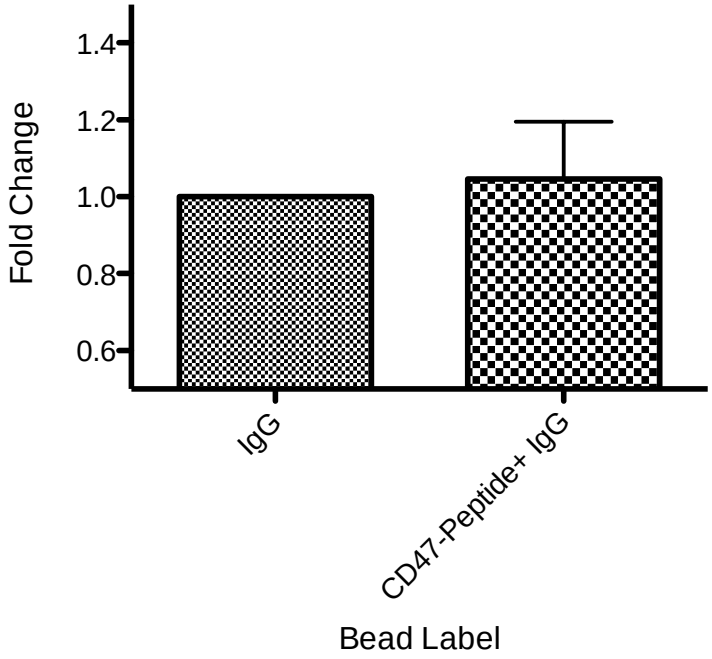


**Fig. 5.1.- Self- beads don't inhibit Neutrophil Phagocytosis**

When hCD47-derived peptide beads were used, there was no significant ($p>0.05$) change in phagocytosis compared to control labeled beads. Phagocytosis rates (beads phagocytized/neutrophil number) were compared between three samples from the same donor for each condition. Total neutrophils counted: Control trials n =748, Peptide trials n=681.

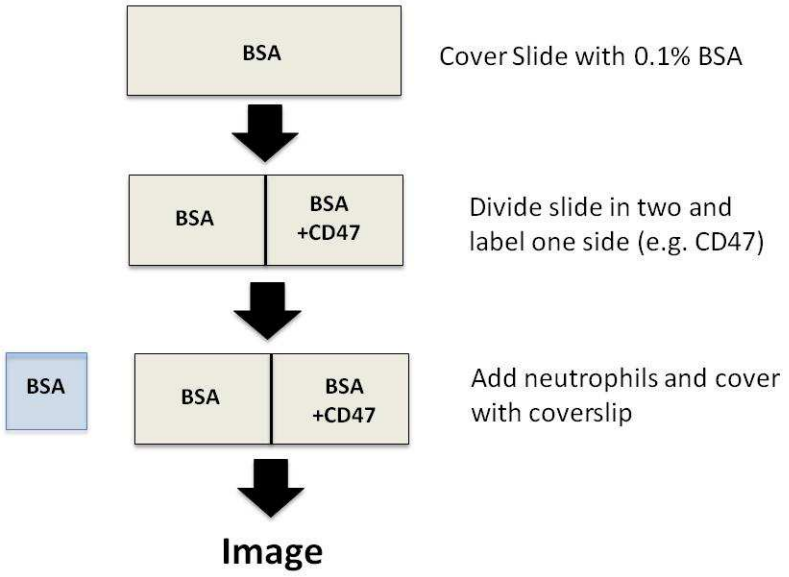


**Fig. 5.2.- Schematic representation of Migration Assay Protocol**

(Described in more detail in Material and Methods)

| hSIRPα variants | Migration (um over 45 minutes) | |
|---|---|---|
| | BSA Surface | CD47/BSA Surface |
| *Donor 1: V1, V2, V3 | 66.54 ± 12.06 | 0 |
| Donor 2: V4, V7, V8, V2 | 26.77 ± 2.4 | 16.55 ± 5.1 |
| *Donor 3: V1, V2, V3 | 117.92 ± 32.6 | 31.84 ±12.1 |
| *Donor 4: V1, V2 | 32.26 ± 11.1 | 0 |
| Donor 5: V2, V4, V7,V8 | 41.19 ± 4.3 | 63.86 ±8.7 |
| *Donor 6: V2,V3 | 13.35 ± 3.2 | 0 |
| *Donor 7: V9, V10 | 23.56 ± 5.9 | 0 |

**Table 5.1: Effect of SIRPα Polymorphisms on Migration in human Neutrophils.**

**(B)** The effect of SIRPα on migration of neutrophils from various donors was tested as previously detailed in Fig. 5.2. Based on the human HapMap data (www.hapmap.org) we defined the possible SIRPα variants (denoted as V1- V10 in the table above) that donors from each geographical location could possess. Donors 1 (L.W, *n = 6 cells*), 3 (J.S, *n = 4 cells*) and 4 (N.S, *n = 4 cells*) are of European descent. Donors 2 (P.S, *n = 6 cells*) and 5 (D.D., *n = 4 cells*) are of Indian/Asian descent. Donor 6 (A.B., *n = 3 cells*) is of Middle Eastern descent and Donor 7 (T.H., *n = 4 cells*) is of Japanese descent. All data are mean ±SEM. (* $p < 0.05$ between surfaces for each donor).

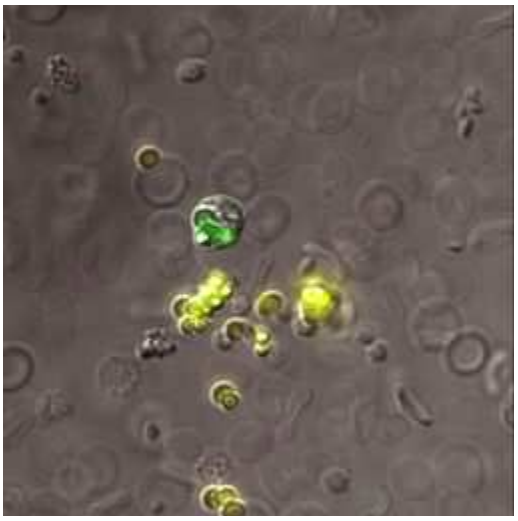

**Fig. S5.1.- Neutrophil Phagocytosis**

Phagocytosis was confirmed using a secondary antibody incapable of cell entry. Image represents a composite image showing bright field, FITC, and TRIC fluorescence. Phagocytized beads fluoresce only in the FITC spectrum (green), while beads outside of the cell fluoresce in both the FITC and TRITC (red) spectra creating a yellow color. Image taken with 60x objective and a digital zoom of 1.5x.

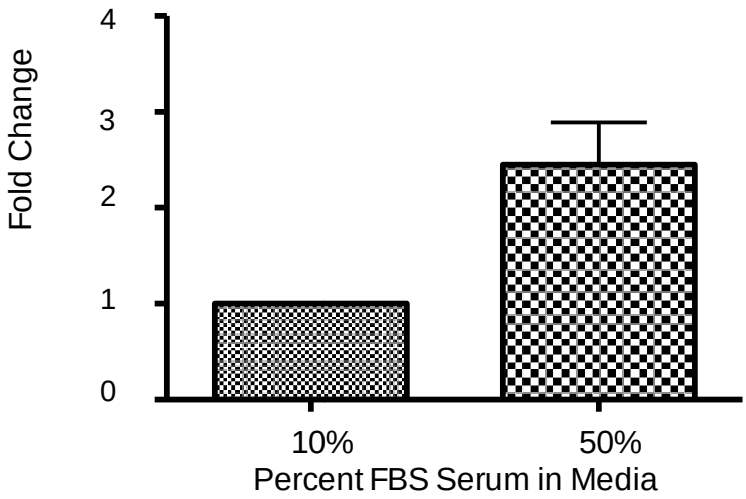


**Fig. S5.2.- Serum Level Affects Neutrophil Phagocytosis**

Changing the serum concentration to 50% FBS led to a 2.4 fold increase in phagocytosis of synthetic 2.1um microbeads by neutrophils, as compared to neutrophils in media containing 10% FBS serum. 50% serum phagocytosis rates are normalized to 10% serum phagocytosis rates. Total neutrophils counted: 10% FBS n =210, 50% FBS n=217.

## 5.5 – References


1. Cannistra, S.A., and J.D. Griffin. 1988. Regulation of the production and function of granulocytes and monocytes Semin.Hematol. 25:173-188.
2. Chin AC, Fournier B, Peatman EJ, Reaves TA, Lee WY, Parkos CA. CD47 and TLR-2 cross-talk regulates neutrophil transmigration. J Immunol. 2009 Nov 1;183(9):5957-63. Epub 2009 Oct 7.
3. Chung J, Gao AG, Frazier WA. Thrombspondin acts via integrin-associated protein to activate the platelet integrin αIIbβ3. J. Biol. Chem 1997;272:14740–14746.
4. Cooper D, Lindberg FP, Gamble JR, Brown EJ, Vadas MA. Transendothelial migration of neutrophils involves integrin-associated protein (CD47). Proc. Natl. Acad. Sci. USA 1995;92:3978–3982. [PubMed: 7732016]
5. Cronstein, B.N., and G. Weissmann. 1993. The adhesion molecules of inflammation Arthritis Rheum.36:147-157.
6. Demeure CE, Tanaka H, Mateo V, Rubio M, Delespesse G, Sarfati M. CD47 engagement inhibits cytokine production and maturation of human dendritic cells. J. Immunol 2000;164:2193–2199.
7. Han X, Sterling H, Chen Y, Saginario C, Brown EJ, Frazier WA, Lindberg FP, Vignery A. CD47, a ligand for the macrophage fusion receptor, participates in macrophage multinucleation. J. Biol. Chem 2000;275:37984–37992.
8. Hatherley, D., S.C. Graham, J. Turner, K. Harlos, D.I. Stuart, and A.N. Barclay. 2008. Paired receptor specificity explained by structures of signal regulatory proteins alone and complexed with CD47 Mol.Cell. 31:266-277.
9. Jaiswal, S., C.H. Jamieson, W.W. Pang, C.Y. Park, M.P. Chao, R. Majeti, D. Traver, N. van Rooijen, and I.L. Weissman. 2009. CD47 is upregulated on circulating hematopoietic stem cells and leukemia cells to avoid phagocytosis Cell. 138:271-285.
10. Liu, Y., H.J. Buhring, K. Zen, S.L. Burst, F.J. Schnell, I.R. Williams, and C.A. Parkos. 2002. Signal regulatory protein (SIRPalpha), a cellular ligand for CD47, regulates neutrophil transmigration J.Biol.Chem. 277:10028-10036.
11. Matozaki, T., Y. Murata, H. Okazawa, and H. Ohnishi. 2009. Functions and molecular mechanisms of the CD47-SIRPalpha signalling pathway Trends Cell Biol. 19:72-80.
12. Oh, H., B. Siano, and S. Diamond. 2008. Neutrophil isolation protocol J.Vis.Exp. (17). pii: 745 doi:10.3791/745.
13. Oldenborg, P.-., A. Zheleznyak, Y.F. Fang, C.F. Lagenaur, H.D. Gresham, and F.P. Lindberg. 2000. Role of CD47 as a Marker of Self on Red Blood Cells. Science. 288:2051- 2054.
14. Parkos, C.A., S.P. Colgan, T.W. Liang, A. Nusrat, A.E. Bacarra, D.K. Carnes, and J.L. Madara. 1996. CD47 mediates post-adhesive events required for neutrophil migration across polarized intestinal epithelia J.Cell Biol. 132:437-450.
15. Pettersen RD, Hestdal K, Olafsen MK, Lie SO, Lindberg FP. CD47 signals T cell death. J. Immunol 1999;162:7031–7040.

16. Smith, J.A. Neutrophils, host defense, and inflammation: a double-edged sword. J Leukoc Biol. 1994 Dec;56(6):672-86.
17. Stachelek, S.J., M.J. Finley, I.S. Alferiev, F. Wang, R.K. Tsai, E.C. Eckells, N. Tomczyk, J.M. Connolly, D.E. Discher, D.M. Eckmann, and R.J. Levy. 2011. The effect of CD47 modified polymer surfaces on inflammatory cell attachment and activation Biomaterials. doi: 10.1016/j.biomaterials.2011.02.053.
18. Takenaka, K., T.K. Prasolava, J.C. Wang, S.M. Mortin-Toth, S. Khalouei, O.I. Gan, J.E. Dick, and J.S. Danska. 2007. Polymorphism in Sirpa modulates engraftment of human hematopoietic stem cells Nat.Immunol. 8:1313-1323.
19. Tsai, R.K., P.L. Rodriguez, and D.E. Discher. 2010. Self inhibition of phagocytosis: The affinity of 'marker of self' CD47 for SIRPalpha dictates potency of inhibition but only at low expression levels Blood Cells. Mol.Dis. doi: 10.1016/j.bcmd.2010.02.016.
20. Zehr, K.J., A. Herskowitz, P.C. Lee, P. Kumar, A.M. Gillinov, and W.A. Baumgartner. 1994. Neutrophil adhesion and complement inhibition prolongs survival of cardiac xenografts in discordant species Transplantation. 57:900-906.

# CHAPTER 6 – CONCLUSIONS AND FUTURE WORK

In this dissertation we have shown that the membrane protein CD47 acts as a ‘Marker of Self’ that impedes phagocytosis of self cells by signaling through a species-specific, highly polymorphic receptor, SIRPα. In each of the preceding chapters we have described various findings that have supported this general notion.

In Chapter 2, we introduced our reductionist approach of designing minimal “self” peptides derived from human-CD47, synthesized with anchoring groups, and attached to virus-size nanoparticles for injection into NOD.SCID gamma (NSG) mice. We found only a weak affinity of hCD47 for NSG-SIRPα, but that was still within the broad range (0.1~5 μM) of affinity of the different human-SIRPα variants. The hCD47-peptides delayed splenic clearance of particles by macrophages with an exponential increase in persistence in circulation. Our reductionist approach thus highlighted the importance of a human ‘Marker of Self’.

In Chapter 3, we applied our reductionist approach to a potential therapeutic application. We showed that “self”-beads and hCD47-beads led to a 16- to 22-fold enhancement of the near-infrared imaging of human tumor xenografts. We also showed that hCD47-beads could shrink lung tumor cells with similar efficiency as the widely used current standard Cremophor® EL-Paclitaxel

(Taxol) treatments, but without the noted toxicity imparted by the Cremophor® EL excipient. We also developed an antibody-targeting approach using this “self” peptide, which allowed us to successfully target the human lung cancer cells with a biotinylated anti-hCD47 antibody. This antibody resulted in more efficient delivery to the tumor site, leading to suppression in tumor growth in just one day.

In Chapter 4, we moved into the molecular level in an effort to understand the low affinity of the signal regulatory protein (SIRPα) to hCD47. We found that this low affinity was necessary to allow for rapid exchange of CD47-SIRPα from an intracellular cis to an intercellular trans interaction. Further confirmation of this competitive binding behavior was demonstrated through measurement of the association constant, $k_{on}$, which exhibited a slower rate for wild-type macrophages. This suggested that the availability of CD47 to interact in trans was influenced by the amount of CD47 that was occupied in cis interactions. The CD47-SIRPα cis interactions appear to partially hinder phagocytosis of foreign particles, but at the same time it is important for macrophages to maintain their own display of the “self” signal to prevent their own phagocytic clearance by other macrophages.

Finally, in Chapter 5 we extended our analysis of marker of “self” to the case of neutrophil transmigration. Our preliminary findings in this regard suggested that the SIRPα polymorphism in the human population affects the

migration process of neutrophils. When higher levels of neutrophil migration on a surface were observed, there was a lower affinity of the SIRPα variants for CD47.

Taken together, the chapters of this dissertation show that we have successfully designed a unique CD47 peptide that mimic the effect of the full-length protein in inhibiting the uptake of nanometer scale particles by macrophages *in vivo*. Our method therefore offers a very attractive platform for potential biomedical applications. The antibody targeting approach developed here revealed the importance and utility of a human marker of “self” in improving drug delivery on nanobeads, which could lead to safer therapies. It remains to be seen how our reductionist approach will perform as a human clinical drug delivery carrier, e.g. filomicelles or toroidal polymers. Similarly, it would be interesting to apply our methods to tissue xenotransplantation. We hope to continue investigating these issues in future research.

Xenograft rejection remains as a major obstacle to clinical transplantation in current medicine. We hope that the methods and evidence provided in this dissertation will contribute to a more thorough understanding of this problem.